Integration of Gap Junction Coupling in Adenosine Signalling of Endothelial Cells

Von der Naturwissenschaftlichen Fakultät der
Gottfried Wilhelm Leibniz Universität Hannover

zur Erlangung des Grades
Doktorin der Naturwissenschaften
(Dr. rer. nat.)

genehmigte Dissertation

von
Almke Bader, M. Sc.

2018

Contents

Abbreviations

2-PAA	2-phenylaminoadenosine
ATP	adenosine triphosphate
BAY	BAY60-6583
cAMP	cyclic adenosine monophosphate
cav-1	caveolin-1
CBX	carbenoxolone
CD	cluster of differentiation
CNG	cyclic nucleotide-gated
cont.	control
Cx	connexin
DAPI	4',6-diamidino-2-phenylindole
dip.	dipyridamole
EL	extracellular loop
Epac	exchange protein directly activated by cAMP
GNOME LP/DT	gold nanoparticle-mediated laser perforation/dye transfer
IL	intracellular loop
KT	KT5720
MRS	MRS1754
PET	polyethylene terephthalate
PKA	protein kinase A
Rp, Rp-cAMPS	Rp-adenosine-3',5'-cyclic monophosphorothioate
SCH	SCH58261
SNAPs	synaptosomal-associated proteins
TEER	transendothelial/transepithelial electrical resistance
TM	transmembrane domain
ZO1	zonula occludens 1

List of Figures

Zusammenfassung

Gap Junctions sind durch den Austausch von Ionen und Metaboliten zwischen benachbarten Zellen an der Bildung von funktionellen Geweben beteiligt. In Endothelzellen sind Gap Junctions essentiell für die Aufrechterhaltung der vaskulären Funktionen. Adenosin ist ein ubiquitäres extrazelluläres Signalmolekül, das durch parakrine Bindung an seine Rezeptoren großflächige zelluläre Reaktionen hervorrufen kann. Im vaskulären System regulieren Adenosinrezeptor-abhängige Signalwege verschiedene Funktionen wie Vasodilatation oder die endotheliale Barrierefunktion. Da Gap Junctions wichtig für diverse Gewebefunktionen sind, ist die Regulierung der Gap Junction-Kopplung durch allgemeine Signalmechanismen im Gewebe nötig. Daher wurde die Regulierung von Gap Junctions durch Adenosin als extrazellulärem Signalmolekül in der vorliegenden Arbeit untersucht.

Die Aktivierung des Adenosinrezeptor-Subtyps A_{2B} führte in der mikrovaskulären Endothelzelllinie hCMEC/D3 durch Aktivierung von *cyclic nucleotide-gated-* (CNG) Kanälen zu einer signifikanten Steigerung der Gap Junction-Kopplung und einer vermehrten Anzahl von Connexin43-Gap-Junction-Plaques. Auf funktionaler Ebene stellt die Regulierung von Gap Junctions durch Adenosinrezeptoraktivierung und der Zusammenhang zu den CNG-Kanälen einen bislang wenig beachteten Signalweg dar. Dieser könnte neue Einblicke beispielsweise in die Regulierung von Entzündungsprozessen liefern.

Die Analyse der Gap Junction-Kopplung erfolgte durch *scrape loading*/Farbstofftransfer-Versuche. Zur Optimierung wurde die Goldnanopartikel-vermittelte Laserperforation/Farbstofftransfer- (GNOME LP/DT) Methode zur nicht-invasiven, zellschonenden Analyse der Gap Junction-Kopplung etabliert. Mit dieser Methode konnten semi-automatisch vergleichbare Ergebnisse wie in *scrape loading*/Farbstofftransfer-Versuchen ermittelt und eine höhere Reproduzierbarkeit erzielt werden. Zusätzlich ist die GNOME LP/DT-Methode für empfindliche Zellen sowie in komplexen, beispielsweise dreidimensionalen Zellkulturmodellen sowie Ko-Kulturen in *transwell inserts* geeignet. Mit solchen Zellkultursystemen kann es die GNOME LP/DT-Methode in Kombination mit transendothelialen Widerstandsmessungen ermöglichen, neue Erkenntnisse zur Rolle der Gap Junctions in der Pyhsiologie der Blut-Hirn-Schranke zu erlangen.

Schlagwörter: Gap Junctions, Adenosinrezeptoren, Goldnanopartikel-vermittelte Laserperforation/Farbstofftransfer

Abstract

By allowing a direct exchange of ions and metabolites between cells, gap junctions participate in the formation of physiological units in tissues. Gap junctions in endothelial cells are essential for maintaining vascular functions. Adenosine is a ubiquitous extracellular signalling molecule that can evoke cellular responses in large tissue areas by binding in a paracrine manner to its receptors. Adenosine receptor-dependent signalling mechanisms regulate several vascular functions, for example vasodilation or endothelial barrier properties. Since gap junctions are important for various tissue functions, it is essential to include the gap junction regulation into general signalling mechanisms within tissues. Therefore, the regulation of gap junction coupling by adenosine receptor signalling was analysed in the presented work.

Activation of the adenosine receptor subtype A_{2B} significantly increased the gap junction coupling and the amount of connexin43 gap junction plaques in microvascular endothelial hCMEC/D3 cells via activation of cyclic nucleotide-gated (CNG) channels. On functional level the regulation of gap junctions upon adenosine receptor activation and especially the involvement of CNG channels is as yet a disregarded signalling link and could provide new insights for example into the regulation of inflammatory conditions.

Analysis of gap junction coupling was performed with scrape loading/dye transfer assays. To improve this technique a gold nanoparticle-mediated laser perforation/dye transfer (GNOME LP/DT) method was established for a non-invasive, cell-friendly analysis of gap junction-dependent cell coupling. The GNOME LP/DT method enabled the analysis of gap junction coupling with similar results as scrape loading/dye transfer assays and was more reproducible. Additionally, the GNOME LP/DT method was successfully applied to sensitive cells and in complex cell culture systems, for example three-dimensional cell culture or co-culture of blood-brain barrier cells in transwell inserts. Applying the GNOME LP/DT method in such cell culture systems in combination with transendothelial resistance measurements can provide new insight into the role of gap junctions in the physiology of the blood-brain barrier.

keywords: gap junctions, adenosine receptors, gold nanoparticle-mediated laser perforation/dye transfer

1 General introduction

1.1 Gap junctions

Gap junctions are channels directly connecting neighbouring cells. They enable intercellular communication by exchange of small molecules through diffusion from one cell to another (Leybaert *et al.* 2017, Nielsen *et al.* 2012). As gap junction channels are permeable to ions, second messengers, metabolites (smaller than $1.5\,\text{kDa}$) and even small RNAs (Brink *et al.* 2012, Nielsen *et al.* 2012), gap junctions play a crucial role in the formation of functional tissue from multiple individual cells. Gap junctions are ubiquitously expressed in almost all animal tissue. Gap junction channels are involved in a plethora of tissue functions including synchronous contraction of smooth muscle cells (Figueroa & Duling 2009), electric conduction in the heart (Dhein 2004), passing maturation signals to oocytes (Nicholson & Bruzzone 1997) and nutrient supply in the lens (Donaldson *et al.* 2001, Berthoud & Ngezahayo 2017).

1.1.1 Connexins and gap junction structure

Gap junctions are formed by connexins in vertebrates (Nicholson 2003, Nielsen *et al.* 2012) and by innexins in invertebrates (Phelan 2005, Yen & Saier 2007). Connexins are membrane-spanning proteins with two conserved extracellular loops, an intracellular loop and N- and C-terminus located in the cytoplasm (Figure 1.1 A, Leybaert *et al.* 2017, Nielsen *et al.* 2012, Kumar & Gilula 1996). Six connexins form a hemichannel, called connexon (Nielsen *et al.* 2012) which as hemichannels at the cell surface can enable the exchange of molecules with the extracellular space (Leybaert *et al.* 2017). Two connexons from adjacent cells can interact through the extracellular loops of the connexins to form a complete gap junction channel (Figure 1.1 B, Foote *et al.* 1998, Kumar & Gilula 1996, Leybaert *et al.* 2017). So far 21 human genes of different connexin isoforms have been identified (Söhl & Willecke 2004, Beyer & Berthoud 2009). The connexin isoforms are distinguished by adding their weight in kDa as suffix to the abbreviation Cx for connexin (Söhl & Willecke 2004, Willecke *et al.* 2002). Gap junctions can be homo- or heteromeric,

concerning the composition of the connexons from different connexin isoforms, or homo- or heterotypic with regard to the two connexons that form a complete gap junction channel (Kumar & Gilula 1996, Nicholson 2003). Some connexin isoforms are expressed only by few specialised cell types while others, like connexin43 (Cx43), are ubiquitously found in almost every tissue (Willecke *et al.* 2002, Leybaert *et al.* 2017).
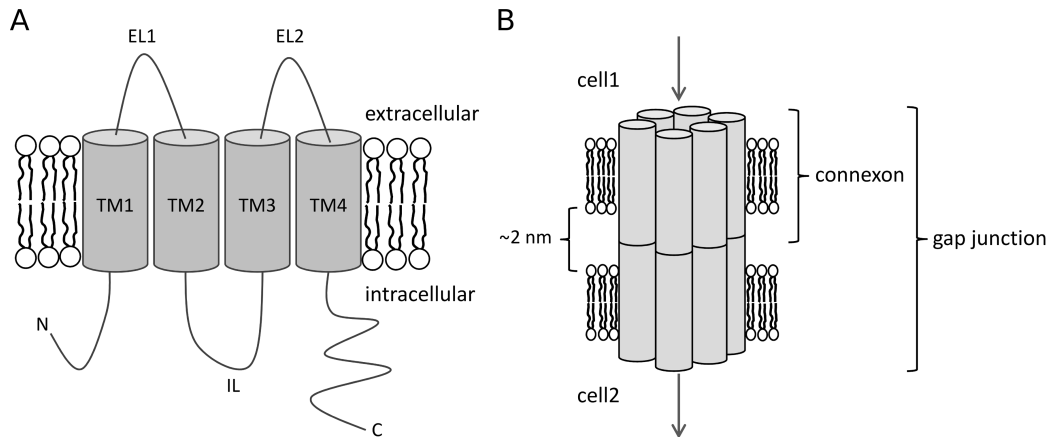
Figure 1.1: Schematic presentation of connexins, connexons and gap junctions. A) Connexin proteins have four transmembrane domains (TM), two extracellular loops (EL), one intracellular loop (IL) and N- and C-terminus are located intracellularly. B) Six connexins form a hemichannel, a connexon; two connexons of adjacent cells build a complete gap junction.

Like other membrane proteins connexins are synthesised in the endoplasmatic reticulum and transported to the membrane via the secretory pathway (Segretain & Falk 2004, Laird 2006). The hexamerisation to connexons can begin as early as in the endoplasmatic reticulum and continue in the Golgi apparatus and *trans*-Golgi network. However, the exact compartment and time point of connexon assembly seems to be isoform-dependent (Laird 2006, Segretain & Falk 2004). The closed hemichannels are inserted into the plasma membrane, probably via regulated transport to distinct membrane areas (Schubert *et al.* 2002, Shaw *et al.* 2007, Rhett & Gourdie 2012, Leybaert *et al.* 2017). Gap junction assembly usually occurs at the edges of so-called gap junction plaques, which contain up to thousands of individual gap junctions (Leybaert *et al.* 2017, Nicholson 2003, Segretain & Falk 2004). Gap junctions can be integrated in specialised membrane domains called lipid rafts, for example those structured by caveolins, that participate in gap junction structuring and regulation (Hervé *et al.* 2012, Schubert *et al.* 2002, Langlois *et al.* 2008, Ampey *et al.* 2016). Several associated scaffolding proteins anchor the gap junction plaques into the cell membrane, mostly via cytoskeletal filaments

(Segretain & Falk 2004, Giepmans 2004, Rhett & Gourdie 2012, Hervé *et al.* 2012). For example, the tight junction-associated protein zonula occludens 1 (ZO1) tethers Cx43 to actin filaments and is involved in gap junction formation and degradation (Rhett *et al.* 2011, Rhett & Gourdie 2012, Thévenin *et al.* 2017, Leybaert *et al.* 2017, Giepmans 2004, Hervé *et al.* 2012). Gap junction degradation occurs via proteasomal or lysosomal pathways (Segretain & Falk 2004, Thévenin *et al.* 2013, Su & Lau 2014) and it is well described that complete gap junctions from both neighbouring cells are internalised in so-called annular junctions (Jordan *et al.* 2001, Berthoud *et al.* 2004, Thévenin *et al.* 2013, Falk *et al.* 2016). Posttranslational modifications of connexins regulate gap junctions and the best-known modifications are phosphorylations through various protein kinases (Leybaert *et al.* 2017). Phosphorylations regulate several steps in the connexin life cycle, including trafficking through the secretory pathway, gap junction assembly, channel gating and degradation (Thévenin *et al.* 2013, Lampe & Lau 2004, Leybaert *et al.* 2017, Moreno & Lau 2007, Solan & Lampe 2005).

1.1.2 Gap junctions in the vascular system

Gap junctions exhibit important functions in the vascular system by enabling the regulation of blood pressure and vascular tone through longitudinal intercellular communication (Johnstone *et al.* 2009, Haefliger *et al.* 2004, Figueroa & Duling 2009). Endothelial cells of the vascular system express the connexin isoforms Cx37, Cx40 and Cx43 and to a lesser extent Cx45 (Figueroa & Duling 2009, Johnstone *et al.* 2009, Begandt *et al.* 2017, Leybaert *et al.* 2017, Haefliger *et al.* 2004) with different distributions depending on vascular bed and vessel size (Johnstone *et al.* 2009, Begandt *et al.* 2017, Leybaert *et al.* 2017). The essential role of vascular connexins has been demonstrated in knock-out mice (Simon & McWhorter 2003, Krüger *et al.* 2000, Kirchhoff *et al.* 2000, Walker *et al.* 2005, Söhl & Willecke 2004). Mice with global knock-out of Cx43 or Cx45 were not viable due to severe vascular and cardiac malformations (Krüger *et al.* 2000, Walker *et al.* 2005, Reaume *et al.* 1995). Endothelial cell-specific deletion of Cx43 resulted in hypotension and bradycardia (Liao *et al.* 2001). Global deletion of Cx40 led to hypertension and cardiac arrhythmias (de Wit *et al.* 2000, Krattinger *et al.* 2007, Simon *et al.* 1998). While deletion of only Cx37 is not lethal and only associated with female infertility (Simon *et al.* 1997), loss of both Cx37 and Cx40 resulted in severe abnormalities in the vascular system and early death (Simon & McWhorter 2003, Figueroa & Duling 2009), indicating an interplay between different connexin isoforms. Furthermore, each connexin isoform seems to have unique functions since exchanging one connexin isoform

with another in knock-out/knock-in experiments usually does not result in complete restoration of the defects associated with the lost connexin isoform (Plum *et al.* 2000, Zheng-Fischhöfer *et al.* 2006, Winterhager *et al.* 2007). Moreover, several vascular pathologies are associated with dysregulation or changed expression of connexins, for example hypertension (Figueroa *et al.* 2006, Figueroa & Duling 2009) or atherosclerosis (Kwak *et al.* 2002, Scheckenbach *et al.* 2011, Blackburn *et al.* 1995). Cx37 and Cx40 are down-regulated in inflammatory conditions associated with atherosclerosis or acute lung injury (Scheckenbach *et al.* 2011, Rignault *et al.* 2007). In contrast, endothelial Cx43 exhibits pro-inflammatory properties and is upregulated in these conditions (Parthasarathi *et al.* 2006, Sarieddine *et al.* 2009, Scheckenbach *et al.* 2011, de Bock *et al.* 2017, Robertson *et al.* 2010, O'Donnell *et al.* 2014) accompanied by increased expression of cell adhesion molecules and increased tissue infiltration by neutrophils (Yuan *et al.* 2015, Sarieddine *et al.* 2009). In accordance, reducing Cx43 levels attenuated progression of atherosclerosis in animal models (Kwak *et al.* 2003, Wong *et al.* 2003), decreased neutrophil recruitment after lung inflammation (Sarieddine *et al.* 2009), attenuated inflammation-induced pulmonary endothelial barrier disruption (O'Donnell *et al.* 2014) and reduced vascular leakage and inflammation in spinal cord injury (Cronin *et al.* 2008).

1.1.3 Gap junctions in blood-brain barrier endothelial cells

The blood-brain barrier forms the physical and metabolic barrier between the cerebral tissue and the blood circulation and therefore enables the maintenance of the cerebral homoeostases (Abbott *et al.* 2006, Correale & Villa 2009, Weiss *et al.* 2009). The blood-brain barrier is composed of specialised microvascular endothelial cells surrounded by a network of pericytes, astrocytes, neurons and microglia (Figure 1.2, Abbott *et al.* 2006, Weiss *et al.* 2009). Blood-brain barrier endothelial cells exhibit specific properties, including tight junction formation (Abbott *et al.* 2006, Weiss *et al.* 2009), low pinocytosis (Sedlakova *et al.* 1999), expression of specialised receptors and transporters (Abbott *et al.* 2006, Weiss *et al.* 2009) and a high amount of mitochondria (Oldendorf *et al.* 1977, Abbott *et al.* 2006).

Gap junction-dependent communication in blood-brain barrier-forming endothelial cells has been proposed to regulate the barrier function of these cells since connexins have been found to be associated with tight junction proteins (Nagasawa *et al.* 2006). Blocking the gap junctions resulted in a significant increase in endothelial permeability (Nagasawa *et al.* 2006). Furthermore, gap junctions between blood-brain barrier endothelial cells were proposed to participate in Ca^{2+} wave spreading induced by bradykinin application
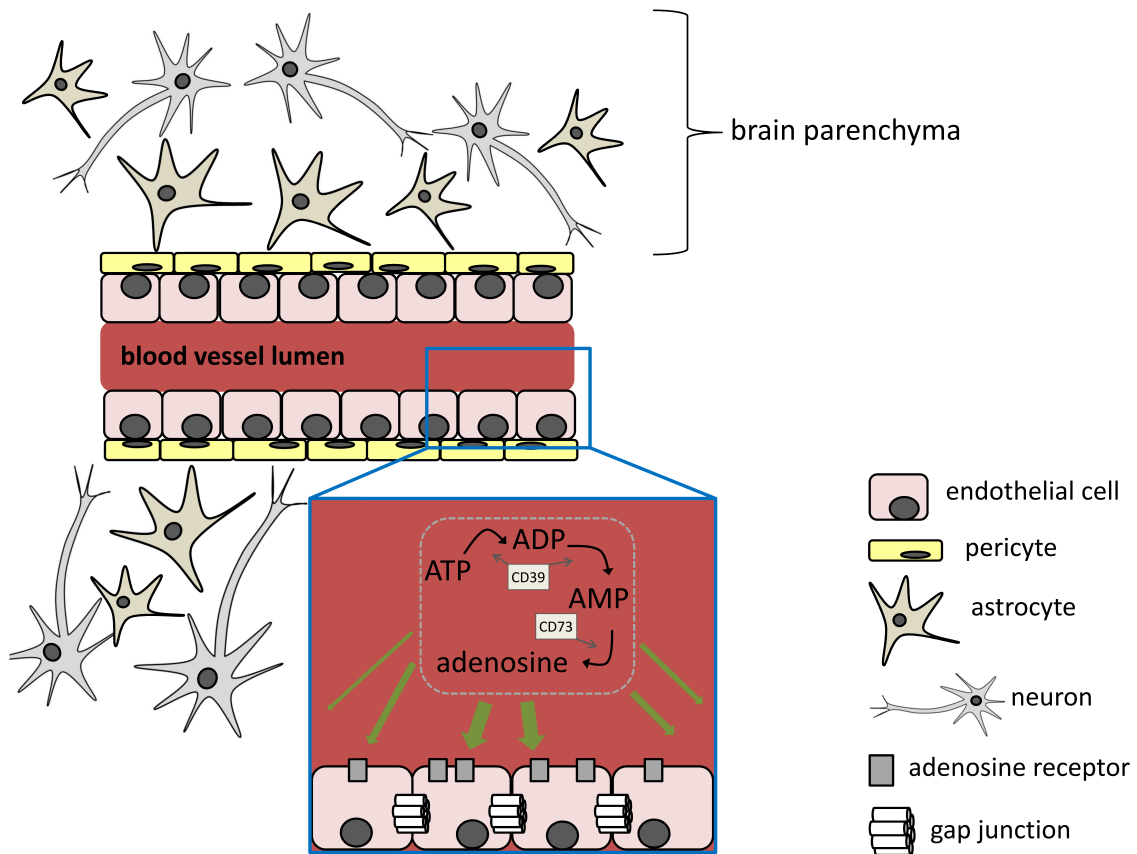
Figure 1.2: Cellular components of the blood-brain barrier. Endothelial cells forming the microvascular capillaries are surrounded by pericytes, astrocytes and neurons. Microglia are not shown. Locally liberated adenosine nucleotides in the blood are broken down by cluster of differentiation (CD) 39 and CD73 to adenosine which activates adenosine receptors present on the surface of microvascular endothelial cells. The connection of microvascular endothelial cells via gap junctions is pointed out.

and associated with increased endothelial permeability (de Bock *et al.* 2012). Recently, upregulation of Cx43 and increased intercellular gap junction coupling was observed in a model of cerebral cavernous malformations, correlating with a redistribution of tight junction proteins (Johnson *et al.* 2018). Apart from these studies little is known about the detailed signalling mechanisms involved in the interplay between gap junctions or connexin hemichannels and barrier properties in the blood-brain barrier (de Bock *et al.* 2014, 2017, Eugenin *et al.* 2012).

Since intercellular communication via gap junctions is essential for the formation of functional tissue from several individual cells, the regulation of gap junction coupling has to be integrated in the general signalling pathways in the tissue. The cells in a tissue are able to sense changes in their extracellular environment for example via extracellular

signalling molecules that activate cell surface receptors. Spreading these signals from cell to cell can occur via gap junctions and several vascular pathologies are associated with dysregulation of gap junctions (Figueroa & Duling 2009, Leybaert *et al.* 2017). Adenosine comprises such an extracellular signalling molecule and adenosine concentrations are often increased in pathological conditions (Fredholm 2007). By activating adenosine receptors various intracellular signalling cascades are induced (Jacobson & Gao 2006, Chen *et al.* 2013, Fredholm 2007, Blackburn *et al.* 2009). These can regulate gap junction coupling as shown before in pituitary folliculostellate cells (Lewis *et al.* 2006) as well as vascular smooth muscle (Begandt *et al.* 2013a) and endothelial cells (Begandt *et al.* 2010, 2013b).

1.2 Adenosine as extracellular signalling molecule

Extracellular adenosine is usually a breakdown product of locally liberated adenosine nucleotides (Figure 1.2, Fredholm 2007). Adenosine triphosphate (ATP) is released from cells for example due to shear stress or mechanical stretch (Bodin *et al.* 1991, Bodin & Burnstock 2001, Hamada *et al.* 1998, Burnstock & Knight 2017), during hypoxic conditions (Eltzschig 2009), or from damaged or dying cells (Burnstock & Knight 2017, Fredholm 2007). Regulated nucleotide release during exocytosis (MacDonald *et al.* 2006, Zhang *et al.* 2007), or through connexin and pannexin hemichannels (Eltzschig *et al.* 2006, Dahl 2015, Lohman & Isakson 2014) is also possible (Fredholm 2007). Adenosine nucleotides are quickly degraded to adenosine through the ectonucleotidases cluster of differentiation (CD) 39 and CD73 (Figure 1.2, Fredholm 2007, Eltzschig 2009, Chen *et al.* 2013, Antonioli *et al.* 2013) that are expressed by most cell types, including endothelial cells (Eltzschig *et al.* 2003, Chadjichristos *et al.* 2010, Mills *et al.* 2011, Kim & Bynoe 2015). Additionally, intracellularly produced adenosine can be transported out of cells along concentration gradients via equilibrative nucleoside transporters (Fredholm 2007, Podgorska *et al.* 2005). The systemic plasma concentration of adenosine is usually in the low nanomolar range (10 to 300 nM, Shryock & Belardinelli 1997, Fredholm 2007, Haskó *et al.* 2008, Ballarín *et al.* 1991) but can rise to micromolar ranges in extreme physiological or pathological conditions (Fredholm 2007, Ho & Rose'Meyer 2013, Eltzschig 2009, Pedata *et al.* 2001). However, spontaneous locally increased adenosine concentrations in non-pathological conditions were measured *in vivo* in various tissue such as the brain (Nguyen *et al.* 2014, Nguyen & Venton 2015). Due to rapid adenosine uptake into the

cells and further degradation (Löffler *et al.* 2007, Eltzschig 2009), locally increased adenosine levels only last for about 10 s (Ho & Rose'Meyer 2013, Eltzschig 2009).

Adenosine activates adenosine receptors that are expressed on the cell surface. Adenosine receptors are G protein-coupled receptors with seven transmembrane domains and are divided in four subtypes, A_1, A_{2A}, A_{2B} and A_3 (Jacobson & Gao 2006, Fredholm 2007, Chen *et al.* 2013). The A_1 and A_3 adenosine receptor subtypes are coupled to G_i or, the A_1 adenosine receptor less frequently, to G_o proteins and generally inhibit the adenylyl cyclase (Jacobson & Gao 2006, Fredholm 2007). The A_{2A} and A_{2B} adenosine receptor subtypes are mainly coupled to G_s proteins and generally increase the cyclic adenosine monophosphate (cAMP) concentration by activating the adenylyl cyclase (Jacobson & Gao 2006, Fredholm 2007). The four receptor subtypes differ in their affinity to adenosine. The A_1, A_{2A} and A_3 adenosine receptor subtypes are activated by low adenosine concentrations that occur in physiological conditions while the A_{2B} adenosine receptor subtype is activated by micromolar adenosine concentrations (Fredholm *et al.* 2001a, Fredholm 2007) mainly observed under extreme physiologic or pathologic conditions (Fredholm 2007).

Knocking-down adenosine receptor expression in animal models revealed a wide range of effects, including altered response to inflammation and ischemia as well as behaviour changes (Fredholm 2007, Chen *et al.* 2013, Blackburn *et al.* 2009). Adenosine receptors are ubiquitously expressed (Chen *et al.* 2013) and have been found to be important for the regulation of vascular function, for example vasodilation (Fredholm *et al.* 2001b, Szentmiklósi *et al.* 1995, Eltzschig 2009), inflammatory responses by endothelial leukocyte adhesion (Yang *et al.* 2006, Lennon *et al.* 1998, Bouma *et al.* 1996, Linden 2011) and vascular barrier function (Eltzschig *et al.* 2003, Eckle *et al.* 2008, Davies *et al.* 2014, Umapathy *et al.* 2010).

1.2.1 Adenosine receptor signalling in the vascular system

In cerebral endothelial cells adenosine signalling has been implicated to play a role in bacteria crossing the blood-brain barrier (Caporarello *et al.* 2017). Furthermore, adenosine receptors were proposed as target for the controlled permeabilisation of the blood-brain barrier (Kim & Bynoe 2015, Carman *et al.* 2011, Gao *et al.* 2014, Bynoe *et al.* 2015). Many studies focused on activation of the A_{2A} adenosine receptor subtype in order to increase the blood-brain barrier permeability (Carman *et al.* 2011, Kim & Bynoe 2015, Gao *et al.* 2014). Other authors proposed that A_{2A} adenosine receptor activation to specifically target blood-brain barrier cells was not reproducible *in vivo* and

previous observations could be explained by an impaired renal function and subsequent retainment of the tracer in the blood (Cheng *et al.* 2016). In contrast to blood-brain barrier-related studies, activation of both the A_{2A} and A_{2B} adenosine receptor subtypes has been reported to be anti-inflammatory (Haskó & Cronstein 2004, Haskó *et al.* 2008, Blackburn *et al.* 2009) and for example enhanced endothelial barrier function and prevented vascular leakage in peripheral endothelial cells, especially in the lung (Eltzschig *et al.* 2003, Eckle *et al.* 2008, Davies *et al.* 2014, Lennon *et al.* 1998, Umapathy *et al.* 2010, Hassanian *et al.* 2014). However, pro-inflammatory roles of the A_{2A} and A_{2B} adenosine receptors have been reported as well (Yang *et al.* 2014, Zhou *et al.* 2011, Sun *et al.* 2006, Karmouty-Quintana *et al.* 2013, Blackburn *et al.* 2009).

A correlation between adenosine-dependent signalling via CD73 and Cx40 has been shown in endothelial cells: Knocking-down endothelial Cx40 expression resulted in a down-regulation of CD73 and subsequently increased leukocyte adhesion and inflammatory response (Chadjichristos *et al.* 2010, Scheckenbach *et al.* 2011). The increased inflammation was attributed to decreased adenosine receptor-dependent signalling due to less degradation of adenosine nucleotides (Chadjichristos *et al.* 2010, Scheckenbach *et al.* 2011). Applying the nucleoside transporter blocker dipyridamole to rat smooth muscle cells (Begandt *et al.* 2013a) or bovine aortic endothelial cells (Begandt *et al.* 2010, 2013b) increased the gap junction coupling via adenosine receptor-dependent activation of cAMP/protein kinase A (PKA) signalling pathways (Begandt *et al.* 2010, 2013a). Application of adenosine also increased Cx43 expression and gap junction coupling in pituitary folliculostellate cells (Lewis *et al.* 2006). This could indicate that increased adenosine levels as occurring for example during hypoxic conditions (Eltzschig 2009, Chen *et al.* 2013, Fredholm 2007) can regulate gap junction coupling and Cx43 expression.

1.2.2 Aim of the first study

Both adenosine receptor-dependent signalling and gap junction-dependent intercellular communication are associated with the same cellular processes, especially in the vascular system, for example cellular responses during inflammation or ischemia (Willebrords *et al.* 2016, Yang *et al.* 2006, Lennon *et al.* 1998, Chen *et al.* 2013, Blackburn *et al.* 2009, Scheckenbach *et al.* 2011, Green & Nicholson 2008). It was shown that gap junction coupling can be regulated by adenosine receptor stimulation (Lewis *et al.* 2006, Begandt *et al.* 2010, 2013a) and this can provide a link for spreading locally induced adenosine signals by gap junction-dependent cellular responses along the vascular wall. The role of gap junctions in the specialised microvascular endothelial cells of the blood-brain bar-

rier still is not conclusive (de Bock *et al.* 2014, 2017, Eugenin *et al.* 2012). In contrast, adenosine-dependent signalling is especially important in the brain for example in response to inflammation or ischemia (Melani *et al.* 2014, Blackburn *et al.* 2009) but also as target for the controlled opening of the blood-brain barrier (Bynoe *et al.* 2015). The aim of the first part of this work was to analyse the regulation of gap junction-dependent intercellular communication after adenosine receptor activation and elucidate which signalling pathways participate in this regulation. We focused on specialised blood-brain barrier microvascular endothelial cells using a human cerebral microvascular cell line as model.

1.3 Analysis of gap junction coupling

Gap junction coupling can be analysed by dye transfer experiments (Abbaci *et al.* 2008) or by measuring electrical conductances between cells with double whole-cell patch-clamp experiments (Neyton & Trautmann 1985, Abbaci *et al.* 2008). For dye transfer studies small, membrane-impermeable but gap junction-permeable dyes are loaded into cells using different methods (Abbaci *et al.* 2008). These include microinjection in single cells and, for loading many cells simultaneously, electroporation or mechanical wounding with the scrape loading technique (Abbaci *et al.* 2008).

1.3.1 Scrape loading/dye transfer

The scrape loading/dye transfer technique (Figure 1.3 A) is a simple method that allows the simultaneous gap junction coupling analysis of numerous cells without the need of special equipment (Abbaci *et al.* 2008, Babica *et al.* 2016, Trosko *et al.* 2000). Loading the cells with the membrane-impermeable dye is achieved by cutting the cell monolayer with a razor blade or a needle in presence of the dye, allowing its infiltration into the cytoplasm of the wounded cells and dye diffusion into neighbouring cells via gap junctions (Abbaci *et al.* 2008, Babica *et al.* 2016). The amount of cells inheriting the dye corresponds to the grade of gap junction coupling and this can be quantified by counting dye-incorporating cells, calculating the dye-incorporating cell area or calculating the dye diffusion distance (Babica *et al.* 2016, Trosko *et al.* 2000, Opsahl & Rivedal 2000, Begandt *et al.* 2010). This method enables the quantification of gap junction coupling in response to different stimuli (Begandt *et al.* 2010, 2013a,b, Babica *et al.* 2016, Opsahl & Rivedal 2000, Trosko *et al.* 2000).
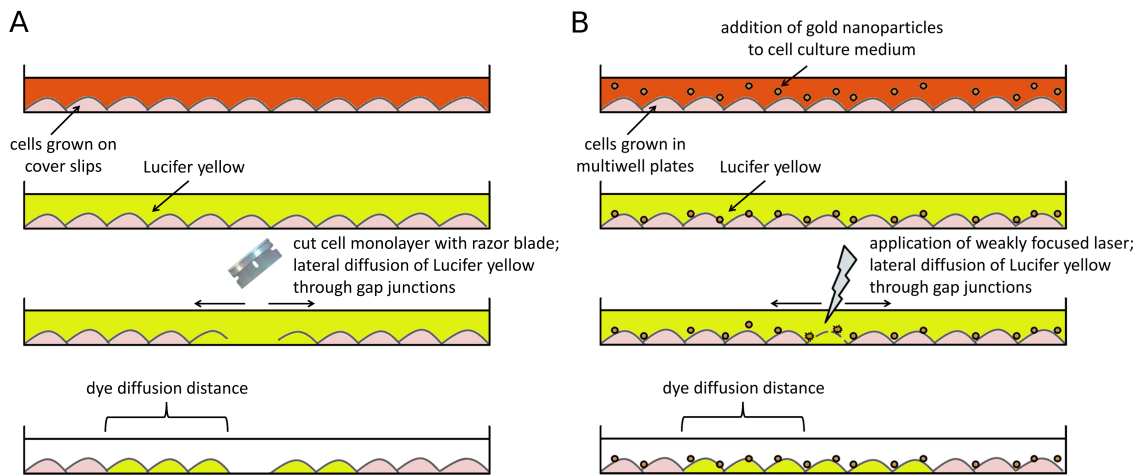
Figure 1.3: Scrape loading/dye transfer in comparison to the gold nanoparticle-mediated approach. A) During the scrape loading/dye transfer assays cells are cut with a razor blade to introduce the fluorescent dye. B) A weakly focused laser beam interacting with gold nanoparticles on the cell surface enables the transient membrane permeabilisation.

Although the scrape loading/dye transfer method is easy to perform without the need of special equipment (Abbaci *et al.* 2008, Babica *et al.* 2016, Begandt *et al.* 2010) it has limitations. Assays are usually performed in two-dimensional cell culture systems of cells grown on hard culture surfaces (Babica *et al.* 2016, Begandt *et al.* 2010), although adaptation of the technique to *ex vivo* animal tissue has been attempted by some groups (Sai *et al.* 2000, Upham *et al.* 2009, Babica *et al.* 2016). Furthermore, gap junction coupling is hard to quantify in cells that do not grow to uniform monolayers or show an elongated or irregular morphology (Babica *et al.* 2016, Trosko *et al.* 2000). Additionally, cellular responses in tissue are not only regulated by neighbouring cells of the same sort, but also by interactions with other cell types. In the blood-brain barrier (Figure 1.2) astrocytes for example actively participate in the regulation of endothelial barrier properties (Abbott *et al.* 2006, Hawkins *et al.* 2015, de Bock *et al.* 2014, 2017). For improved modelling of the blood-brain barrier consisting of endothelial cells, astrocytes, pericytes and neurons, co-culture of multiple cell types provides a much more *in vivo*-like setting (Gromnicova *et al.* 2013, Sreekanthreddy *et al.* 2015, Thomsen *et al.* 2015, Zhang *et al.* 2011, Czupalla *et al.* 2014, Wilhelm *et al.* 2011, Hatherell *et al.* 2011). To enhance the transferability of cell culture-based *in vitro* experiments to *in vivo* conditions, three-dimensional cell culture is preferable. With respect to endothelial cells this can be combined with cultivation under continuous flow conditions as found *in vivo* (Cucullo *et al.* 2008, 2011,

Adriani *et al.* 2017, Wilhelm *et al.* 2011, Sellgren *et al.* 2015). Since scrape loading/dye transfer assays are not applicable in these cell culture systems, other methods need to be established that enable the quantitative analysis of gap junction coupling in complex cell culture models as well as in animal tissue.

1.3.2 Gold nanoparticle-mediated laser perforation

Laser-based perforation of cells to specifically deliver molecules like DNA, RNA or proteins has proved to be a cell-friendly method (Stevenson *et al.* 2010). In particular gold nanoparticle-mediated laser perforation is well established for the application in therapeutics and diagnostics (Schomaker *et al.* 2015, Kong *et al.* 2017). In this approach gold nanoparticles (diameter 200 nm) are added to the cell culture medium and allowed to sink and attach to the cell surface (Heinemann *et al.* 2013, Kalies *et al.* 2013). Then a laser beam is applied and thermal as well as plasmon resonance effects lead to a temporal membrane permeabilisation (Figure 1.3 B, Heinemann *et al.* 2013, Schomaker *et al.* 2015). The permeabilisation does not need a focused system which simplifies the construction of the set-up (Heinemann *et al.* 2013). So far, gold nanoparticle-mediated laser perforation was shown to be an efficient and cell-friendly method to introduce different molecules into cells, including dextran-coupled dyes (Heinemann *et al.* 2013, Schomaker *et al.* 2014), siRNA (Heinemann *et al.* 2013), morpholinos (Kalies *et al.* 2013) and proteins (Heinemann *et al.* 2014), and was successfully applied to primary human cells (Krawinkel *et al.* 2016).

1.3.3 Aim of the second study

Considering the easy application of gold nanoparticle-mediated laser perforation (Heinemann *et al.* 2013, Kalies *et al.* 2013) we aimed to utilise this method to load the gap junction-permeable dye Lucifer yellow into cells and analyse the gap junction coupling in an assay as simple as the scrape loading/dye transfer technique (Figure 1.3 B). Furthermore, with respect to the non-invasive character of this method, the technique is potentially appclicable to gap junction analysis of more complex cell culture models. The applicability of this method in co-cultures of different cell types of the blood-brain barrier (Hatherell *et al.* 2011, Hawkins *et al.* 2015, Thomsen *et al.* 2015) and three-dimensional culture of the endothelial cells (Adriani *et al.* 2017, Cucullo *et al.* 2008, 2011) was tested with the perspective of adaption for *ex vivo* or even *in vivo* analysis of animal tissue.

2 Cyclic nucleotide-gated channels link adenosine receptors and gap junctions in cerebral endothelial cells

Contribution: I designed the experiments together with A. N., performed most of the experiments, analysed the data, prepared all the figures and wrote the manuscript together with A. N.

Adenosine receptors regulate gap junction coupling of the human cerebral microvascular endothelial cells hCMEC/D3 by Ca^{2+} influx through cyclic nucleotide-gated channels

Almke Bader[1], Willem Bintig[2], Daniela Begandt[3], Anne Klett[1], Ina G. Siller[1], Carola Gregor[4], Frank Schaarschmidt[5], Babette Weksler[6], Ignacio Romero[7], Pierre-Olivier Couraud[8,9,10], Stefan W. Hell[4] and Anaclet Ngezahayo[1,11]

[1]*Institute of Biophysics, Leibniz University Hannover, Hannover, Germany*
[2]*Institute of Biochemistry, Charité Universitätsmedizin Berlin, Berlin, Germany*
[3]*Walter Brendel Centre of Experimental Medicine, Department of Cardiovascular Physiology and Pathophysiology, Biomedical Center, Ludwig-Maximilians-Universität München, Planegg-Martinsried, Germany*
[4]*Department of NanoBiophotonics, Max Planck Institute for Biophysical Chemistry, Göttingen, Germany*
[5]*Institute of Biostatistics, Leibniz University Hannover, Hannover, Germany*
[6]*Weill Medical College of Cornell University, New York, NY, USA*
[7]*Department of Biological Sciences, The Open University, Walton Hall, Milton Keynes, UK*
[8]*INSERM, U1016, Institut Cochin, Paris, France*
[9]*CNRS, UMR8104, Paris, France*
[10]*Université Paris Descartes, Paris, France*
[11]*Center for Systems Neuroscience Hannover, University of Veterinary Medicine Hannover Foundation, Hannover, Germany*

The Journal of Physiology

Key points

- Gap junction channels are essential for the formation and regulation of physiological units in tissues by allowing the lateral cell-to-cell diffusion of ions, metabolites and second messengers.
- Stimulation of the adenosine receptor subtype A$_{2B}$ increases the gap junction coupling in the human blood–brain barrier endothelial cell line hCMEC/D3.
- Although the increased gap junction coupling is cAMP-dependent, neither the protein kinase A nor the exchange protein directly activated by cAMP were involved in this increase.
- We found that cAMP activates cyclic nucleotide-gated (CNG) channels and thereby induces a Ca^{2+} influx, which leads to the increase in gap junction coupling.
- The report identifies CNG channels as a possible physiological link between adenosine receptors and the regulation of gap junction channels in endothelial cells of the blood–brain barrier.

Abstract The human cerebral microvascular endothelial cell line hCMEC/D3 was used to characterize the physiological link between adenosine receptors and the gap junction coupling in endothelial cells of the blood–brain barrier. Expressed adenosine receptor subtypes and connexin (Cx) isoforms were identified by RT-PCR. Scrape loading/dye transfer was used to evaluate the impact of the A$_{2A}$ and A$_{2B}$ adenosine receptor subtype agonist 2-phenylaminoadenosine (2-PAA) on the gap junction coupling. We found that 2-PAA stimulated cAMP synthesis and enhanced gap junction coupling in a concentration-dependent manner. This enhancement was accompanied by an increase in gap junction plaques formed by Cx43. Inhibition of protein kinase A did not affect the 2-PAA-related enhancement of gap junction coupling. In contrast, the cyclic nucleotide-gated (CNG) channel inhibitor L-*cis*-diltiazem, as well as the chelation of intracellular Ca^{2+} with BAPTA, or the absence of external Ca^{2+}, suppressed the 2-PAA-related enhancement of gap junction coupling. Moreover, we observed a 2-PAA-dependent activation of CNG channels by a combination of electrophysiology and pharmacology. In conclusion, the stimulation of adenosine receptors in hCMEC/D3 cells induces a Ca^{2+} influx by opening

CNG channels in a cAMP-dependent manner. Ca^{2+} in turn induces the formation of new gap junction plaques and a consecutive sustained enhancement of gap junction coupling. The report identifies CNG channels as a physiological link that integrates gap junction coupling into the adenosine receptor-dependent signalling of endothelial cells of the blood–brain barrier.

Introduction

Gap junctions are intercellular channels that connect the cytoplasm of adjacent cells. They provide the possibility to exchange ions and small molecules (< 1.5 kDa) such as metabolites or second messengers between neighbouring cells. Gap junctions consist of two hemi-channels, the so-called connexons, each comprising six protein sub-units, the connexins (Cxs). So far, 21 genes for different Cx isoforms have been identified in humans (Söhl & Willecke 2004; Beyer & Berthoud 2009). They are expressed in a tissue-specific manner and are named according to their molecular weight (e.g. Cx43 has a molecular weight of 43 kDa; Söhl & Willecke 2004). Of these isoforms Cx37, Cx40, Cx43 and to a lesser extent Cx45 are commonly found in cells of the vascular wall (Haefliger *et al.* 2004; Johnstone *et al.* 2009; Figueroa & Duling 2009). They form gap junctions that mainly participate in the regulation of blood pressure and blood flow (Haefliger *et al.* 2004; Johnstone *et al.* 2009; Figueroa & Duling 2009).

In cerebral endothelial cells of different species, the expression of Cx37, Cx40, Cx43 and Cx45 has been shown (Nagasawa *et al.* 2006; Avila *et al.* 2011; Bock *et al.* 2012; Kaneko *et al.* 2015). At the functional level, Cxs were found to be closely associated with tight junction proteins in porcine blood–brain barrier (BBB) endothelial cells. It was also observed that chemical agents that close gap junctions such as 18*β*-glycyrrhetinic acid affected the barrier function of these cells (Nagasawa *et al.* 2006). The association of Cxs with the endothelial tight junctions, which constitute the morphological basis of the barrier function of the BBB, suggests possible regulatory inter-actions as well as a co-regulation of gap junction coupling and tight junctions by signalling mechanisms in BBB endothelial cells.

One of the signalling mechanisms involved in the physiology of the BBB is adenosine-stimulated signalling. Adenosine is a metabolite ubiquitously present in tissues (Fredholm 2007; Blackburn *et al.* 2009). As an extracellular mediator, adenosine is produced by rapid (< 1ms) conversion of released adenine nucleotides like ATP or ADP through a series of ectonucleotidases such as CD73 and CD39 (Fredholm 2007; Eltzschig 2009).

Under pathophysiological conditions such as ischaemia, hypoxia or inflammation, external adenosine achieves high (100-fold) and sustained concentrations, stimulating various cells in large portions of organs such as the brain (Sands & Palmer 2005; Fredholm 2007; Eltzschig 2009; Blackburn *et al.* 2009; Melani *et al.* 2014). Local increases of external adenosine by transient adenosine nucleotide release have also been observed in the brain under non-pathophysiological conditions (Nguyen *et al.* 2014; Nguyen & Venton 2015) and can occur in the vasculature as well, especially in response to changed fluid flow (Bodin *et al.* 1991; Bodin & Burnstock 2001). As an external mediator, locally produced adenosine can affect the cells in an autocrine or paracrine manner by binding to the adenosine receptor subtypes A_1, A_{2A}, A_{2B} or A_3. These receptors are G protein-coupled receptors which regulate the synthesis of cAMP in the cells and have a plethora of actions on the cells depending on the cell-specific signalling regulated by cAMP. A_1 and A_3 subtypes inhibit the synthesis of cAMP via G_i proteins, while A_{2A} and A_{2B} subtypes stimulate the production of cAMP via G_s proteins (Fredholm 2007; Eltzschig 2009).

In endothelial cells of the BBB, the expression of A_1, A_{2A} and A_{2B} adenosine receptor subtypes was shown at mRNA and protein levels (Schaddelee *et al.* 2003; Mills *et al.* 2011; Carman *et al.* 2011). In animal experiments, adenosine-dependent signalling was demonstrated as a regulator of the BBB (Carman *et al.* 2011; Gao *et al.* 2014). However, the specific contribution of the participating cells (blood cells, endothelial cells, pericytes, glial cells or neurons) was not determined in those experiments and contradictory results have been published. While many authors claimed that adenosine signalling affected endothelial barrier function, Cheng *et al.* (2016)

have shown that the classical adenosine receptor agonist 5′-*N*-ethylcarboxamidoadenosine (NECA) could stimulate cerebral extravasation of fluorescein and dextran without directly affecting the BBB (Cheng *et al.* 2016). The authors argued that NECA impaired renal function, resulting in retention of the tracer in the blood. This led to an increased concentration of the tracer in brain tissue (Cheng *et al.* 2016). Since adenosine receptor-dependent signalling in the BBB was proposed as a potential target for pharmacological therapies of pathophysiological conditions such as hypoxia, ischaemia or stroke (Blackburn *et al.* 2009; Melani *et al.* 2014), or for controlled opening of the BBB to deliver drugs into the CNS (Carman *et al.* 2011; Gao *et al.* 2014; Kim & Bynoe 2015; reviewed by Bynoe *et al.* 2015), it is of interest to decipher the physiology of this signalling in the different cells of the BBB. Using the human cerebral microvascular endothelial cell line hCMEC/D3, which has been proposed as a suitable *in vitro* model for BBB endothelial cells (Weksler *et al.* 2005, 2013), we show in the present study that adenosine receptor signalling enhances gap junction coupling. We identify cyclic nucleotide-gated (CNG) channels as the physiological link which allows an integration of the adenosine receptors and gap junction communication in a signalling unit in the BBB endothelial cells.

Methods

Materials

2-PAA, MRS1754, SCH58261, forskolin, 8-Br-cAMP, 8-Br-cGMP, dibutyryl-cGMP (db-cGMP) and Lucifer Yellow were purchased from Sigma-Aldrich (Taufkirchen, Germany). BAPTA AM was obtained from Santa Cruz Biotechnology (Heidelberg, Germany). EGTA AM was purchased from Biomol (Hamburg, Germany). CGS21680 was from Merck Millipore (Darmstadt, Germany). L-*cis*-diltiazem was from Abcam (Cambridge, UK). 8-Cyclopentyl-1,3-dipropylxanthine (DPCPX), KT5720 and SQ22536 were from Enzo Life Sciences (Lörrach, Germany). Rp-cAMPS and 8-pCPT-2′-*O*-Me-cAMP were from Biolog Life Science Institute (Bremen, Germany).

2-PAA was dissolved in a mixture (1:1) of ethanol and buffer solution (121 mM NaCl, 5.4 mM KCl, 25 mM Hepes, 0.8 mM MgCl$_2$, 5.5 mM glucose, 6 mM NaHCO$_3$, 1.8 mM CaCl$_2$, pH 7.4) while MRS1754, SCH58261, CGS21680, BAPTA AM, EGTA AM, KT5720 and 8-pCPT-2′-*O*-Me-cAMP were dissolved in DMSO. All inhibitors were added 20–30 min prior to addition of 2-PAA. The vehicles DMSO or ethanol were added to control cells in all experiments at maximal concentrations of 0.2% or 0.3%, respectively. At these concentrations the vehicles by themselves did not affect the cells in any experiment.

Cell culture

The human cerebral endothelial cell line hCMEC/D3 was cultured as described before (Weksler *et al.* 2005) in EBM-2 medium (Lonza, Basel, Switzerland) supplemented with 5% fetal calf serum (Biochrom, Berlin, Germany), 1 mg ml^{-1} penicillin, 0.1 mg ml^{-1} streptomycin (Biochrom), 1.4 μM hydrocortisone, 5 μg ml^{-1} ascorbic acid, 10 mM Hepes, 1 ng ml^{-1} bFGF (Sigma-Aldrich), and chemically defined lipid concentrate (Thermo Fisher Scientific, Darmstadt, Germany) diluted 1:100. The cells were maintained in a cell culture incubator in a humidified atmosphere with 5% CO$_2$ at 37 °C. The cell culture media was renewed every two to three days. Cells up to passage 36 were used for experiments.

Scrape loading/dye transfer

hCMEC/D3 cells were seeded at a density of 3×10^5 cells per coverslip on glass coverslips coated with collagen I (Trevigen, Gaithersburg, MD, USA). Cells were allowed to form a monolayer for 48 h before 2-PAA was added to the cell culture medium for the indicated time periods. Scrape loading/dye transfer experiments were performed as described previously (Begandt *et al.* 2010). The cell monolayers were washed with Ca^{2+}-free buffer (121 mM NaCl, 5.4 mM KCl, 25 mM Hepes, 0.8 mM MgCl$_2$, 5.5 mM glucose, 6 mM NaHCO$_3$, 1 mM EGTA, pH 7.4) and then incubated in 0.25% Lucifer Yellow in Ca^{2+}-free buffer for 2 min. The monolayers were scraped with a razor blade and incubated for another 5 min to allow dye uptake by the injured cells and lateral dye diffusion in the cell monolayer. The cells were then washed twice, first with Ca^{2+}-free and then with Ca^{2+}-containing buffer before fixing with 4% formaldehyde in phosphate buffered saline (PBS, 137 mM NaCl, 2.7 mM KCl, 10 mM Na$_2$HPO$_4$, 1.8 mM KH$_2$PO$_4$, pH 7.4) for 10 min. The cells were stored in PBS at 4 °C prior to microscopic analysis.

Four images along the scrape with a size of 1273 μm x 1273 μm were acquired from each coverslip with a confocal Nikon Eclipse TE2000-E laser scanning microscope (Nikon GmbH, Düsseldorf, Germany) and the software EZ-C1 (Nikon GmbH). A home-made ImageJ (http://imagej.nih.gov/ij) plugin and Matlab- or Octave-based software was used to calculate the lateral diffusion distance of Lucifer Yellow within the monolayer (Begandt *et al.* 2010). For the graphical presentation of the data the dye diffusion distances were normalized to those found in vehicle-treated cells. All experiments were repeated at least five times using at least three different cell passages.

To evaluate the time dependency we used the non-linear curve fit assistant of Origin 7 (OriginLab) to fit the measured dye diffusion distances at different time points for 2-PAA concentrations of 1 μM, 10 μM, 20 μM and

50 μM to an exponential asymptotic curve defined by the equation:

$$y(t) = a + (b - a)\,e^{-t}$$

In this equation, b represents the relative dye diffusion distance measured at the time point 0 h and a represents the asymptotic value of the dye diffusion distance that would be achieved by 2-PAA treatment for an infinite time. From the asymptote a, the half-maximal increase in the dye diffusion distances was calculated as $(a - b)/2 + 100$ and the corresponding time point was considered as $t_{1/2}$. To analyse the concentration dependency, we used the non-linear curve fit assistant of Origin 7 to fit the dye diffusion distances obtained after treatment with 2-PAA concentrations ranging from 0.01 μM to 100 μM for 1 h to a sigmoidal Boltzmann function given by the equation:

$$y = \frac{A_1 - A_2}{1 + e^{\frac{x - x_0}{dx}}} + A_2$$

In the equation, A_1 represents the diffusion distance obtained for 0.01 μM 2-PAA and A_2 is the theoretical maximal diffusion distance calculated from the data. We estimated the half-maximal increase as the value $(A_1 + A_2)/2$ (which corresponds to $x = x_0$) and the corresponding concentration was estimated as EC$_{50}$ concentration for 2-PAA.

Knock-down of the A$_{2B}$ adenosine receptor subtype

For siRNA-mediated knock-down of the A$_{2B}$ adenosine receptor subtype, 2.5×10^5 cells were seeded on collagen I-coated coverslips and grown for 24 h to a confluence of about 60%. The cell culture media was exchanged to Opti-MEM (Thermo Fisher Scientific). Two different anti-A$_{2B}$ adenosine receptor siRNAs (Qiagen, Hilden, Germany, SI02662982 and SI02662975) and Silencer Select Negative Control No. 2 siRNA (Thermo Fisher Scientific) were diluted in JetPrime dilution buffer (Polyplus transfection, Illkirch, France). Per well 1.5 μl JetPrime transfection reagent (Polyplus transfection) were added. The transfection mix was incubated for 10 min at room temperature before addition to the cells to a final siRNA concentration of 50 nM per well. After 6–7 h the transfection medium was exchanged for normal cell culture medium and the cells were cultivated for further 48 h before scrape loading/dye transfer experiments and quantification of A$_{2B}$ adenosine receptor mRNA was performed.

RT-PCR

The RNeasy Mini kit (Qiagen) or the PeqGOLD Total RNA kit (Peqlab, Erlangen, Germany) were used for total RNA isolation according to the manufacturer's protocols. Briefly, cells were washed with PBS containing 1 mg ml^{-1}

EDTA. Lysis buffer was then added and the cell lysate was collected in a new reaction tube. The RNA was eluted from the spin columns with 40–50 μl RNase-free water. The RNA concentration was measured with a Nanodrop2000c spectrophotometer (Peqlab).

After removal of genomic DNA with DNaseI (Thermo Fisher Scientific), 500 ng of total RNA were reverse transcribed into cDNA in a 20 μl reaction mixture containing 0.2 μg of random hexamer primers, 10 μM of each dNTP, 1 $\times$ reaction buffer, 1 U RiboLock RNase inhibitor and 1 U MML-V reverse transcriptase (Thermo Fisher Scientific). A first incubation phase at 25 °C for 5 min was followed by a second incubation phase at 37 °C for 1 h before the reaction was stopped at 70 °C for 5 min. Alternatively the Maxima First Strand cDNA synthesis kit for RT-qPCR with dsDNase (Thermo Fisher Scientific) was used. Up to 5 μg of total RNA were incubated with 1 μl dsDNAse and 1 $\times$ dsDNAse buffer for 30 min at 37 °C. Then 1 $\times$ reaction buffer and 2 μl enzyme mix were added in a final volume of 20 μl. The reaction was carried out for 10 min at 25 °C followed by 30 min at 65 °C and 5 min at 85 °C. Complete removal of genomic DNA was confirmed before reverse transcription for all samples by PCR analysis using the DNase-treated RNA as template.

The primer pairs for gene expression analysis of Cx isoforms, adenosine receptors and CNG channel subtypes are given in Table 1. The correct amplification of all genes was verified by sequencing of the amplificates. PCR was performed in a 25 μl reaction mixture containing 62.5 ng cDNA, 0.2 μM of each primer and 1 $\times$ GoTaq G2 Green Mastermix (Promega, Mannheim, Germany) or KAPA ReadyMix with dye (Kapa Biosystems, Wilmington, MA, USA) or OneTaq Quick-Load Master Mix with standard buffer (New England Biolabs, Ipswich, MA, USA) in a peqSTAR Universal 2$\times$ gradient PCR cycler (Peqlab). The PCR reaction started with an initial denaturation at 95 °C for 3 min followed by 35 cycles of denaturation at 95 °C for 10 s, annealing of primers at 60 °C for 30 s and elongation at 72 °C for 45 s and a final elongation at 72 °C for 5 min. Each PCR was run with an appropriate positive and negative control for each primer pair. The PCR products were separated in 2% agarose gels stained with GelRed (Biotium, Hayward, CA, USA).

Real time PCR was used to quantify the expression of Cx isoforms after 2-PAA treatment and to analyse the knock-down of the A$_{2B}$ adenosine receptor subtype after siRNA transfection. The glyceraldehyde 3-phosphate dehydrogenase (gapdh) and beta-actin (actB) genes were used as housekeeping genes for normalization. For real time PCR the KAPA SYBR FAST Universal mastermix (Kapa Biosystems) was used and PCR was performed in a peqSTAR 96Q real time PCR cycler (Peqlab). Real time PCR was carried out with an initial denaturation at 95 °C

　　　　CNG channels as link between adenosine receptors and gap junctions　　　　

Table 1. List of all primer pairs used for gene expression analyses and quantitative real time PCR

Target gene		Primer sequence 5′-3′	Amplicon size (bp)
gapdh	For	GGGGAGCCAAAAGGGTCATCATCT	701
	Rev	TGTGCTCTTGCTGGGGCTGGTG	
adora1	For	ATCCCTCTCCGGTACAAGATG	550
	Rev	TCTGGATGCGGAAGGCATAG	
adora2A	For	ATCGCAGTGGGTGTGCTCGC	455
	Rev	GCCGCCAGGAAGATCCGCAAA	
adora2B	For	GTGCCACCAACAACTGCACAGAAC	518
	Rev	CTGACCATTCCCACTCTTGACATC	
adora3	For	GTGCTTCCAGCTCTGCTCCCA	518
	Rev	GCCAGTGGGCCTAGCTCTCG	
cx30	For	GCTACCTGCTGCTGAAAGTG	326
	Rev	CGTTGTGTATGAATGGAGCA	
cx32	For	CCTGGAGGAGGTGAAGAGGC	250
	Rev	GCCAGAGGCAGCTAGCATGA	
cx36	For	CTGCCCAGTCTTTGTCTGCT	119
	Rev	CAACAGGATCCTCCCGATCAT	
cx37	For	GGACCATGGAGCCCGTGTTTGTGT	443
	Rev	AGAGCTGCTGGGACGACTTGGGGG	
cx40	For	CCGTATGCTCGTGCTGGGCA	465
	Rev	CTGCGGCAGACATGCAGGGT	
cx43	For	AGCAAAAGAGTGGTGCCCAGG	494
	Rev	TGATGTAGGTTCGCAGCAACCCC	
cx45	For	GGCTTCCAAGTCCACCCGTTTTAT	453
	Rev	ATCCAAGCGTTCCTGAGCCATCC	
cngA1	For	TCAAGGAAGGCAAACTCGCT	511
	Rev	GAGTCGATGGGCCCACTTTC	
cngA2	For	AAAATGGGCAATCGACGCAC	436
	Rev	CAATGCTGGAGAGGCAGTTG	
cngA3	For	GCTACTTCGGGGAGATCAGC	483
	Rev	CCCTGTGAAGCAGGAGACAG	
cngA4	For	CAGAGACCCGCACAGCTTAC	447
	Rev	AGTCAATAACTCGCCGCTCC	
cngB1	For	CCCCTCGGAAGACCAAGATG	451
	Rev	TTCTGCTCCAGCCACAGAAG	
cngB3	For	TGAGCTAAGGAAACACTACAGGAC	524
	Rev	TGGTGTCATCCATGCAGGC	
*gapdh**	For	GCTCATTTCCTGGTATGAC	274
	Rev	ACAGGGTACTTTATTGATGGT	
*actB**	For	ATATGAGATGCGTTGTTACAG	257
	Rev	CAAAAGCCTTCATACATCTC	
*cx37**	For	CCCAGCAGCTCTGCTTCTAA	274
	Rev	TGCTGACTCTGTCTGTGCTC	
*cx40**	For	AAATGCCCCACCTTGGTGAT	265
	Rev	GGTTCGAGAGAGGACAACAG	
*cx43**	For	AAGCTCTGTGCTCCAAGTTAC	254
	Rev	GTTTGCCTAAGGCGCTCCA	
*cx45**	For	CTGGACAACAGGGCATACCA	269
	Rev	GGAACACCCAGAAGCGTACA	
*gapdh**	For	TTGAGGTCAATGAAGGGGTC	117
	Rev	GAAGGTGAAGGTCGGAGTCA	
*actB**	For	CCTTGCACATGCCGGAG	112
	Rev	GCACAGAGCCTCGCCTT	
*adora2B**	For	TTCTGGCCGTGGCAGTC	100
	Rev	AGGACAGCAATGACCCCT	

*Primers for real time PCR.

A. Bader and others

for 3 min followed by 40 cycles of denaturation at 95 °C for 15 s and annealing of primers and elongation at 55 to 65 °C, depending on the primers, for 30 s. Amplification of target sequences was confirmed by melting curve analysis and gel electrophoresis. The $\Delta\Delta$ct method of the cycler software peqSTAR 96Q (Peqlab) was used for quantification of the relative mRNA amounts. At least three experiments with three different cell passages were performed for each treatment and each gene expression study.

Western blot

For isolation of total protein, cells grown in 60 mm diameter cell culture plates were washed twice with ice-cold PBS and removed from the culture plate surface with a cell scraper in the presence of 1 ml PBS. The cells were centrifuged for 4 min at 900 × *g* at 4 °C. The cell pellet was resuspended in 15 μl RIPA buffer (25 mM Tris HCl, pH 7.6, 150 mM NaCl, 1% non-idet P-40, 1% sodium desoxycholate, 0.1% SDS, freshly added 1% phosphatase inhibitor mix II (Serva, Heidelberg, Germany), 0.5% protease inhibitor cocktail (Roche, Waiblingen, Germany), 1.5 mM PMSF) and kept for 15 min on ice before centrifugation for 15 min at 14,000 × *g* at 4 °C. The protein concentration in the supernatant was determined with a Bradford assay (Sigma-Aldrich) using bovine serum albumin (BSA) as standard. The protein solution was mixed with 1 × Laemmli buffer (13 mM Tris HCl, 2% glycerol, 0.4% SDS, 0.002% Bromophenol Blue, 10 mM DTT, pH 6.8) and heated at 70 °C for 10 min. Aliquots of 30 μg of protein per lane were separated in a 5% SDS-polyacrylamide stacking gel and a 8% or 12% separation gel. The proteins were transferred onto a nitrocellulose membrane using a semi-dry blotting system (transfer buffer: 25 mM Tris HCl, pH 8.3, 192 mM glycine, 0.1% SDS, 20% methanol). Afterwards, the membranes were blocked in 5% non-fat dry milk powder in TBS (50 mM Tris HCl, 75 mM NaCl, pH 7.4) containing 0.1% Tween 20 (TBS-T) for 2 h at room temperature. Anti-β-tubulin antibody for the loading control (Sigma-Aldrich, T4026) was diluted 1:7500, anti-CNGA2 antibody (Alomone Labs, Jerusalem, Israel, APC-045) was diluted 1:750 and anti-Cx37 antibody (Abcam, ab58918) was diluted 1:700 in TBS-T and applied to the membranes at 4 °C overnight. After washing, the secondary anti-rabbit and the secondary anti-mouse antibody (each diluted 1:10,000 in TBS-T, Sigma-Aldrich, A9169 and A9044) were each applied for 1 h at room temperature. The detection was carried out with SuperSignal West chemiluminescent substrate (Thermo Fisher Scientific) and imaged with a CCD camera imaging system (Intas Science Imaging, Göttingen, Germany). The presence of CNGA2 and Cx37 protein was confirmed in at least five different cell passages.

Measurement of intracellular cAMP concentration

Approximately 4.5×10^5 hCMEC/D3 cells per well were seeded in a 24 multiwell plate and grown for 48 h until confluent. Measurement of cAMP levels was performed using the cAMP-Screen Chemiluminescent Immuno-assay System (Thermo Fisher Scientific) according to the manufacturer's instructions with slight modifications as described below. 100 μl of lysis buffer were added per well to the cells and incubated for 30 min at 37 °C with gentle agitation. 90 μl of lysed cell suspension were added to each well of the supplied ELISA 96 multiwell plate. 30 μl of the diluted cAMP-AP conjugate and 60 μl of the anti-cAMP antibody were added per well, followed by an incubation for 1 h at 37 °C with gentle agitation. Afterwards the wells were washed three times with 200 μl wash buffer before addition of 100 μl chemiluminescent substrate and incubation for 30 min at room temperature. Luminometric measurement was performed with a Varioskan Flash plate reader (Thermo Fisher Scientific) with a measurement time of 1 s per well. Defined cAMP concentrations served as standard. Chemiluminescence values of treated cell samples were normalized to those obtained from vehicle-treated cell samples. The results are given as the mean ± SEM from at least six different cell passages.

Ca²⁺ imaging

The evaluation of changes of the intracellular Ca^{2+} concentration was performed by ratiometric Ca^{2+} imaging with Fura-2 (Merck Millipore, Darmstadt, Germany) as described previously (Bintig *et al.* 2009). Cells grown on coverslips were loaded with 2 μM Fura-2 AM dissolved in buffer (140 mM NaCl, 5 mM KCl, 10 mM HEPES, 1 mM MgCl$_2$, 10 mM glucose, 2 mM CaCl$_2$, pH 7.4) for 20 min at room temperature. The coverslips were transferred to a perfusion chamber mounted on an inverted microscope (Zeiss, Oberkochen, Germany) and perfused with buffer to remove external Fura-2. Fura-2 in single cells was excited at 340 and 380 nm using a monochromator polychrome II (T.I.L.L Photonics GmbH, Planegg, Germany) equipped with a 75 W XBO xenon lamp. Fluorescence emission at 510 nm was recorded with a digital CCD camera (C4742-95, Hamamatsu Photonics Deutschland GmbH, Herrsching am Ammersee, Germany) controlled by Aquacosmos software (Hamamatsu Photonics GmbH). The Ca^{2+} concentration was accessed as the ratio of the fluorescence intensities elicited by excitation at 340 nm and 380 nm ($R = F_{340}/F_{380}$). At the beginning of the measurement, the cells were perfused with 0.3% ethanol-containing buffer as vehicle control. 2-PAA-containing buffer was applied 1–2 min later, and the data were recorded for the following 20 min. For control experiments, the cells

were continuously superfused with the vehicle-containing buffer. For all cells, the ratio R measured during the first 1–2 min was averaged to generate a value R_0 and the standard deviation (SD) was calculated. A Ca^{2+} increase in a cell was assumed if the ratio R of the respective cell achieved a value higher than $R_0 + 2 \times$ SD over a period of at least 5 s within 20 min. The percentage of cells with an increased Ca^{2+} signal is given as the mean $\pm$ SEM for five different cell passages with at least 20 cells measured per passage.

Electrophysiology

CNG channel opening was analysed using the whole-cell patch-clamp technique. hCMEC/D3 cells were settled on coverslips placed in a perfusion chamber containing buffer (140 mM NaCl, 5 mM KCl, 2 mM $CaCl_2$, 1 mM $MgCl_2$, 10 mM glucose, 10 mM Hepes, pH 7.4). The perfusion chamber was mounted on a Ti-E inverted fluorescence microscope (Nikon GmbH) equipped with a CCD Orca-Flash 4 camera (Hamamtsu Photonics Deutschland GmbH) and the software NIS-Elements AR (Nikon GmbH). A whole-cell configuration was established using an EPC 10 USB Double (HEKA Elektronik Dr Schulze GmbH, Lambrecht/Pfalz, Germany) coupled to PulseMaster software (HEKA Elektronik Dr Schulze GmbH). The patch pipette filling solution was composed of 125 mM potassium gluconate, 15 mM CsCl, 0.2 mM $CaCl_2$, 2.5 mM MgATP, 2 mM Na_2ATP, 5 mM EGTA, 5.5 mM glucose, 10 mM Hepes (pH 7.25). The cells were clamped at −60 mV. Membrane currents were elicited by voltage pulses between −150 and 100 mV for 250 ms in 10 mV steps in the presence of buffer with 0.3% ethanol, or 20 μM 2-PAA, or buffer containing 2-PAA and 100 μM L-*cis*-diltiazem or L-*cis*-diltiazem alone. The results were obtained from two to four different cell passages measuring at least nine cells for each treatment.

Immunofluorescence

For immunostaining 7.5×10^4 cells were seeded on collagen I-coated coverslips (diameter 10 mm) and grown for 48 h to a confluence of more than 70%. The cells were washed with PBS and fixed with 4% formaldehyde in PBS for 20 min at 4 °C. Blocking was performed with 0.5% BSA in PBS for 30 min at 37 °C. The primary antibodies anti-Cx37 (1:100, Sigma-Aldrich, SAB2100920 or Abcam, ab58918), anti-Cx40 (1:100, Sigma-Aldrich, SAB1304973), anti-Cx43 (1:4000, Sigma-Aldrich, C6219) and anti-Cx45 (1:50, Sigma-Aldrich, AV36631) were diluted as indicated in PBS containing 0.3% Triton X-100 and 0.5% BSA (only for anti-Cx40 antibody) and added to the cells overnight at 4 °C. The secondary fluorescein-conjugated anti-rabbit antibody (Merck

Millipore, 401314) was diluted 1:100 in PBS containing 0.3% Triton X-100 and added to the cells with 2 μM DAPI (Sigma-Aldrich) for 1 h at 37 °C. The cells were washed with PBS and stored at 4 °C.

Immunostaining was imaged using the Eclipse TE2000-E inverse confocal laser scanning microscope (Nikon GmbH) with a ×60 water immersion objective and the software EZ-C1 (Nikon GmbH). Six sections of 212 μm x 212 μm were recorded of each coverslip. Cx40 and Cx43 were visible as green 'dots' either within the cytoplasm of the cells or as 'plaques' in the cell membranes between adjacent cells. For quantification, the number of cells containing Cx43 as 'plaques' in the cell membrane was counted in blinded samples. The percentage of vehicle-treated cells containing membrane-localized Cx43 was compared to the percentage of 2-PAA-treated cells containing Cx43 in the cell membrane. The experiments were repeated 12 times with at least three individual cell passages.

For evaluation of the Cx43 gap junction plaque size, additional super-resolution stimulated emission depletion (STED) microscopy was applied. Staining was performed as described above, but without nuclear staining. The secondary goat anti-rabbit AlexaFluor488-conjugated antibody was diluted 1:1000. The STED set-up (Urban *et al.* 2011) included a pulsed-laser diode (Toptica Photonics, Graefelfing, Germany) with excitation at 488 nm and 100 ps pulses. The pulses for the STED beam were delivered by a Ti:Sapphire laser (MaiTai; Spectra-Physics, Darmstadt, Germany) operating at 80 MHz and emitting light pulses at 795 nm that were converted to 595 nm by an optical parametric oscillator (APE, Berlin, Germany) and stretched to 400 ps by dispersion. The power of the STED beam was 20–30 mW in the back focal aperture of the objective lens. The STED focal doughnut was created with a vortex phase plate (RPC Photonics, Rochester, NY, USA) introduced into the path of the expanded STED beam. The STED and excitation pulses were synchronized via external triggering of the laser diode. Both beams were overlapped using custom-made dichroic mirrors and focused into the 1.2 NA objective lens (PL APO, CORR CS, 63, water; Leica, Wetzlar, Germany). The fluorescence was collected by the same lens, separated by a dichroic mirror, filtered with a 535/50 band-pass filter and imaged onto a multimode optical fibre connected to a single-photon avalanche photodiode (PerkinElmer, Waltham, MA, USA). Images were recorded with resonant mirror scanning (15 kHz, SC-30; EOPC, Glendale, NY, USA) along the *x*-axis and piezo-stage scanning (P-733; Physik Instrumente, Karlsruhe, Germany) along the *y*-axis.

Membrane areas between adjacent cells with Cx43 gap junction plaques were selected from confocal imaging and magnified with STED imaging. Areas of 18 μm x 18 μm were recorded with STED imaging. The plaque sizes in STED and corresponding confocal images were

A. Bader and others

determined using the particle analyser tool of ImageJ after conversion into a 16-bit image, applying the auto threshold MaxEntropy and selection of the plaque areas in the corresponding confocal images. For statistical analysis of plaque areas and the number of distinguishable plaques, linear mixed effects models (Pinheiro & Bates 2000) were used. Total area of plaques per image and number of distinguishable plaques per cell were log-transformed before analysis. The model for comparing microscopy methods involved treatments, methods and their interaction as fixed effects and random effects for replicates, replicate-method-interaction and individual images. For the comparison of treatments, microscopy methods were analysed separately; the mixed models included treatments as fixed effects and random effects for replications, and treatment-replication interaction. After model fitting, all pairwise comparisons of least square means of microscopy methods and treatments were tested using Kenward-Roger degrees of freedom. Analysis was performed in R-3.2.2 (https://www.R-project.org/) using add-on packages lsmeans 2.20–23 and lme4 1.1–10. 4.

Statistical analysis

Statistical analysis was performed with a Student's paired two-sided *t* test. Cells from the same passage treated at the same time were considered as pairs. All treatments were compared to the corresponding vehicle controls and treatments with inhibitors were additionally compared to samples treated with 2-PAA only. Results with a *P* value < 0.05 were considered to be statistically significant. The exact *P* values are stated in the respective Results section.

Results

The aim of the present report was to study how stimulation of the adenosine receptors affects gap junction coupling of endothelial cells of the BBB. We first tested for the expression of the different adenosine receptor isoforms as well as of the vascular Cx isoforms in the hCMEC/D3 cells, which are an accepted *in vitro* model for human BBB endothelial cells (Weksler *et al.* 2005, 2013).

RT-PCR showed that the adenosine receptors A_1, A_{2A} and A_{2B} were expressed in hCMEC/D3 cells at the mRNA level (Fig. 1*A*). The hCMEC/D3 cells also expressed Cx37, Cx40, Cx43 and Cx45 mRNA (Fig. 1*B*). The Cx isoforms Cx30, Cx32 and Cx36 that are expressed in other cerebral cell types (Eugenin *et al.* 2012) were not found in hCMEC/D3 cells (Fig. 1*B*). Cxs form gap junction channels which assemble in gap junction plaques that are easily recognized in immunocytochemistry experiments. Correspondingly, we found gap junction plaques composed of Cx40 and Cx43, while Cx37 and Cx45 were not observed in the membrane areas between

contacting cells. For Cx37 and Cx45, a diffuse staining in the intracellular space was observed (Fig. 1*C*).

To activate adenosine receptors, we applied 2-phenylaminoadenosine (2-PAA), a non-hydrolysable agonist for A_{2A} and A_{2B} adenosine receptors (Bruns *et al.* 1986; Choksi *et al.* 1997; Wilson & Batra 2002), to the hCMEC/D3 cells. With scrape loading/dye transfer assays, we analysed the gap junction coupling by measuring the dye diffusion distance in cell monolayers treated with 2-PAA (20 μM) for 15 min to 6 h (Fig. 2*A*). We found that compared to vehicle-treated cells, the dye diffusion distance increased rapidly within the first 45 min of 2-PAA application and reached an asymptotic maximum of approximately 135% after a 2-PAA treatment period of 1 h (Fig. 2*B*; Student's paired *t* test compared to vehicle-treated cells: $P = 4.5 \times 10^{-3}$). For concentrations above 1 μM, the kinetic of the 2-PAA-induced increase in gap junction coupling was not concentration dependent as shown by the times for the half-maximal increase ($t_{1/2}$) of approximatively 39 min calculated by fitting the dye diffusion distances for 1 μM, 10 μM, 20 μM and 50 μM 2-PAA applied for 15 min to 6 h to an exponential asymptotic function (Table 2). With respect to the concentration dependency, we applied 2-PAA at various concentrations between 0.01 μM and 100 μM for 1 h (Fig. 2*C*). The dye diffusion distance in the cells increased beginning with 0.01 μM 2-PAA (107%, Student's paired *t* test compared to vehicle-treated cells: $P = 5.3 \times 10^{-2}$) and achieved a maximal increase of 130–140% at 20–50 μM (Student's paired *t* test compared to vehicle-treated cells: $P < 2.2 \times 10^{-3}$). An EC_{50} of 1.9 μM was evaluated with a curve fit to a sigmoidal Boltzmann function (Fig. 2*C*).

The increase in gap junction coupling was not related to a change in the expression of the Cxs since quantitative real time PCR showed that the quantity of the mRNA for Cx37, Cx40, Cx43 and Cx45 was not significantly changed by an application of 2-PAA for 1 or 6 h (data not shown). At the morphological level, the 2-PAA-related enhancement of the gap junction coupling correlated to an increase in cells with gap junction plaques composed of Cx43 (Fig. 3*A*). It is noteworthy that the other Cx isoforms were not affected. We observed 73% of cells with Cx43 gap junction plaques in control conditions and found an increase to 80% of cells with Cx43 gap junction plaques after 2-PAA treatment for 1 h (Fig. 3*B*; Student's paired *t* test compared to vehicle-treated cells: $P = 1.6 \times 10^{-2}$, $n = 12$). Evaluation of the STED microscopy showed that compared to the corresponding confocal microscopic images, in STED microscopic images the mean area of the plaques per image was reduced to one-third ($P < 1.0 \times 10^{-4}$) but the total amount of individually distinguishable particles increased 10-fold ($P < 1.0 \times 10^{-4}$, Fig. 3*C*). The different treatments were compared for each microscopic method individually. A

significant increase in the total plaque area per image was found for 2-PAA-treated cells both in the confocal images (123% of the vehicle control, $P = 4.9 \times 10^{-2}$) and in the images generated with STED microscopy (144% compared to ethanol-treated cells, $P = 4.5 \times 10^{-2}$).

In recent publications we showed that the adenosine transporter inhibitor dipyridamole increased the gap junction coupling in aortic endothelial cells by activating adenosine receptors and subsequently the cAMP–PKA pathway (Begandt *et al.* 2010, 2013*b*). Therefore, we analysed whether the same pathway is activated in the BBB endothelial cells. We found that 2-PAA (20 μM) stimulated the synthesis of cAMP to 124% compared to the vehicle (Fig. 4*A*; Student's paired *t* test compared to vehicle-treated cells: $P = 8.5 \times 10^{-4}$). The adenylyl cyclase inhibitor SQ22536 (400 μM) applied concomitantly with 2-PAA suppressed the increase in the intracellular cAMP concentration evoked by 2-PAA alone with a relative
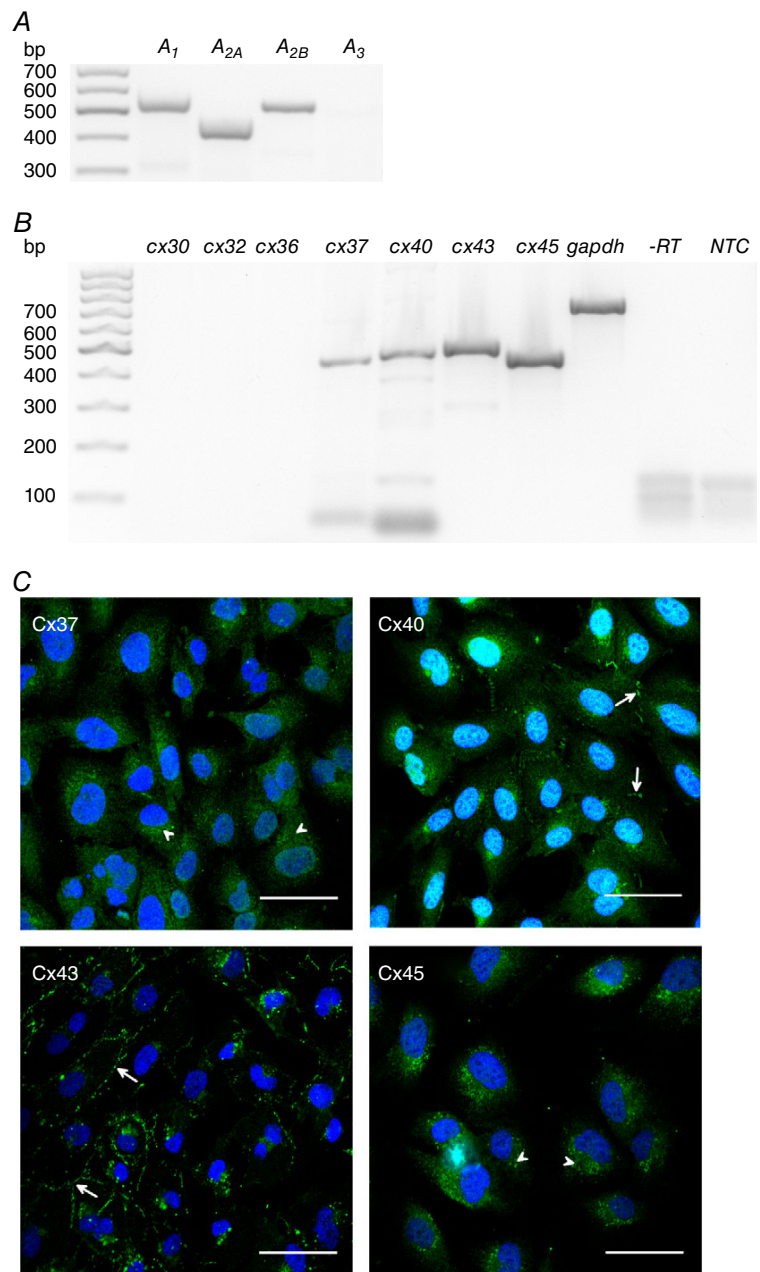
Figure 1. Expression of adenosine receptor subtypes and Cx isoforms in hCMEC/D3 cells
The mRNA of the adenosine receptor subtypes A$_1$, A$_{2A}$ and A$_{2B}$ (*A*) and of the Cx isoforms Cx37, Cx40, Cx43 and Cx45 (*B*) was detected with RT-PCR. Cx30, Cx32 and Cx36 were absent in hCMEC/D3 cells. -RT is the reverse transcription control with gapdh primers to confirm the absence of genomic DNA contamination. NTC is the negative control without template exemplarily shown for gapdh primers. *C*, immunofluorescence images of the different Cx isoforms in hCMEC/D3 cells (green). While Cx37 and Cx45 showed a diffuse intracellular staining (arrowheads), Cx40 and Cx43 staining showed gap junction plaques between neighbouring cells (arrows). Nuclei were counterstained with DAPI (blue). Scale bars represent 50 μm. [Colour figure can be viewed at wileyonlinelibrary.com]

cAMP concentration of 91% compared to the vehicle control (Fig. 4A; Student's paired t test compared to 2-PAA-treated cells: $P = 2.4 \times 10^{-3}$, $n = 7$). Consequently, we found that SQ22536 attenuated the 2-PAA-induced enhancement of the dye diffusion distance in scrape loading/dye transfer experiments (Fig. 4B; relative dye diffusion distance of 109% for 2-PAA with SQ22536 compared to 121% for 2-PAA alone, Student's paired t test compared to 2-PAA-treated cells: $P = 2.6 \times 10^{-2}$, $n = 7$). Additionally, a general increase in the intracellular cAMP concentration either by activation of adenylyl cyclase using forskolin (0.5 μM) or by application of the membrane permeable cAMP analogue 8-Br-cAMP (1 mM) significantly increased the gap junction coupling (Fig. 4B; relative diffusion distance of 123% for forskolin and 129% for 8-Br-cAMP, Student's paired t test compared to vehicle-treated cells: $P = 4.6 \times 10^{-8}$, $n = 23$ for forskolin

and $P = 3.3 \times 10^{-2}$, $n = 7$ for 8-Br-cAMP), suggesting a cAMP-dependent mechanism might also be induced by 2-PAA.

As agonist of adenosine receptors, 2-PAA predominantly targets A_{2A} and A_{2B} adenosine receptor subtypes (Bruns *et al.* 1986; Choksi *et al.* 1997; Wilson & Batra 2002). However, since 2-PAA is an adenosine derivate, an action on the A_1 adenosine receptor subtype, which was also expressed in hCMEC/D3 cells, cannot be completely excluded. The classical pathway of the A_1 adenosine receptor subtype is activation of G_i, thereby inhibiting the adenylyl cyclase. This pathway seemed unlikely since we found that 2-PAA increased cAMP in the cells and the adenylyl cyclase inhibitor SQ22536 antagonized the 2-PAA-related increase in the dye diffusion distance (Fig. 4A and B). A second pathway of A_1 adenosine receptor activation is related
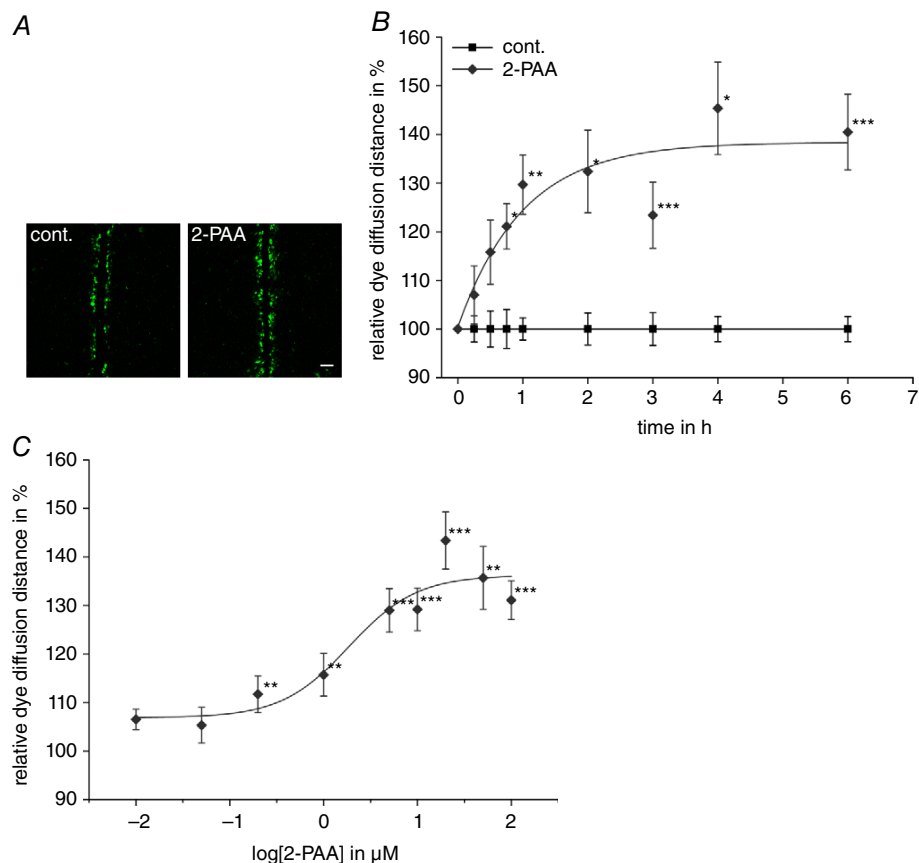
Figure 2. Enhancement of gap junction coupling by 2-PAA
A, representative micrographs of scrape loading/dye transfer experiments in hCMEC/D3 cells treated with the vehicle (cont., 0.3% ethanol) or 2-PAA (20 μM) for 1 h. Scale bar represents 100 μm. *B*, the time-dependent increase in the dye diffusion distance induced by 2-PAA (20 μM) as found by scrape loading/dye transfer assays relative to the vehicle control (cont., 0.3% ethanol). *C*, the concentration dependency of 2-PAA on the increased dye diffusion distance. The data points represent the relative dye diffusion distance achieved in cell monolayers after application of 2-PAA for 1 h. All results were analysed using Student's t test. *Significant differences to the vehicle control: *$P < 0.05$, **$P < 0.01$, ***$P < 0.001$. [Colour figure can be viewed at wileyonlinelibrary.com]

CNG channels as link between adenosine receptors and gap junctions

Table 2. The time for the half-maximal increase in the dye diffusion distance for 2-PAA concentrations ranging from 1 μM to 50 μM

Concentration of 2-PAA (μM)	Maximal relative dye diffusion distance (%)	Time for the half-maximal dye diffusion increase (min)
1	111.9	46
10	125.5	40
20	138.4	40
50	151.0	31

The maximal relative dye diffusion distance and the time for the half-maximal increase were estimated by fitting the data points for the corresponding 2-PAA concentration to a single exponential equation (Fig. 2*B*).

to cGMP accumulation (Kurtz *et al.* 1988; Serpa *et al.* 2014; Pinto *et al.* 2016). Therefore we analysed whether A$_1$ adenosine receptor- and cGMP-dependent pathways may be involved in the 2-PAA-induced enhancement of the gap junction coupling. We found that DPCPX (25 nM), an A$_1$ adenosine receptor subtype antagonist, had no effect on the 2-PAA-induced increase in the dye diffusion distance (Fig. 4*C*; relative dye diffusion distance of 122% for 2-PAA with DPCPX compared to 131% for 2-PAA alone, Student's paired *t* test compared to 2-PAA-treated cells: $P = 0.11$, $n = 9$). Moreover, the membrane permeable cGMP analogues db-cGMP (1 mM) and 8-Br-cGMP (1 mM) did not influence the dye diffusion distance (relative dye diffusion distance of 96% for both db-cGMP and 8-Br-cGMP,

Student's paired *t* test compared to vehicle-treated cells: $P = 0.36$ for db-cGMP and 0.57 for 8-Br-cGMP, $n = 7$, respectively).

With respect to the A$_{2A}$ and A$_{2B}$ adenosine receptor subtypes, MRS1754 (0.5 μM), a specific antagonist of the A$_{2B}$ adenosine receptor subtype, almost completely antagonized the effect of 20 μM 2-PAA on the gap junction coupling (Fig. 4*C*; relative dye diffusion distance of 113% for 2-PAA with MRS1754 compared to 131% for 2-PAA alone, Student's paired *t* test compared to 2-PAA-treated cells: $P = 1.2 \times 10^{-5}$, $n = 15$). In contrast, the A$_{2A}$ adenosine receptor subtype antagonist SCH58261 (0.5 μM) only had a slight inhibitory effect on the increased dye diffusion distance after 2-PAA application (Fig. 4*C*; relative diffusion distance of 122% for 2-PAA with SCH58261 compared to 131% for 2-PAA alone, Student's paired *t* test compared to 2-PAA-treated cells: $P = 2.5 \times 10^{-2}$, $n = 15$). The combination of all three adenosine receptor inhibitors with 2-PAA led to the same result as the combination of 2-PAA with only MRS1754 (Fig. 4*C*; relative dye diffusion distance of 111% for 2-PAA with all three inhibitors compared to 131% for 2-PAA alone, Student's paired *t* test compared to 2-PAA-treated cells: $P = 8.3 \times 10^{-3}$, $n = 9$). Additionally, the specific A$_{2A}$ adenosine receptor agonist CGS21680 (25 nM and 50 nM) did not affect the gap junction coupling of hCMEC/D3 cells with maximal dye diffusion distances of 105% compared to the vehicle control (Fig. 4*D*; Student's paired *t* test compared to vehicle-treated cells: $P > 0.38$, $n = 5$). The siRNA-mediated knock-down of the A$_{2B}$ adenosine receptor subtype also confirmed the importance of this receptor subtype in the observed
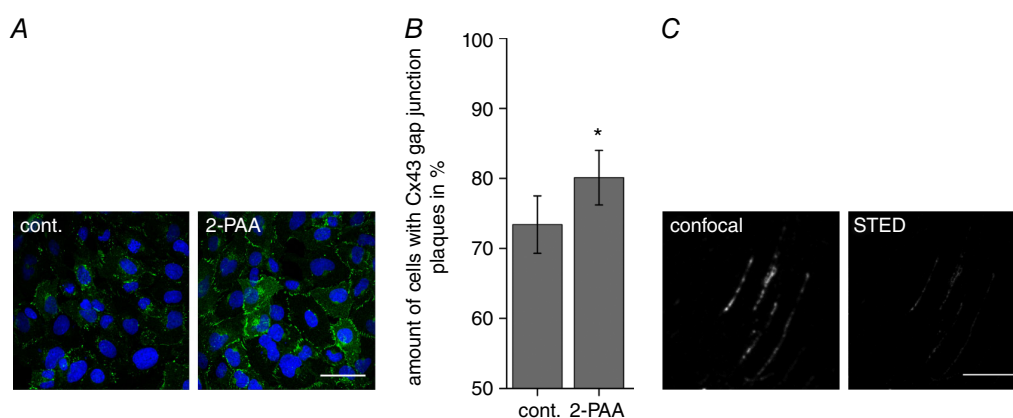
Figure 3. 2-PAA induced the formation of gap junction plaques between hCMEC/D3 cells

A, representative microscopic images of Cx43 (green) immunofluorescence in hCMEC/D3 cells after 20 μM 2-PAA treatment for 1 h. Nuclei were counterstained with DAPI (blue). Scale bar represents 50 μm. *B*, the amount of hCMEC/D3 cells with Cx43 gap junction plaques was significantly increased after 2-PAA treatment (20 μM) for 1 h compared to the vehicle control (cont., 0.3% ethanol). The results were analysed using Student's *t* test. *Significant differences to the vehicle control: *$P < 0.05$. *C*, exemplary confocal and STED images with increased resolution of individual Cx43 gap junction plaques. Scale bar represents 5 μm. [Colour figure can be viewed at wileyonlinelibrary.com]

A. Bader and others
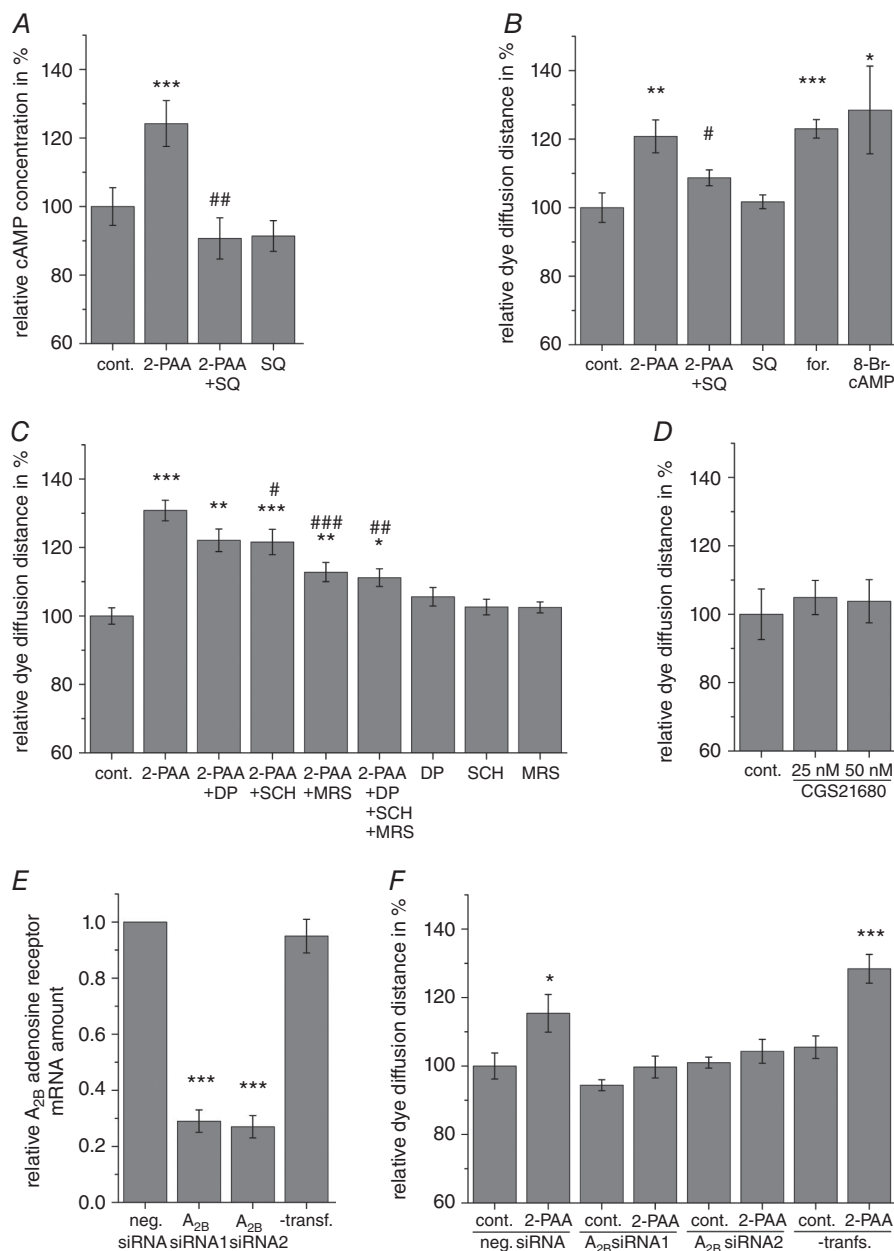
Figure 4. The pharmacology of the 2-PAA-related increase in gap junction coupling
A, 2-PAA (20 μM) increased the intracellular cAMP concentration. This increase could be blocked by the adenylyl cyclase inhibitor SQ22536 (SQ, 400 μM). *B*, the increase in the dye diffusion distance in scrape loading/dye transfer assays was significantly attenuated by the adenylyl cyclase inhibitor SQ22536 (SQ, 400 μM). The adenylyl cyclase activator forskolin (for., 0.5 μM) and the cAMP analogue 8-Br-cAMP (1 mM) significantly increased the dye diffusion distance within 1 h similar to 2-PAA. *C*, the increased dye diffusion distance by 2-PAA (20 μM, 1 h) was not significantly affected by the A_1 adenosine receptor subtype antagonist DPCPX (DP, 25 nM) and only slightly affected by the A_{2A} adenosine receptor subtype antagonist SCH58261 (SCH, 0.5 μM). The A_{2B} adenosine receptor subtype antagonist MRS1754 (MRS, 0.5 μM) alone or together with DPCPX and SCH58261 nearly completely blocked the 2-PAA-induced increase in the dye diffusion distance. *D*, the A_{2A} adenosine receptor subtype-specific agonist CGS21680 did not change the dye diffusion distance. *E*, transfection of the hCMEC/D3 cells with two different anti-A_{2B} adenosine receptor siRNAs (A_{2B} siRNA) significantly decreased the mRNA amount of the A_{2B} adenosine receptor after 48 h compared to transfection with negative control (neg.) siRNA. Cells that were not treated with

transfection reagent (-transf.) served as control. *F*, the transfection with both anti-A_{2B} adenosine receptor siRNAs (A_{2B} siRNA) attenuated the increase in the dye diffusion distance after 2-PAA (20 μM) application compared to cells transfected with negative control (neg.) siRNA. The result of cells that were not treated with transfection reagent (-transf.) is shown as control. The relative dye diffusion distances were normalized to vehicle-treated cells transfected with negative control siRNA. All results were analysed using Student's *t* test. *Significant differences to the vehicle control: *$P < 0.05$, **$P < 0.01$, ***$P < 0.001$; #significant differences to 2-PAA: #$P < 0.05$, ##$P < 0.01$, ###$P < 0.001$.

2-PAA-related enhancement of gap junction coupling. Transfection of the hCMEC/D3 cells with siRNA specific for A_{2B} adenosine receptor mRNA led to significant decreases in A_{2B} adenosine receptor mRNA amounts of 29% and 27% for siRNA1 and siRNA2, respectively, compared to cells transfected with negative control siRNA after 48 h (Fig. 4*E*; Student's paired *t* test compared to negative control siRNA-transfected cells: $P = 5.7 \times 10^{-7}$ for siRNA1 and $P = 1.8 \times 10^{-7}$ for siRNA2, $n = 8$). Scrape loading/dye transfer experiments showed that 2-PAA (20 μM, 1 h) enhanced the dye diffusion distance in cells transfected with negative control siRNA (Fig. 4*F*; relative dye diffusion distance of 115% for 2-PAA, Student's paired *t* test compared to vehicle-treated cells: $P = 2.8 \times 10^{-2}$, $n = 8$). In cells that were transfected with anti-A_{2B} adenosine receptor siRNAs the effect of 2-PAA on the dye diffusion distance was significantly reduced (Fig. 4*F*; relative dye diffusion distances of 106% and 103% for siRNA1 and siRNA2, respectively, for 2-PAA treatment compared to the respective vehicle-treated cells, Student's paired *t* test compared to vehicle-treated cells: $P = 0.20$ for siRNA1 and $P = 0.41$ for siRNA2, $n = 8$). The observed reduced increase in the dye diffusion distance induced by 2-PAA in cells transfected with negative control siRNA as compared to non-transfected cells (Fig. 4*F*) seems to reflect a general stress induced in the cells by the transfection.

As second messenger, cAMP can activate the protein kinase A (PKA; Tasken & Aandahl 2004), the exchange protein directly activated by cAMP (Epac; Banerjee & Cheng 2015), and cyclic nucleotide-gated (CNG) channels (Kaupp & Seifert 2002). We used pharmacological approaches in combination with patch-clamp and Ca^{2+} measurements to evaluate the involvement of the different cAMP-dependent pathways in the 2-PAA-induced enhancement of the gap junction coupling in the hCMEC/D3 cells. We found that the PKA inhibitors Rp-cAMPS (200 μM) and KT15720 (1 μM) did not affect the 2-PAA-related enhancement of the gap junction coupling in the cerebral microvascular endothelial cells hCMEC/D3 (Fig. 5*A*; relative dye diffusion distances of 132% for 2-PAA alone and 133% with Rp-cAMPS and 123% with KT5720, respectively, Student's paired *t* test compared to 2-PAA-treated cells: $P = 0.20$, $n = 17$ for 2-PAA with Rp-cAMPS and $P = 0.95$, $n = 9$ for 2-PAA with KT5720). Furthermore, the specific Epac activator 8-pCPT-2′-*O*-Me-cAMP (100 μM) did not induce an

increase in the gap junction coupling in the hCMEC/D3 cells with a dye diffusion distance of 98% compared to the vehicle control (Fig. 5*A*; Student's paired *t* test compared to vehicle-treated cells: $P = 0.65$, $n = 5$). We therefore hypothesized that the 2-PAA-related enhancement of the gap junction coupling in these cells was related to an activation of CNG channels. Accordingly, we found that the CNG channel inhibitor L-*cis*-diltiazem (100 μM) suppressed the 2-PAA-related enhancement of the gap junction coupling (Fig. 5*B*; relative dye diffusion distance of 102% for 2-PAA with L-*cis*-diltiazem compared to 125% for 2-PAA alone, Student's paired *t* test compared to 2-PAA-treated cells: $P = 1.8 \times 10^{-2}$, $n = 7$). We therefore analysed the expression and activation of CNG channels in hCMEC/D3 cells.

There are six different subunits known to form CNG channels, A1, A2 and A3 and the three modulatory subunits A4, B1 and B3 (Kaupp & Seifert 2002). RT-PCR experiments showed that the hCMEC/D3 cells expressed the A1, the A2 and the B1 subunits of the CNG channels (Fig. 5*C*). Western blotting confirmed the presence of the particularly cAMP-sensitive A2 subunit (Kaupp & Seifert 2002; Cheng *et al.* 2008) in the cells (Fig. 5*D*). Correspondingly, the patch-clamp technique showed that the application of 20 μM 2-PAA increased a whole-cell current registered in the cells (Fig. 5*E*; Student's paired *t* test compared to vehicle-treated cells: $P < 0.08$, $n = 9$). The increase in the current was abolished by simultaneous application of the CNG channel blocker L-*cis*-diltiazem (100 μM; Fig. 5*E*; Student's paired *t* test compared to vehicle-treated cells: $P > 0.25$, $n = 15$).

CNG channels are rather unselective channels permeable to cations. Beside Na^+ influx and K^+ efflux, the CNG channels also allow Ca^{2+} entry into the cells. Accordingly, Ca^{2+} imaging experiments with Fura-2 showed an increased Ca^{2+} signal in more cells treated with 2-PAA (61%) compared to cells treated with the vehicle (30%; Fig. 6*A*; Student's paired *t* test compared to vehicle-treated cells: $P = 1.7 \times 10^{-2}$, $n = 5$). The increase in the Ca^{2+} signal was slow and rapid transient Ca^{2+} spikes were rarely observed, suggesting that the fractional Ca^{2+} current was reduced, as the CNG channels are permeable to both Ca^{2+} and Na^+ (Kaupp & Seifert 2002). We therefore replaced the external Na^+ by 5′-*N*-ethylcarboxamidoadenosine (NMDG) and repeated the Ca^{2+} imaging. In the absence of external Na^+, 2-PAA more readily induced rapid transient

Ca^{2+} spikes (Fig. 6*B*). To analyse whether Ca^{2+} was necessary for the 2-PAA-related enhancement of the gap junction coupling, 2-PAA (20 μM) was applied after preloading the cells with BAPTA (10 μM) as chelator of intracellular Ca^{2+} or in the absence of extracellular Ca^{2+}. Under these conditions, the 2-PAA-related enhancement of the dye diffusion distance was strongly reduced (Fig. 6*C*; relative dye diffusion distances of 109% for 2-PAA with BAPTA and 113% for 2-PAA without extracellular Ca^{2+} compared to 126% for 2-PAA alone, Student's paired *t* test compared to 2-PAA-treated cells: $P = 2.1 \times 10^{-3}$, $n = 12$ for 2-PAA with BAPTA and Student's paired *t*

test compared to 2-PAA-treated cells with extracellular Ca^{2+}: $P = 5.1 \times 10^{-3}$, $n = 17$ for 2-PAA in absence of extracellular Ca^{2+}).

Collectively, the data presented in this report identify CNG channels as a previously unrecognized physiological link between adenosine receptors and gap junction coupling in human cerebral microvascular endothelial cells. Specifically, we show that following activation of predominantly A_{2B} adenosine receptors in hCMEC/D3 cells, the second messenger cAMP leads to the opening of CNG channels, allowing a Ca^{2+} influx that evokes the increase in gap junction coupling.
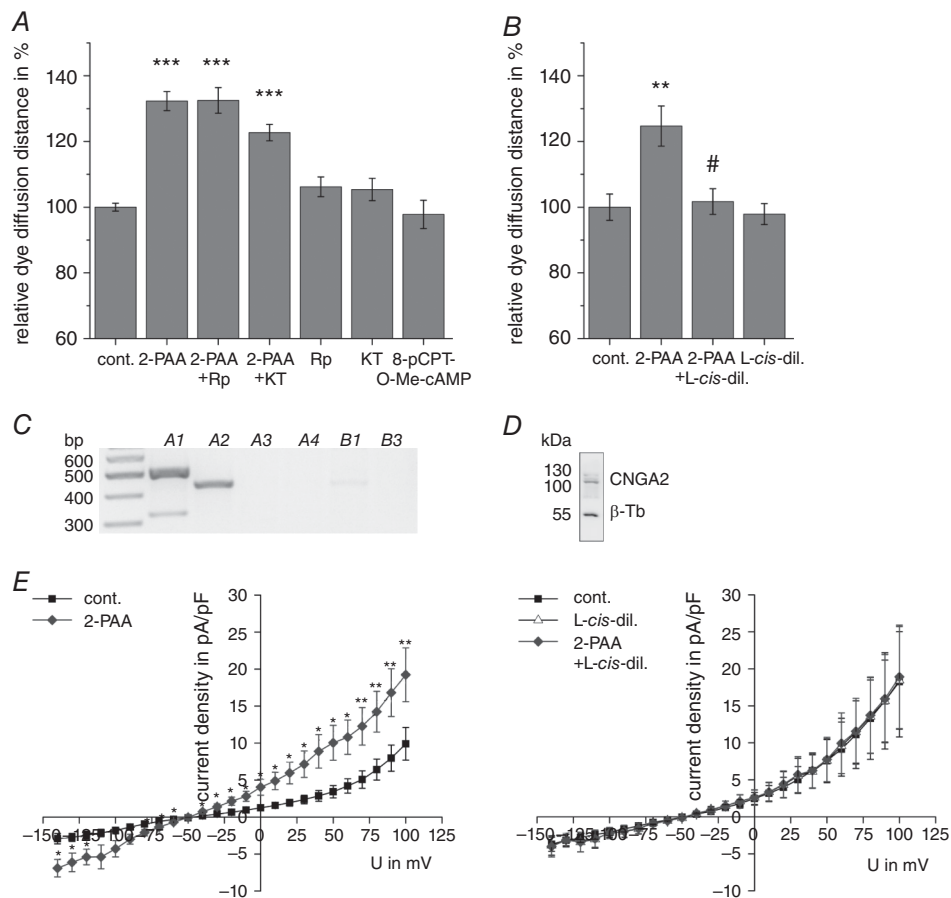
Figure 5. The signalling mechanism induced by 2-PAA
A, the increase in the dye diffusion distance induced by 2-PAA (20 μM, 1 h) was not blocked by the protein kinase A inhibitors Rp-cAMPS (Rp, 200 μM) and KT5720 (KT, 1 μM). Additionally, the activator of the exchange protein directly activated by cAMP, 8-pCPT-*O*-Me-cAMP (100 μM) did not affect the dye diffusion distance. *B*, the cyclic nucleotide-gated (CNG) channel inhibitor L-*cis*-diltiazem (L-*cis*-dil., 100 μM) could prevent the increase in the dye diffusion distance induced by 2-PAA (20 μM, 1 h) relative to the vehicle control (cont., 0.3% ethanol) in scrape loading/dye transfer assays. *C*, RT-PCR showed that the CNG channel subunits A1, A2 and B1 were expressed in hCMEC/D3 cells. *D*, furthermore, the cAMP-sensitive subunit CNGA2 was confirmed to be expressed at protein level with β-tubulin (β-Tb) serving as loading control. *E*, in whole-cell patch-clamp experiments, 2-PAA (20 μM) increased the current measured in hCMEC/D3 cells. This increased current was completely abolished by simultaneous application of the CNG channel blocker L-*cis*-diltiazem (L-*cis*-dil., 100 μM) with 2-PAA. All results were analysed using Student's *t* test. *Significant differences to the vehicle control: *$P < 0.05$, **$P < 0.01$, ***$P < 0.001$; #significant differences to 2-PAA: #$P < 0.05$.

Discussion

By allowing the exchange of ions and metabolites between cells, the gap junction coupling permits the formation of physiological units in tissues. A prerequisite for a regulation of these units is the physiological integration of the gap junction coupling in the general signalling pathways of the cells within a tissue. In the present report we used hCMEC/D3 cells as an accepted *in vitro* model for human BBB endothelial cells (Weksler *et al.* 2005, 2013) and found that adenosine receptor-dependent signalling regulated the gap junction coupling in these cells via activation of CNG channels (Figs 2 and 5).

In accordance with other studies on BBB endothelial cells (Nagasawa *et al.* 2006; Avila *et al.* 2011; Bock *et al.* 2012; Kaneko *et al.* 2015), RT-PCR analysis revealed that Cx37, Cx40, Cx43 and Cx45 were expressed in hCMEC/D3 cells (Fig. 1*B*). Transcripts of three other isoforms, Cx30, Cx32 and Cx36, that are known to be expressed in other cerebral cell types (Eugenin *et al.* 2012) were not found in hCMEC/D3 cells (Fig. 1*B*). Immunofluorescence staining showed that in hCMEC/D3 cells Cx40 and Cx43 formed gap junction plaques while Cx37 and Cx45 were solely stained in the intracellular space (Fig. 1*C*). The structural and physiological significance of the absence of Cx37 and Cx45 in gap junction plaques is not clear. It is possible that Cx37 and Cx45 are not inserted into the membrane of the cells. The expression of Cxs independently of gap junction channel formation has for example been proposed to modulate cell migration (Kameritsch *et al.* 2012) or act as tumour suppressors (McLachlan *et al.* 2006). Alternatively Cx37 and Cx45 could form gap junction hemichannels or gap junction channels which are not clustered like the Cx43 and Cx40 plaques and are therefore not easily recognizable with fluorescence microscopy (Nakagawa *et al.* 2011). In endothelial cells, particularly those derived from the BBB, the existence and functional role of hemichannels has been proposed (Bock *et al.* 2012; Kaneko *et al.* 2015). These hemichannels are permeable to metabolites such as ATP (Stout *et al.* 2002; Kang *et al.* 2008) and pathophysiological conditions like hypoxia or ischaemia are known to increase their open probability (Davidson *et al.* 2012; Kaneko *et al.* 2015). Furthermore, the presence of non-clustered gap junction channels containing Cx37 and Cx45 is possible as it is known that the different Cxs form gap junction channels with variable dynamics (Thomas *et al.* 2005; Stout *et al.* 2015).

Considering gap junction coupling, we found that in hCMEC/D3 cells the adenosine receptor agonist 2-PAA enhanced the gap junction coupling (Fig. 2), which achieved its maximum within 45–60 min (Fig. 2*B*). At the morphological level, the 2-PAA-induced increase in gap junction coupling was only paralleled by an increased formation of Cx43 gap junction plaques as well as increased Cx43 gap junction plaque size between adjacent cells as revealed by quantitative evaluation of confocal and STED microscopic images (Fig. 3). Although no effect of 2-PAA on the localization of Cx37, Cx45 or Cx40 was discernible (data not shown), the increased presence of Cx43 in the membrane in response to 2-PAA treatment suggests that the increase in gap junction coupling may primarily be related to an increased formation of gap junction channels between the cells. However, changes in
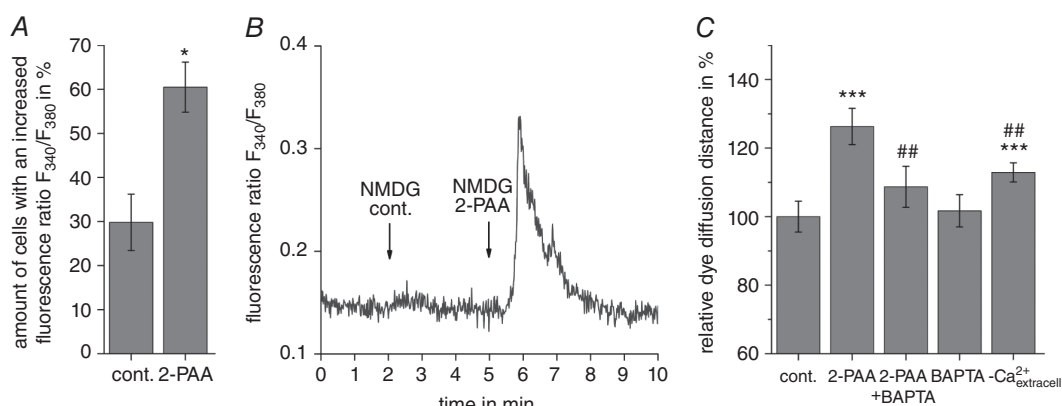
Figure 6. The 2-PAA-induced increase in gap junction coupling was Ca^{2+} dependent
A, application of 2-PAA (20 μM) increased the intracellular Ca^{2+} signal (fluorescence ratio F_{340}/F_{380}). The columns show the results obtained by counting the amount of cells with an increased $[Ca^{2+}]_i$ after treatment with the vehicle control (cont., 0.3% ethanol) or 2-PAA (20 μM) in presence of 140 mM external Na^+. *B*, a representative rapid transient Ca^{2+} signal induced by application of 2-PAA (20 μM) when external Na^+ was replaced by NMDG. *C*, the 2-PAA-induced increase in the dye diffusion distance was abolished when 2-PAA (20 μM, 1 h) was applied on cells preloaded with the Ca^{2+} chelator BAPTA (10 μM) or in absence of external Ca^{2+} (- $Ca^{2+}_{extracell.}$). All results were analysed using Student's *t* test. *Significant differences to the vehicle control: *$P < 0.05$: ***$P < 0.001$; #significant differences to 2-PAA: ##$P < 0.01$.

A. Bader and others

the biophysical properties of the gap junction channels such as an increase in single gap junction channel conductance or the open probability of the channels may be secondarily involved as well. An increase in gap junction channels can be achieved by enhanced gene expression, Cx synthesis, less connexon degradation or enhanced connexon trafficking to the membrane. The increase in gap junction coupling can also be achieved by the insertion of new connexons into the membrane or a reduced removal of the gap junctions from the membrane. The synthesis and trafficking, as well as the removal, of gap junction channels are processes which necessitate a time too long (Jordan *et al.* 1999; Falk *et al.* 2014) to explain the observed rapid 2-PAA-induced increase in gap junction coupling within 30 min (Fig. 2*B*), which is therefore more compatible with 2-PAA stimulated formation of gap junction channels in the membrane.

Regarding the kinetics of the effect of adenosine receptor stimulation on the physiological function of the BBB in animal models, an increase in the BBB permeability was visible within 15–30 min (Carman *et al.* 2011). However, while the animal model reflects systemic reactions integrating all cells in a tissue, the specific contribution of the different cell types, e.g. endothelial cells, is very difficult to estimate. Other authors have analysed how adenosine receptor stimulation affected the BBB function using isolated microvascular endothelial cells. It was found that the A_{2A} adenosine receptor-specific agonist regadenoson (lexiscan) and the non-specific adenosine receptor agonist NECA decreased the transendothelial electrical resistance (TEER) of the cells within 5–15 min of application (Gao *et al.* 2014; Kim & Bynoe 2015), which is faster than the effect of 2-PAA on the gap junction coupling described in the present report (Fig. 2*B*). The pharmacology shows that the decrease of the TEER was mainly due to the stimulation of the A_{2A} adenosine receptors (Gao *et al.* 2014; Kim & Bynoe 2015). 2-PAA, which was used in the present report, stimulates both A_{2A} and A_{2B} adenosine receptor subtypes (Bruns *et al.* 1986; Choksi *et al.* 1997; Wilson & Batra 2002). Accordingly, we found that 2-PAA increased the cellular cAMP concentration and that the adenylyl cyclase inhibitor SQ22536 suppressed the increased cAMP synthesis (Fig. 4*A*). SQ22536 also reduced the 2-PAA-related increase in gap junction coupling (Fig. 4*B*), which showed that cAMP was necessary for the 2-PAA-induced increase in gap junction coupling. It is noteworthy that SQ22536 did not completely suppress the 2-PAA-induced increase in gap junction coupling, suggesting that other mechanisms could be involved in the 2-PAA-induced enhancement of gap junction coupling in the cells. Although 2-PAA is described as an agonist for A_{2A} and A_{2B} adenosine receptors (Bruns *et al.* 1986; Choksi *et al.* 1997; Wilson & Batra 2002) and we found that 2-PAA stimulation induced cAMP synthesis, as an adenosine derivative 2-PAA might be able to bind to A_1 adenosine

receptors, which are linked to G_i or to the synthesis of cGMP (Kurtz *et al.* 1988; Eltzschig 2009; Serpa *et al.* 2014; Pinto *et al.* 2016). The following findings, however, argue against the involvement of the A_1 adenosine receptor in the action of 2-PAA on the gap junction coupling. First, we found that 2-PAA induced a cAMP increase (Fig. 4*A*), which is incompatible with activation of A_1 adenosine receptors, which, via G_i, preferentially inhibits adenylyl cyclase (Fredholm 2007; Eltzschig 2009). Secondly, the A_1 adenosine receptor antagonist DPCPX did not influence the 2-PAA-related enhancement of the gap junction coupling (Fig. 4*C*), and additionally cGMP analogues were not able to mimic the effect of 2-PAA on the gap junction coupling. Hence, an action of 2-PAA that involves binding to A_1 adenosine receptors and activation of cGMP synthesis seems very unlikely. The results therefore suggest that 2-PAA acted solely by binding to G_s coupled receptors, which activated adenylyl cyclase to synthesize cAMP. Nine different adenylyl cyclase isoforms can be expressed in cells (Seifert *et al.* 2012) and none of the widely used adenylyl cyclase inhibitors is able to inhibit all isoforms equally well (Seifert *et al.* 2012). Therefore we assume that even in the presence of SQ22536, 2-PAA could still induce cAMP synthesis to some extent, which could affect the gap junction coupling in a statistically non-significant manner as observed in this report. Regarding the A_{2A} and A_{2B} adenosine receptor subtypes which are both linked to G_s and stimulation of adenylyl cyclase, the A_{2A} adenosine receptor antagonist SCH58261 and the A_{2B} adenosine receptor antagonist MRS1754, as well as the A_{2A} adenosine receptor-specific agonist CGS21680, revealed that the 2-PAA-related increase in gap junction coupling was mainly dependent on stimulation of the A_{2B} adenosine receptor subtype and not the A_{2A} adenosine receptor subtype (Fig. 4*C* and *D*). The predominant role of the A_{2B} adenosine receptor subtype in the regulation of gap junction coupling in cerebral endothelial cells presented here is also sustained by the transient knock-down of the A_{2B} adenosine receptor subtype using siRNA. We found that when expression of the A_{2B} adenosine receptor subtype was decreased, 2-PAA could no longer significantly increase the gap junction coupling in hCMEC/D3 cells (Fig. 4*F*). It is noteworthy that neither the pharmacological inhibition nor the siRNA-dependent knock-down of the A_{2B} adenosine receptor could completely suppress the effect of 2-PAA. With siRNA we achieved a knock-down of mRNA levels of over 70% (Fig. 4*E*) and with the pharmacological inhibitors our aim was to avoid high inhibitor concentrations, which are not specific anymore and might induce unintended side-effects on the cells. We therefore assume that under our experimental conditions, a reduced activation of adenosine receptors by 2-PAA was still possible, thereby inducing an increase in gap junction coupling. This increase was, however, not statistically significant. Moreover, an involvement

of the A_{2A} adenosine receptor subtype to a low extent cannot completely be ruled out. However, our results obtained using hCMEC/D3 cells as model suggest that the regulation of gap junction coupling in cerebral microvascular cells is mainly related to A_{2B} adenosine receptor subtypes.

Activation of the A_{2B} adenosine receptor subtype and subsequent upregulation of its expression in endothelial cells has been proposed as a mechanism for preventing vascular leakage (Eltzschig *et al.* 2003; Eckle *et al.* 2008) and inflammatory signalling (Yang *et al.* 2006; Blackburn *et al.* 2009). Additionally, it was found that activation of the A_{2B} adenosine receptor subtype stimulated the expression of vascular endothelial growth factor and angiogenesis in microvascular endothelial cells (Feoktistov *et al.* 2002; Du *et al.* 2015). Our findings identify gap junction coupling as another target of the A_{2B} adenosine receptor-related signalling in endothelial cells of the microvascular system. Whether and how gap junction coupling is integrated in, for example, the anti-inflammatory or angiogenic properties of A_{2B} adenosine receptor stimulation is an exciting topic for future research; to this end the present report clearly shows the physiological link between A_{2B} adenosine receptor activation and cAMP-dependent regulation of gap junction coupling.

The enhancement of gap junction coupling in different cells by cAMP- and PKA-dependent pathways is an accepted mechanism (Mehta *et al.* 1992; Atkinson *et al.* 1995; Paulson *et al.* 2000; Lampe & Lau 2004). A general increase in the cAMP concentration by application of forskolin or 8-Br-cAMP also increased the gap junction coupling in hCMEC/D3 cells (Fig. 4*B*). Recently, we showed that the adenosine transporter inhibitor dipyridamole induced an enhancement of gap junction coupling in aortic endothelial cells as well as in aortic smooth muscle cells through activation of adenosine receptors, an effect that was suppressed in presence of PKA inhibitors (Begandt *et al.* 2010, 2013*a,b*). In the present report the PKA inhibitors Rp-cAMPS and KT5720 were not able to suppress the 2-PAA-related enhancement of gap junction coupling in hCMEC/D3 cells (Fig. 5*A*). Additionally, an activator of Epac, another effector of cAMP, also failed to affect the gap junction coupling (Fig. 5*A*), suggesting that another cAMP-dependent mechanism is activated in these BBB endothelial cells.

CNG channels constitute a third target for cAMP. RT-PCR experiments showed that the CNG channel subunits A1, A2 and B1 were expressed in hCMEC/D3 cells (Fig. 5*C*). Western blotting confirmed that the especially cAMP-sensitive A2 subunit of CNG channels (Kaupp & Seifert 2002; Cheng *et al.* 2008) is expressed in hCMEC/D3 cells (Fig. 5*D*). Electrophysiological patch-clamp experiments showed that 2-PAA increased the current in the cells (Fig. 5*E*) without significantly affecting the membrane potential. However,

the CNG channel inhibitor L-*cis*-diltiazem antagonized the 2-PAA-related current changes (Fig. 5*E*), suggesting that 2-PAA induced the opening of CNG channels. It could be expected that BBB endothelial cells might express CNG channels since expression and a physiological role of CNG channels in various endothelial systems has been shown previously (Zhang *et al.* 2002; Cheng *et al.* 2003; Cheng *et al.* 2008). Moreover, it was shown that an adenosine receptor-related increase in cAMP enhanced the membrane current and intracellular Ca^{2+} concentration in endothelial cells and that these effects were both blocked by CNG channel inhibitors (Cheng *et al.* 2008). Interestingly, in those experiments it was also the A_{2B} adenosine receptor subtype that led to the CNG channel activation (Cheng *et al.* 2008), which is in accordance with our results.

With respect to gap junction coupling of hCMEC/D3 cells, L-*cis*-diltiazem suppressed the 2-PAA-related enhancement of gap junction coupling as shown by scrape loading/dye transfer experiments (Fig. 5*B*). This indicates that activation of CNG channels was required for the 2-PAA-induced enhancement of gap junction coupling. Interestingly, L-*cis*-diltiazem also attenuated the increase in gap junction coupling induced by the adenylyl cyclase activator forskolin (data not shown), indicating that cAMP-dependent activation of CNG channels was crucial for the cAMP-mediated effect on the gap junction coupling. As cation permeable channels, the CNG channels can affect the membrane potential of the cells and allow a Ca^{2+} influx into the cells (Kaupp & Seifert 2002). Since we did not observe a significant change in the membrane potential of the cells when we applied 2-PAA in the whole-cell patch-clamp experiments (Fig. 5*E*), we concluded that the 2-PAA-related increase in gap junction coupling necessitated a Ca^{2+} influx. The finding that the 2-PAA-related increase in gap junction coupling was reduced if 2-PAA was applied to cells preloaded with the internal Ca^{2+} chelator BAPTA or if 2-PAA was applied in the absence of external Ca^{2+} (Fig. 6*C*) support this conclusion. Preloading the cells with BAPTA also attenuated the forskolin-induced increase in gap junction coupling (data not shown), indicating the importance of Ca^{2+} in the action mechanism of cAMP on the gap junction coupling. Additionally, Ca^{2+} imaging showed that 2-PAA led to a slow and moderate increase in the intracellular Ca^{2+} signal (Fig. 6*A*). A rapid and transient increase in Ca^{2+} could, however, be observed if 2-PAA was applied in the absence of external Na^+ (Fig. 6*B*). These results suggest that 2-PAA induced an activation of CNG channels but that under normal extracellular Na^+ concentrations the fractional Ca^{2+} current is reduced. We therefore assume that under normal conditions, the intracellular Ca^{2+} increase was mostly related to a locally restricted Ca^{2+} increase in the vicinity of the membrane rather than to a general influx of Ca^{2+} into the cytoplasmic

A. Bader and others

space. This assumption is supported by comparison of the results obtained when 2-PAA was applied to cells pre-loaded with the Ca^{2+} chelators EGTA or BAPTA. BAPTA antagonized the 2-PAA-induced increase in gap junction coupling, but EGTA did not (data not shown). This might be because BAPTA diffuses readily, coming into close proximity with the cell membrane (Rousset *et al.* 2004), and is therefore able to efficiently chelate Ca^{2+} that is located right underneath the cell membrane, while EGTA, due to its limited diffusion, mainly chelates the Ca^{2+} in the core of the cells and does not reach the membrane region (Rousset *et al.* 2004). Furthermore, BAPTA can effectively chelate Ca^{2+} derived from nano- and microdomains due to its faster Ca^{2+} binding rate constant (Parekh 2008; Fakler & Adelman 2008). Overall, the results suggest that 2-PAA by binding to A_{2B} adenosine receptors activates adenylyl cyclase which synthesises cAMP. cAMP in turn induces a locally restricted Ca^{2+} influx through CNG channels. This Ca^{2+} stimulates insertion of connexons in the membrane and leads to an increase in gap junction plaques between the cells, resulting in an increase in gap junction coupling.

To our knowledge, a physiological link between the A_{2B} adenosine receptor, CNG channels and gap junction coupling as shown in this report (Fig. 7) has not been described before. The detailed mechanism by which the reinforcement of gap junction plaques and gap junction coupling in hCMEC/D3 cells is achieved by a Ca^{2+} influx through CNG channel activation is currently a matter of speculation. Protein kinase C (PKC) or Ca^{2+}/calmodulin-dependent protein kinase II (CaMKII)-dependent pathways do not seem to play a role, since the PKC activator TPA did not enhance gap junction coupling in the hCMEC/D3 cells. Moreover, inhibitors of PKC (bisindolylmaleimide II) and of CaMKII (KN93) did not significantly affect the 2-PAA-related enhancement of gap junction coupling (data not shown). Considering the relatively fast increase in gap junction coupling and the observation of a parallel increased formation of gap junction plaques, we propose that the increased Ca^{2+} induced formation of new gap junction channels in the membrane in a secretion process of connexon containing vesicles.
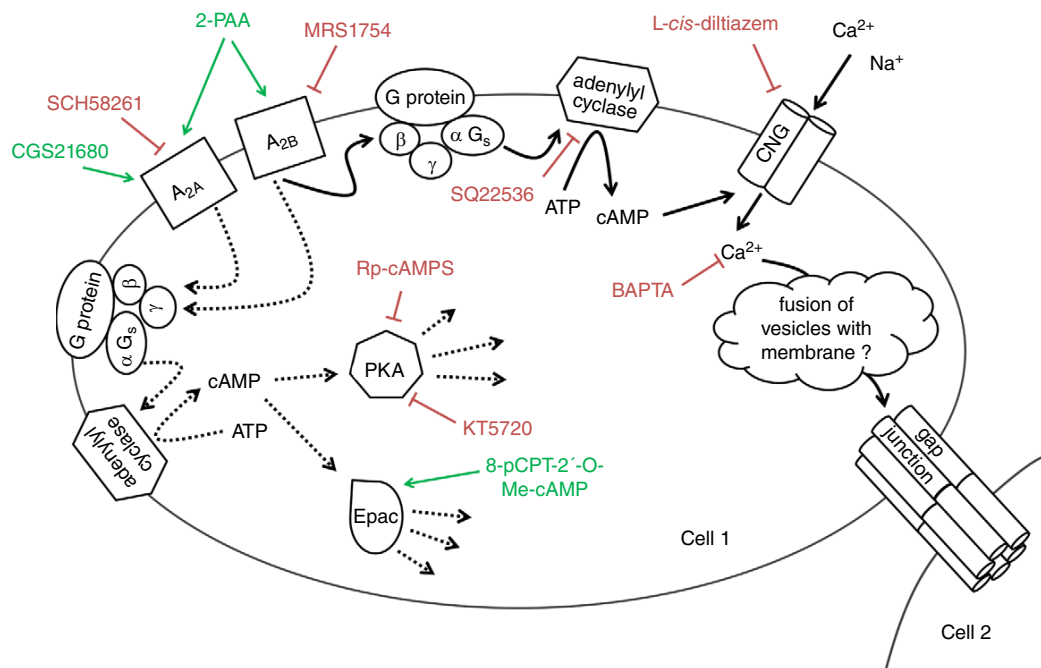
Figure 7. Proposed mechanism of action of 2-PAA to increase the gap junction coupling in hCMEC/D3 cells (continuous arrows)
The stimulation of A_{2B} adenosine receptors induces synthesis of cAMP which leads to a Ca^{2+} influx by opening CNG channels. We hypothesise that Ca^{2+} in turn induces the increase in gap junction plaques resulting in an enhancement of the gap junction coupling. The increase in the gap junction plaques is related by an as-yet-unidentified mechanism which is probably a fusion of connexon-containing vesicles with the cell membrane. The green arrows indicate activation, the red bars indicate inhibition. The dotted arrows indicate other possible adenosine receptor-dependent signalling mechanisms which were found not to be involved in the regulation of gap junction coupling in the cerebral microvascular endothelial cells in the present report. [Colour figure can be viewed at wileyonlinelibrary.com]

References

Atkinson MM, Lampe PD, Lin HH, Kollander R, Li XR & Kiang DT (1995). Cyclic AMP modifies the cellular distribution of connexin43 and induces a persistent increase in the junctional permeability of mouse mammary tumor cells. *J Cell Sci* **108**, 3079–3090.

Avila MA, Sell SL, Hawkins BE, Hellmich HL, Boone DR, Crookshanks JM, Prough DS & DeWitt DS (2011). Cerebrovascular connexin expression: effects of traumatic brain injury. *J Neurotrauma* **28**, 1803–1811.

Banerjee U & Cheng X (2015). Exchange protein directly activated by cAMP encoded by the mammalian rapgef3 gene: structure, function and therapeutics. *Gene* **570**, 157–167.

Begandt D, Bader A, Dreyer L, Eisert N, Reeck T & Ngezahayo A (2013*a*). Biphasic increase of gap junction coupling induced by dipyridamole in the rat aortic A-10 vascular smooth muscle cell line. *J Cell Commun Signal* **7**, 151–160.

Begandt D, Bader A, Gerhard L, Lindner J, Dreyer L, Schlingmann B & Ngezahayo A (2013*b*). Dipyridamole-related enhancement of gap junction coupling in the GM-7373 aortic endothelial cells correlates with an increase in the amount of connexin 43 mRNA and protein as well as gap junction plaques. *J Bioenerg Biomembr* **45**, 409–419.

Begandt D, Bintig W, Oberheide K, Schlie S & Ngezahayo A (2010). Dipyridamole increases gap junction coupling in bovine GM-7373 aortic endothelial cells by a cAMP-protein kinase A dependent pathway. *J Bioenerg Biomembr* **42**, 79–84.

Beyer EC & Berthoud VM (2009). The family of connexin genes. In *Connexins: A Guide*, eds Harris AL & Locke D, pp. 3–26. Springer, New York.

Bintig W, Baumgart J, Walter WJ, Heisterkamp A, Lubatschowski H & Ngezahayo A (2009). Purinergic signalling in rat GFSHR-17 granulosa cells: an in vitro model of granulosa cells in maturing follicles. *J Bioenerg Biomembr* **41**, 85–94.

Blackburn MR, Vance CO, Morschl E & Wilson CN (2009). Adenosine receptors and inflammation. *Handb Exp Pharmacol* **193**, 215–269.

Bock M de, Culot M, Wang N, da CA, Decrock E, Bol M, Bultynck G, Cecchelli R & Leybaert L (2012). Low extracellular Ca^{2+} conditions induce an increase in brain endothelial permeability that involves intercellular Ca^{2+} waves. *Brain Res* **1487**, 78–87.

Bodin P, Bailey D & Burnstock G (1991). Increased flow-induced ATP release from isolated vascular endothelial cells but not smooth muscle cells. *Br J Pharmacol* **103**, 1203–1205.

Bodin P & Burnstock G (2001). Evidence that release of adenosine triphosphate from endothelial cells during increased shear stress is vesicular. *J Cardiovasc Pharmacol* **38**, 900–908.

Bruns RF, Lu GH & Pugsley TA (1986). Characterization of the A_2 adenosine receptor labeled by [^{3}H]NECA in rat striatal membranes. *Mol Pharmacol* **29**, 331–346.

Bynoe MS, Viret C, Yan A & Kim DG (2015). Adenosine receptor signaling: a key to opening the blood–brain door. *Fluids Barriers CNS* **12**, 20.

Carman AJ, Mills JH, Krenz A, Kim DG & Bynoe MS (2011). Adenosine receptor signaling modulates permeability of the blood–brain barrier. *J Neurosci* **31**, 13272–13280.

Cheng CC, Yang YL, Liao KH & Lai TW (2016). Adenosine receptor agonist NECA increases cerebral extravasation of fluorescein and low molecular weight dextran independent of blood–brain barrier modulation. *Sci Rep* **6**, 23882.

Cheng KT, Chan FL, Huang Y, Chan WY & Yao X (2003). Expression of olfactory-type cyclic nucleotide-gated channel (CNGA2) in vascular tissues. *Histochem Cell Biol* **120**, 475–481.

Cheng KT, Leung YK, Shen B, Kwok YC, Wong CO, Kwan HY, Man YB, Ma X, Huang Y & Yao X (2008). CNGA2 channels mediate adenosine-induced Ca^{2+} influx in vascular endothelial cells. *Arterioscler Thromb Vasc Biol* **28**, 913–918.

Choksi NY, Hussain A & Booth RG (1997). 2-Phenylaminoadenosine stimulates dopamine synthesis in rat forebrain in vitro and in vivo via adenosine A_2 receptors. *Brain Res* **27**, 151–155.

Davidson JO, Green CR, Nicholson LF, O'Carroll SJ, Fraser M, Bennet L & Gunn AJ (2012). Connexin hemichannel blockade improves outcomes in a model of fetal ischemia. *Ann Neurol* **71**, 121–132.

Du X, Ou X, Song T, Zhang W, Cong F, Zhang S & Xiong Y (2015). Adenosine A_{2B} receptor stimulates angiogenesis by inducing VEGF and eNOS in human microvascular endothelial cells. *Exp Biol Med (Maywood)* **240**, 1472–1479.

Eckle T, Faigle M, Grenz A, Laucher S, Thompson LF & Eltzschig HK (2008). A_{2B} adenosine receptor dampens hypoxia-induced vascular leak. *Blood* **111**, 2024–2035.

Eltzschig HK (2009). Adenosine: an old drug newly discovered. *Anesthesiology* **111**, 904–915.

Eltzschig HK, Ibla JC, Furuta GT, Leonard MO, Jacobson KA, Enjyoji K, Robson SC & Colgan SP (2003). Coordinated adenine nucleotide phosphohydrolysis and nucleoside signaling in posthypoxic endothelium: role of ectonucleotidases and adenosine A_{2B} receptors. *J Exp Med* **198**, 783–796.

Eugenin EA, Basilio D, Sáez JC, Orellana JA, Raine CS, Bukauskas F, Bennett MV & Berman JW (2012). The role of gap junction channels during physiologic and pathologic conditions of the human central nervous system. *J Neuroimmune Pharmacol* **7**, 499–518.

Fakler B & Adelman JP (2008). Control of K_{Ca} channels by calcium nano/microdomains. *Neuron* **59**, 873–881.

Falk MM, Kells RM & Berthoud VM (2014). Degradation of connexins and gap junctions. *FEBS Lett* **588**, 1221–1229.

Feoktistov I, Goldstein AE, Ryzhov S, Zeng D, Belardinelli L, Voyno-Yasenetskaya T & Biaggioni I (2002). Differential expression of adenosine receptors in human endothelial cells: role of A_{2B} receptors in angiogenic factor regulation. *Circ Res* **90**, 531–538.

Figueroa XF & Duling BR (2009). Gap junctions in the control of vascular function. *Antioxid Redox Signal* **11**, 251–266.

Fredholm BB (2007). Adenosine, an endogenous distress signal, modulates tissue damage and repair. *Cell Death Differ* **14**, 1315–1323.

A. Bader and others *J Physiol* 595.8

Gao X, Qian J, Zheng S, Changyi Y, Zhang J, Ju S, Zhu J & Li C (2014). Overcoming the blood–brain barrier for delivering drugs into the brain by using adenosine receptor nanoagonist. *ACS Nano* **8**, 3678–3689.

Haefliger JA, Nicod P & Meda P (2004). Contribution of connexins to the function of the vascular wall. *Cardiovasc Res* **62**, 345–356.

Johnstone S, Isakson B & Locke D (2009). Biological and biophysical properties of vascular connexin channels. *Int Rev Cell Mol Biol* **278**, 69–118.

Jordan K, Solan JL, Dominguez M, Sia M, Hand A, Lampe PD & Laird DW (1999). Trafficking, assembly, and function of a connexin43-green fluorescent protein chimera in live mammalian cells. *Mol Biol Cell* **10**, 2033–2050.

Kameritsch P, Pogoda K & Pohl U (2012). Channel-independent influence of connexin 43 on cell migration. *Biochim Biophys Acta* **1818**, 1993–2001.

Kaneko Y, Tachikawa M, Akaogi R, Fujimoto K, Ishibashi M, Uchida Y, Couraud PO, Ohtsuki S, Hosoya K & Terasaki T (2015). Contribution of pannexin 1 and connexin 43 hemichannels to extracellular calcium-dependent transport dynamics in human blood–brain barrier endothelial cells. *J Pharmacol Exp Ther* **353**, 192–200.

Kang J, Kang N, Lovatt D, Torres A, Zhao Z, Lin J & Nedergaard M (2008). Connexin 43 hemichannels are permeable to ATP. *J Neurosci* **28**, 4702–4711.

Kaupp UB & Seifert R (2002). Cyclic nucleotide-gated ion channels. *Physiol Rev* **82**, 769–824.

Kim DG & Bynoe MS (2015). A_{2A} adenosine receptor regulates the human blood–brain barrier permeability. *Mol Neurobiol* **52**, 664–678.

Kurtz A, Della Bruna R, Pfeilschifter J & Bauer C (1988). Role of cGMP as second messenger of adenosine in the inhibition of renin release. *Kidney Int* **33**, 798–803.

Lampe PD & Lau AF (2004). The effects of connexin phosphorylation on gap junctional communication. *Int J Biochem Cell Biol* **36**, 1171–1186.

McLachlan E, Shao Q, Wang HL, Langlois S & Laird DW (2006). Connexins act as tumor suppressors in three-dimensional mammary cell organoids by regulating differentiation and angiogenesis. *Cancer Res* **66**, 9886–9894.

Mehta PP, Yamamoto M & Rose B (1992). Transcription of the gene for the gap junctional protein connexin43 and expression of functional cell-to-cell channels are regulated by cAMP. *Mol Biol Cell* **3**, 839–850.

Melani A, Pugliese AM & Pedata F (2014). Adenosine receptors in cerebral ischemia. *Int Rev Neurobiol* **119**, 309–348.

Mills JH, Alabanza L, Weksler BB, Couraud P-O, Romero IA & Bynoe MS (2011). Human brain endothelial cells are responsive to adenosine receptor activation. *Purinergic Signal* **7**, 265–273.

Nagasawa K, Chiba H, Fujita H, Kojima T, Saito T, Endo T & Sawada N (2006). Possible involvement of gap junctions in the barrier function of tight junctions of brain and lung endothelial cells. *J Cell Physiol* **208**, 123–132.

Nakagawa S, Gong XQ, Maeda S, Dong Y, Misumi Y, Tsukihara T & Bai D (2011). Asparagine 175 of connexin32 is a critical residue for docking and forming functional heterotypic gap junction channels with connexin26. *J Biol Chem* **286**, 19672–19681.

Nguyen MD, Lee ST, Ross AE, Ryals M, Choudhry VI & Venton BJ (2014). Characterization of spontaneous, transient adenosine release in the caudate-putamen and prefrontal cortex. *PLoS One* **9**, e87165.

Nguyen MD & Venton BJ (2015). Fast-scan cyclic voltammetry for the characterization of rapid adenosine release. *Comput Struct Biotechnol J* **13**, 47–54.

Parekh AB (2008). Ca^{2+} microdomains near plasma membrane Ca^{2+} channels: impact on cell function. *J Physiol* **586**, 3043–3054.

Paulson AF, Lampe PD, Meyer RA, TenBroek E, Atkinson MM, Walseth TF & Johnson RG (2000). Cyclic AMP and LDL trigger a rapid enhancement in gap junction assembly through a stimulation of connexin trafficking. *J Cell Sci* **113**, 3037–3049.

Pinheiro JC & Bates DM (2000). Mixed-effects models in S and S-PLUS. In *Statistics and Computing*, eds Chambers J, Eddy W, Härdle W, Sheather S & Tierney L. Springer, New York.

Pinto I, Serpa A, Sebastião AM & Cascalheira JF (2016). The role of cGMP on adenosine A1 receptor-mediated inhibition of synaptic transmission at the hippocampus. *Front Pharmacol* **7**, 103.

Rousset M, Cens T, Vanmau N & Charnet P (2004). Ca^{2+}-dependent interaction of BAPTA with phospholipids. *FEBS Lett* **576**, 41–45.

Sands WA & Palmer TM (2005). Adenosine receptors and the control of endothelial cell function in inflammatory disease. *Immunol Lett* **101**, 1–11.

Schaddelee MP, Voorwinden HL, van Tilburg EW, Pateman TJ, Ijzerman AP, Danhof M & Boer AG de (2003). Functional role of adenosine receptor subtypes in the regulation of blood–brain barrier permeability: possible implications for the design of synthetic adenosine derivatives. *Eur J Pharm Sci* **19**, 13–22.

Seifert R, Lushington GH, Mou TC, Gille A & Sprang SR (2012). Inhibitors of membranous adenylyl cyclases. *Trends Pharmacol Sci* **33**, 64–78.

Serpa A, Sebastião AM & Cascalheira JF (2014). Modulation of cGMP accumulation by adenosine A1 receptors at the hippocampus: influence of cGMP levels and gender. *Eur J Pharmacol* **5**, 83–90.

Söhl G & Willecke K (2004). Gap junctions and the connexin protein family. *Cardiovasc Res* **62**, 228–232.

Stout CE, Costantin JL, Naus CC & Charles AC (2002). Intercellular calcium signaling in astrocytes via ATP release through connexin hemichannels. *J Biol Chem* **277**, 10482–10488.

Stout RF Jr, Snapp EL & Spray DC (2015). Connexin type and fluorescent protein fusion tag determine structural stability of gap junction plaques. *J Biol Chem* **290**, 23497–23514.

Tasken K & Aandahl EM (2004). Localized effects of cAMP mediated by distinct routes of protein kinase A. *Physiol Rev* **84**, 137–167.

Thomas T, Jordan K, Simek J, Shao Q, Jedeszko C, Walton P & Laird DW (2005). Mechanisms of Cx43 and Cx26 transport to the plasma membrane and gap junction regeneration. *J Cell Sci* **118**, 4451–4462.

Urban NT, Willig KI, Hell SW & Nagerl UV (2011). STED nanoscopy of actin dynamics in synapses deep inside living brain slices. *Biophys J* **101**, 1277–1284.

Weksler B, Romero IA & Couraud PO (2013). The hCMEC/D3 cell line as a model of the human blood brain barrier. *Fluids Barriers CNS* **10**, 16.

Weksler BB, Subileau EA, Perrière N, Charneau P, Holloway K, Leveque M, Tricoire-Leignel H, Nicotra A, Bourdoulous S, Turowski P, Male DK, Roux F, Greenwood J, Romero IA & Couraud PO (2005). Blood–brain barrier-specific properties of a human adult brain endothelial cell line. *FASEB J* **19**, 1872–1874.

Wilson CN & Batra VK (2002). Lipopolysaccharide binds to and activates A_1 adenosine receptors on human pulmonary artery endothelial cells. *J Endotoxin Res* **8**, 263–271.

Yang D, Zhang Y, Nguyen HG, Koupenova M, Chauhan AK, Makitalo M, Jones MR, St HC, Seldin DC, Toselli P, Lamperti E, Schreiber BM, Gavras H, Wagner DD & Ravid K (2006). The A_{2B} adenosine receptor protects against inflammation and excessive vascular adhesion. *J Clin Invest* **116**, 1913–1923.

Zhang J, Xia SL, Block ER & Patel JM (2002). NO upregulation of a cyclic nucleotide-gated channel contributes to calcium elevation in endothelial cells. *Am J Physiol Cell Physiol* **283**, C1080–C1089.

Additional information

Competing interests

The authors declare no conflict of interests.

Author contributions

Experiments were performed in the laboratory of A.N. A.B., W.B., D.B. and A.N. contributed to the conception and design of the work as well as writing and revising the manuscript. A.B., W.B., A.K., I.G.S., C.G., F.S. and A.N. contributed to the acquisition, analysis, or interpretation of data for the work. B.W., I.R. and P.O.C. provided the hCMEC/D3 cells and revised the work critically. S.W.H. provided the STED microscopy and a secondary antibody and also revised the work critically. All authors have approved the final version of the manuscript and agree to be accountable for all aspects of the work. All persons designated as authors qualify for authorship, and all those who qualify for authorship are listed.

3 Gold nanoparticle-mediated laser perforation is a new method for gap junction coupling analysis in a semi-automatic high-throughput approach

Contribution: I designed the experiments together with D. B. and A. N., performed part of the experiments, analysed part of the data, prepared some of the figures and wrote the manuscript together with D. B. and A. N.

CrossMark

Gold nanoparticle-mediated (GNOME) laser perforation: a new method for a high-throughput analysis of gap junction intercellular coupling

Daniela Begandt[1] · **Almke Bader**[1] · **Georgios C. Antonopoulos**[2] · **Markus Schomaker**[2] ·
Stefan Kalies[2] · **Heiko Meyer**[2,3] · **Tammo Ripken**[2] · **Anaclet Ngezahayo**[1,4]

Abstract The present report evaluates the advantages of using the gold nanoparticle-mediated laser perforation (GNOME LP) technique as a computer-controlled cell optoperforation to introduce Lucifer yellow (LY) into cells in order to analyze the gap junction coupling in cell monolayers. To permeabilize GM-7373 endothelial cells grown in a 24 multiwell plate with GNOME LP, a laser beam of 88 μm in diameter was applied in the presence of gold nanoparticles and LY. After 10 min to allow dye uptake and diffusion through gap junctions, we observed a LY-positive cell band of 179 ± 8 μm width. The presence of the gap junction channel blocker carbenoxolone during the optoperforation reduced the LY-positive band to 95 ± 6 μm. Additionally, a forskolin-related enhancement of gap junction coupling, recently found using the scrape loading technique, was also observed using GNOME LP. Further, an automatic cell imaging and a subsequent semi-automatic quantification of the images using a java-based ImageJ-plugin were performed in a high-throughput sequence. Moreover, the GNOME LP was used on cells such as RBE4 rat brain endothelial cells, which cannot be mechanically scraped as well as on three-dimensionally cultivated cells, opening the possibility to implement the GNOME LP technique for analysis of gap junction coupling in tissues. We conclude that the GNOME LP technique allows a high-throughput automated analysis of gap junction coupling in cells. Moreover this non-invasive technique could be used on monolayers that do not support mechanical scraping as well as on cells in tissue allowing an in vivo/ex vivo analysis of gap junction coupling.

Keywords Scrape loading · Dye transfer · Gap junction · Gold nanoparticle-mediated laser perforation · GNOME · In vivo · Vascular · Endothelial cells

Introduction

Gap junctions are intercellular channels that directly connect the cytoplasm of neighboring cells. They enable the exchange of small molecules (<2 kDa), e. g. metabolites or second messengers. Therefore, gap junction-dependent cell-cell coupling is very important for the communication and coordination of cells in a multicellular tissue (Nielsen et al. 2012; Goodenough and Paul 2009; Harris 2007). Non-functional gap junction channels as a result of specific gene mutations or physiological dysregulation can lead to pre- or postnatal death, as well as severe diseases such as deafness or cataracts (Kelsell et al. 2001; Zoidl and Dermietzel 2010; Figueroa and Duling 2009; Willecke et al. 2002), which demonstrate the importance of gap junctions for tissue homeostasis (Nielsen et al. 2012; Goodenough and Paul 2009).

Intercellular gap junction coupling can be analyzed using the transfer of hydrophilic gap junction permeable dyes such as Lucifer yellow (LY) (Abbaci et al. 2008; el-Fouly et al. 1987). The dye is introduced into a single cell or a limited

Daniela Begandt and Almke Bader contributed equally to this publication.

✉ Anaclet Ngezahayo
ngezahayo@biophysik.uni-hannover.de

[1] Institute of Biophysics, Leibniz University Hannover, Herrenhäuser Str. 2, D-30419 Hannover, Germany

[2] Biomedical Optics Department, Laser Zentrum Hannover e. V., Hannover, Germany

[3] Department of Cardiothoracic, Transplantation and Vascular Surgery, Hannover Medical School, Hannover, Germany

[4] Center for Systems Neuroscience Hannover, University of Veterinary Medicine Hannover Foundation, Hannover, Germany

number of cells and the subsequent diffusion of the dye through gap junction channels into neighboring cells is evaluated. Dye transfer experiments primarily differ in the method of dye introduction into the cells. The introduction of dye into single cells through microinjection capillaries is an option, which necessitates a micro injector and technical skills that require extensive training (Abbaci et al. 2008). Additionally, the repetitive injection of single cells to achieve a statistically relevant population is a time consuming process. Therefore, the technique is often reduced to proof-of-concept experiments rather than experiments for the quantitative evaluation of gap junction coupling. In contrast, cells grown to a monolayer can be examined by introducing the dye using the scrape loading/dye transfer (SL/DT) technique (Abbaci et al. 2008; el-Fouly et al. 1987). For this method, cells have to be grown to confluence on a hard and even surface such as glass cover slips. In presence of a dye such as LY, the cell monolayer is mechanically scraped with a sharp tool, for instance a razor blade or needle. The dye infiltrates into the cytoplasm of the wounded cells at the edge of the scrape and can diffuse through gap junctions into neighboring cells (Begandt et al. 2010, 2013). The dye diffusion distance within the cell monolayer can then be used for the estimation of gap junction coupling and for a quantitative evaluation of the regulation of gap junction coupling by physiological and pharmacological agents in various cell types (Begandt et al. 2010, 2013; Lee et al. 2010; Xia et al. 2009; Ke et al. 2013).

The SL/DT technique is a simple and convenient method that enables the analysis of gap junction coupling within large cell populations. However, there are also limitations to this method. First, the process of scraping single cover slips is time consuming and necessitates different mechanical steps that can affect gap junction coupling. Second, the geometry of mechanical scrapes varies greatly, which limits the possibility of automation of the imaging and quantification processes. Third, in cells that form a mechanically instable monolayer, the scraping leads to undesirable disruptions of the cell monolayer or a detachment of the cells from the cultivation surface. Therefore, less invasive methods for dye loading, which can be easily automated, are needed to achieve an accurate and high-throughput analysis of gap junction coupling in cell networks. Moreover, a non-invasive technique promises the possibility of gap junction coupling analysis in three dimensional (3D) tissues in and/or ex vivo.

Various laser perforation (optoperforation) techniques promise to be new cell friendly permeabilization methods that allow the uptake of various molecules into cells, while not affecting the cellular viability (Stevenson et al. 2010). A high-throughput variant of the laser perforation technique is the gold nanoparticle-mediated (GNOME) laser perforation (Schomaker et al. 2010; Heinemann et al. 2013; Kalies et al. 2014). During GNOME laser

perforation (GNOME LP), the cell permeabilization is induced by heating effects generated by a laser beam weakly focused at gold nanoparticles (diameter 200 nm) that are adhered on the cell membrane. To date, GNOME LP has been successfully used for the cellular introduction of dextran-coupled dyes as well as siRNA and morpholinos into different cell types (Heinemann et al. 2013; Kalies et al. 2013, 2014; Schomaker et al. 2014). During these experiments, it could be shown that the permeabilization of the cells supported a cell viability of more than 90 %. We propose to adapt the GNOME LP method to a GNOME LP/dye transfer (GNOME LP/DT) technique that can be used to analyze intercellular gap junction coupling in cell monolayers. This technique will offer many advantages, such as the avoidance of mechanical invasiveness, the possibility of automated cell permeabilization, cell imaging as well as experiment evaluation. Additionally we applied the GNOME LP/DT technique to 3D cultivated cells to test the in vivo/ex vivo applicability of the method.

Materials and methods

Chemicals

Carbenoxolone (CBX), forskolin, Hoechst 33342, tetramethylrhodamine isothiocyanate (TRITC)-dextran, average weight 4.4 kDa, and Lucifer yellow (LY) were purchased from Sigma-Aldrich (Munich, Germany). Gold nanoparticles (AuNP, 7×10^8 particles/ml) with a size of 200 nm were delivered from Kisker Biotech (Steinfurt, Germany). For dye transfer experiments, cells were cultivated for 6 h in presence of forskolin (100 µM) or DMSO (0.2 %). Untreated cells and cells treated with dimethylsulfoxide (DMSO), which was used in all experiments as vehicle for forskolin, served as reference.

Cell culture

Bovine GM-7373 aortic endothelial cells (Deutsche Sammlung von Mikroorganismen und Zellkulturen GmbH, Braunschweig, Germany) were cultivated using Dulbecco's Modified Eagle's/Ham's F-12 Medium (DMEM/Ham's F-12, Biochrom, Berlin, Germany) and the rat brain endothelial cell line RBE4 was cultivated with a mixture of Ham's F-10 and alpha-MEM medium (Biochrom). Both media were supplemented with 10 % fetal calf serum (FCS), penicillin and streptomycin (100 U/ml and 0.1 mg/ml, respectively). Additionally, basic fibroblast growth factor (Sigma-Aldrich) with a final concentration of 1 ng/ml was added to the RBE4 medium. The cultures were maintained at 37 °C in a cell culture incubator with a humidified atmosphere containing 5 % CO_2. The culture medium was renewed every 2–3 days.

Scrape Loading/Dye Transfer (SL/DT)

For SL/DT experiments, cover slips (Ø 10 mm) were placed into the wells of a 24 multiwell plate containing 0.5 ml of the corresponding culture medium. The cells were seeded at a density of about 4×10^5 cells/well. Additional cultivation for 24–48 h allowed the cells to adhere and form a monolayer on the cover slip. Analyses of functional gap junction coupling were performed using the SL/DT technique as previously described (Begandt et al. 2010). Briefly, the cells were washed with a bath solution containing 121 mM NaCl, 5.4 mM KCl, 6 mM NaHCO3, 5.5 mM glucose, 0.8 mM MgCl2, 1 mM EGTA, and 25 mM HEPES (pH 7.4, 295 mOsmol/l). The scrape was introduced with a razor blade in presence of 0.25 % LY dissolved in bath solution and incubated for 10 min. Afterwards the cells were washed twice with the bath solution containing 1.8 mM CaCl2. The cells were fixed for 10 min in 4 % formaldehyde dissolved in phosphate buffer saline (PBS) composed of 137 mM NaCl, 2.8 mM KCl, 10 mM Na_2HPO_4 and 1.8 mM KH_2PO_4 (pH 7.4, 295 mOsmol/l) and were stored in PBS for further microscopic analysis. In CBX (100 μM) experiments, the chemical was also present during the scraping and washing steps.

Gold Nanoparticle-mediated Laser Perforation/Dye Transfer (GNOME-LP/DT)

For GNOME LP/DT experiments, the cells were seeded at a density of about 4×10^5 cells/well in a 24 multiwell plate and were cultivated for 24–48 h until they reached confluence. Prior to the experiments, AuNP (0.5 μg/cm^2) were added to the cells for 3–6 h to allow the particles to adhere onto the cell surface. A modified SL/DT protocol was used for the GNOME LP/DT experiments. The cells were washed with the bath solution as described for SL/DT and then were laser-permeabilized in the presence of 0.25 % LY alone or with 0.4 % TRITC-dextran dissolved in bath solution. The laser system set-up and laser treatment was performed according to Heinemann et al. (2013). The set-up included a 532 nm Nd:YAG microchip laser (Horus Laser, Limoges, France), enabling 850 ps laser pulses with a repetition rate of 20 kHz, a telescope for the adjustment of the laser diameter and a half-wave plate combined with a polarizing beam-splitter (Thorlabs, Newton, USA) for adjustment of the laser power. A motorized stage (Carl Zeiss, Jena, Germany) with controller unit (Prior Scientific, Cambridge, UK) and a scanner (Müller Elektronik, Spaichingen, Germany) enabled the positioning and scanning of the multiwell plates. The laser power and the scanning velocity as well as the selection of individual wells were controlled by a self-developed, LabView-based software (Heinemann et al. 2013). To perform GNOME LP/DT, in each well of a 24 multiwell plate, a line of cells was optoperforated by a 35 mW laser beam of 88 μm in diameter

with a scanning velocity of 40 mm/s. After variable dye diffusion times, the cells were washed twice with fresh Ca^{2+}-containing bath solution as described above for manual SL/DT experiments. The fixation and conservation of the cells were performed as described for SL/DT experiments. In CBX experiments, the chemical was also present during the optoperforation and the washing steps.

Quantification of SL/DT Experiments

The SL/DT experiments were documented with a confocal laser scanning microscope (Nikon, Düsseldorf, Germany) using the software program EZ-C1 3.50 (Nikon). A view area of 1024 × 1024 pixels (1273 × 1273 μm) was recorded. The settings for gain, brightness and contrast were not changed for all images within a set of experiments and no editing of the images occurred prior to quantification. The estimation of the dye transfer was performed with the software ImageJ (http://rsbweb.nih.gov/ij/docs/menus/analyze.html) as previously described (Begandt et al. 2010). Briefly, the dye diffusion distance was calculated on the basis of plot profiles generated along the scrape from which the background brightness was subtracted. Per cover slip four micrographs each with six frames with a size of 300 × 100 pixels (length × width) were analyzed with a MATLAB-based software (Begandt et al. 2010). For each treatment, at least four experiments were performed from which the average dye diffusion distance and SEM were calculated.

Quantification of GNOME LP/DT Experiments

To automatically document the GNOME LP/DT experiments, images were obtained with an Orca Flash 4.0 camera (Hamamatsu Photonics, Herrsching am Ammersee, Germany) mounted onto an Eclipse Ti microscope (Nikon) using the NIS elements AR 4.21 software (Nikon). The tool Multipoint ND acquisition was used to generate three images with 2048 × 2048 pixels (3367 × 3367 μm) per well. Two images documented the dye uptake and diffusion in the cells and one image was obtained away from the perforation line, which documented a section of cells that did not contain the dye. The latter image was used for estimation of the background. A constant exposure was used for all images. The automatic focus module of the Eclipse Ti microscope was used to keep the cells in focus during the automatic imaging of the cells in the wells. To analyze the data obtained through the automatic documentation of the 24 multiwell plate, a Java-based ImageJ-plugin was designed which omitted the manual generation of the plot profiles by allowing a robust and automatic detection of the dye-infiltrated cell region in a set of fluorescence images. The plugin detected the boundary of the fluorescent cell band and performed an average intensity projection along the direction of the band. Furthermore, the plugin provided an

alert for detecting image artifacts and outliers in the dye-loaded cell area, allowing the user to correct the boundary of the cell band if necessary. The results were passed to the MATLAB-based software described in a previous publication (Begandt et al. 2010) for calculation of the dye diffusion distance. For each treatment, the average dye diffusion distance and SEM from at least six experiments (at least four passages) were calculated.

Three-dimensional cultivation of cells

To allow the GM-7373 cells to form a 3D pseudo capillary, the cells were introduced into glass capillaries with an inner diameter of 0.58 mm or 1.1 mm, respectively. The cells were allowed to proliferate and to cover the inner surface of the capillaries for 48 h. The AuNP were introduced in the capillaries and allowed to adhere onto the cells for at least 3 h. To avoid an inhomogeneous distribution of the particles the glass capillaries were gently agitated during the AuNP incubation period. A LY-containing bath solution was introduced into the capillaries using a small pipette tip and the capillaries were placed in the GNOME set-up for optoperforation as described above. After washing and fixation of the cells the nuclei were stained with Hoechst 33342. Images of the cells grown in the capillaries were generated using the z-stack tool of the EZ-C1 software and the volume render tool of the software EZ-C1 Free Viewer (Nikon). The dye diffusion distance in untreated cells was compared to that found in cells permeabilized in the presence of CBX.

Statistical analysis

All experiment sets were performed in at least three cell passages. For statistical analyses, a paired two-sample Student's *t*-test was used. The significance is given as * for $P < 0.05$, ** for $P < 0.01$ and *** for $P < 0.001$ for at least four experiments for each treatment.

Results

Gap junction coupling analysis: comparison between SL/DT and GNOME LP/DT

The analysis of gap junction-dependent intercellular coupling is often performed by the SL/DT technique (Abbaci et al. 2008; el-Fouly et al. 1987; Begandt et al. 2010). This simple technique can be used to access the degree of gap junction coupling and to screen the effect of various substances on gap junction coupling in different cells (Fig. 1) (Begandt et al. 2010, 2013). In GM-7373 endothelial cells, a LY diffusion distance of approximately 142 ± 2 μm was measured 10 min following the onset of the SL/DT experiment (Fig. 1b). The

presence of the gap junction channel blocker CBX during SL/DT reduced the dye diffusion distance to 57 ± 3 μm (paired Student's *t*-test, compared to untreated cells; df = 5, $t = 32.08$, $P = 5.5 \times 10^{-7}$), which represents the first row of cells that were injured during scraping (Fig. 1b). The comparison between the results obtained in the absence or presence of the gap junction blocker CBX clearly indicates that the lateral diffusion distance of the LY of 85 ± 3 μm in the untreated cell monolayer was due to gap junction coupling. Conversely, the SL/DT experiments showed that the adenylyl cyclase activator forskolin significantly increased gap junction coupling of the GM-7373 endothelial cells (Fig. 1b). In cells cultivated in the presence of forskolin for 6 h before SL/DT experiments, a dye diffusion distance of 165 ± 2 μm was observed after a diffusion time of 10 min (paired Student's *t*-test, compared to DMSO-treated cells; df = 5, $t = -12.61$, $P = 5.6 \times 10^{-5}$). This increase in the diffusion distance was solely due to a forskolin-dependent action on gap junction coupling and did not involve DMSO, which was also present (0.2 %) in the experiments. In cells that were cultivated for 6 h with DMSO only, a diffusion distance of 137 ± 3 μm was observed (Fig. 1b, paired Student's *t*-test, compared to untreated cells; df = 5, $t = 1.32$, $P = 0.25$). After subtraction of the value found when SL/DT was performed in presence of CBX, the dye diffusion distance found in cells treated with forskolin and DMSO alone was 108 ± 4 μm and 80 ± 4 μm, respectively, indicating a forskolin-related enhancement of the gap junction coupling of 135 %.

We tested whether optoperforation-based GNOME LP could be used to introduce the dye into the cells to allow the analysis of gap junction coupling in cell monolayers establishing thereby a new method named GNOME LP/dye transfer (GNOME LP/DT). In our experimental set-up the GNOME LP/DT uses a laser beam with a diameter of 88 μm, which, by interacting with large gold nanoparticles (Ø 200 nm) in vicinity of the cell membrane, permeabilizes the plasma membrane (Heinemann et al. 2013; Kalies et al. 2014). It has been shown before that gold nanoparticles with a size of 200 nm are best suited for the cell friendly delivery of several substances, for example dextrans or siRNA (Kalies et al. 2013). With the GNOME LP/DT LY was introduced into the GM-7373 endothelial cells. As in SL/DT experiments, the cells were allowed to laterally transmit LY for 10 min after the GNOME LP process. A 179 ± 8 μm wide band of LY-positive cells was found (Fig. 2). The width of the LY-positive cell band was reduced to 112 μm when the cells were fixed immediately after the GNOME LP/DT process without allowing additional time for dye diffusion. The width of the LY-positive cell band was increased to 267 μm when the diffusion time following laser application was changed to 15 min (Fig. 2a). Additionally, when the gap junction blocker CBX was present during GNOME LP/DT experiments a dye diffusion distance of only 95 ± 6 μm was found corresponding to approximately 2–3
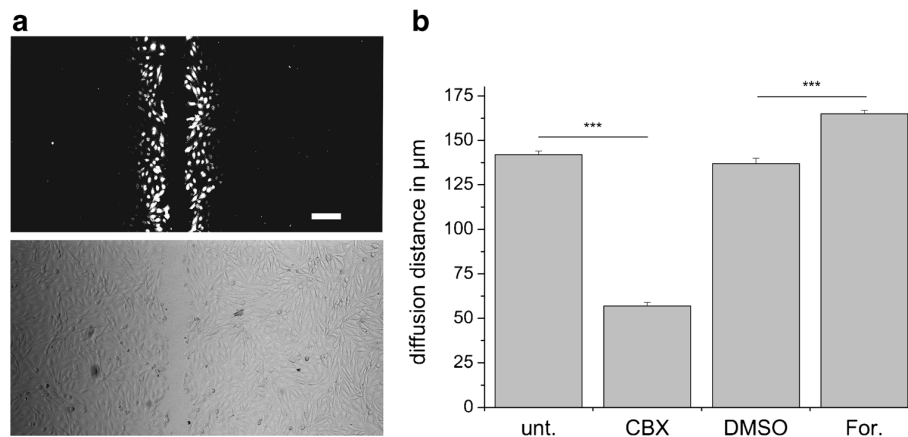
Fig. 1 SL/DT experiment with endothelial GM-7373 cells using the fluorescent dye LY. **a** A typical fluorescent micrograph and correspondent differential interference contrast (DIC) image of cells loaded with LY. **b** Quantitative evaluation of SL/DT experiments performed on cells cultivated with forskolin (For.), DMSO, and under control conditions, as well as cells treated with carbenoxolone (CBX). Cultivation of the cells with forskolin (100 μM) for 6 h increased the dye diffusion distance compared to cultivation of the cells with DMSO (0.2 %), which was used as the solvent for forskolin. Results are shown as average ± SEM from at least four experiments, asterisks indicate $P < 0.001$. The scale bar represents 100 μm

rows of cells (Fig. 2b, paired Student's *t*-test, compared to untreated cells; df = 3, $t = 12.61$, $P = 1.1 \times 10^{-3}$). The results indicate that when gap junction channels were blocked by CBX, LY entered only into the cells that were within the laser beam. Similarly, we performed GNOME LP/DT in the concomitant presence of LY and a gap junction impermeable TRITC-dextran (4.4 kDa). While LY diffused through the gap junctions into the cells that were not within the range of the laser beam, TRITC-dextran was only found in the cells that were directly permeabilized by the laser beam (Fig. 2c). It is striking that the band of the TRITC-dextran-positive cells had the same width as the band of the LY-positive cells found when LY was introduced into CBX-treated cells (Fig. 2c). The results indicate that the LY-positive cell band larger than 95 μm that was found when GNOME LP/DT was performed in the absence of CBX (Fig. 2b) corresponded to a lateral diffusion of LY through gap junction channels in the cell monolayer. For a diffusion time of 10 min, this dye diffusion distance in the monolayer of untreated cells related to gap junction coupling was found to be 83 ± 7 μm.

The SL/DT technique showed that forskolin enhanced the gap junction coupling in GM-7373 endothelial cells (Fig. 1; Begandt et al. 2010). We therefore tested whether GNOME LP/DT, could also detect this forskolin-related effect. We performed GNOME LP/DT on cells cultivated for 6 h in the presence of forskolin and allowed a dye diffusion for 10 min. The width of the LY-positive cell band was found to be 239 ± 11 μm (Fig. 2b, paired Student's *t*-test, compared to DMSO-treated cells; df = 3, $t = -8.27$, $P = 3.7 \times 10^{-3}$). Notably, DMSO did not affect the gap junction coupling (paired Student's *t*-test, compared to untreated cells; df = 3, $t = 1.62$, $P = 0.20$). A 166 ± 4 μm wide LY-positive cell band was observed in cells cultivated for 6 h with DMSO (0.2 %) (Fig. 2b). Similar to the SL/DT experiments, the 95 μm wide band of LY-positive cells, which represents the cells directly permeabilized by the laser beam as shown by application of GNOME LP/DT in presence of CBX, was subtracted from the measured dye diffusion distance observed in all other experiments. Relative to the cells cultivated in the presence of DMSO (70 ± 6 μm), cell cultivation with forskolin for 6 h increased the dye diffusion distance to 143 ± 9 μm, which correlates to an enhancement of the gap junction coupling of 203 %.

GNOME LP/DT opens new possibilities to high throughput screening

As mentioned above, one limitation of the SL/DT technique is the geometric variability of the mechanic scrape, which hinders the automation of experiment processing (Fig. 1). Using GNOME LP/DT, we could generate an accurate band of LY-positive cells (Fig. 2), allowing the automatic imaging and the implementation of a subsequent semi-automatic evaluation of the images using an ImageJ-plugin. The GNOME LP/DT-treated multiwell plate was mounted on a motorized microscope table. Subsequently, the fluorescent images of each well of the 24 multiwell plate were obtained using a multipoint memory tool. The images were further processed with a custom-made ImageJ-plugin based on Java. Using this tool, the dye diffusion plot profiles (Begandt et al. 2010) were automatically generated and saved. These data were passed to the homemade MATLAB-based software described for the SL/DT experiments, which then calculated the dye diffusion distance.
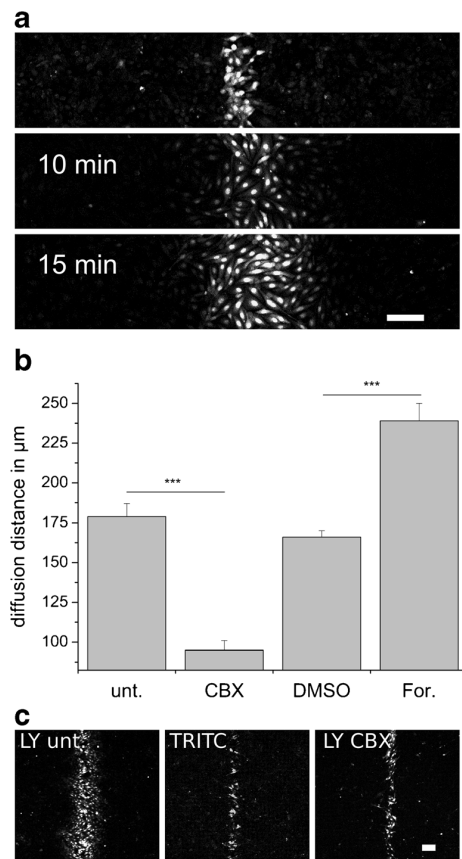
Fig. 2 Analysis of gap junction coupling of GM-7373 cells using GNOME LP/DT. **a** Fluorescent micrographs of LY-loaded cells using GNOME LP/DT. The width of the LY-positive cell band increased with the diffusion time following the GNOME LP/DT process. **b** For quantification, a diffusion time of 10 min was selected. In cells that were cultivated in the presence of forskolin (For., 100 μM) for 6 h, GNOME LP/DT revealed an increase of the diffusion distance compared to cells cultivated with DMSO (0.2 %). **c** Concomitant introduction of LY (left) and TRITC-dextran (center) using GNOME LP/DT. The band of TRITC-dextran-positive cells was narrow compared to the band of LY-positive cells. It is striking that the band of TRITC-dextran-positive cells was comparable to that of LY-positive cells observed when LY was introduced into the cells in presence of CBX (right). The quantitative results in **b** are given as average from at least six experiments ± SEM, asterisks indicate $P < 0.001$. Scale bars represent 100 μm

GNOME LP/DT increases the number of investigable cell types and tissues

Another major limitation of the SL/DT technique is that for some cell types, such as HUVEC or RBE4 cells, we observed that during SL/DT, the cells at the edge of the scrape were squeezed or shredded, rendering an estimation of the dye diffusion distance in the monolayer very difficult (Fig. 3a). As an optical method, GNOME LP/DT did not alter the mechanical adhesion of the cells on the culture surface. Because the detachment of the cells could be avoided, an evaluation of the
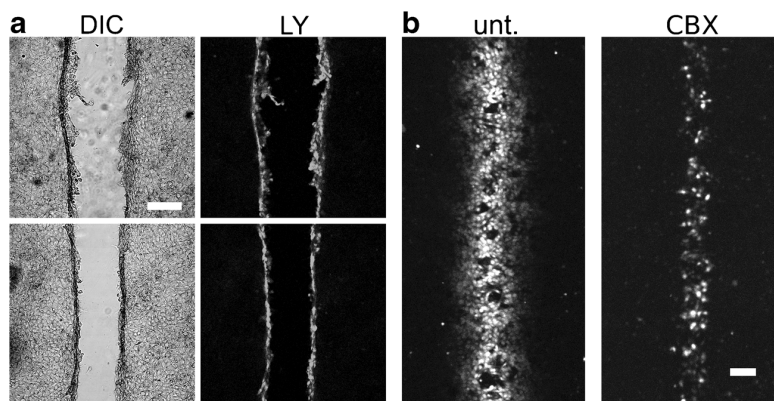
gap junction coupling in RBE4 cells was possible. Using the optoperforation-based GNOME LP/DT, we found LY-loaded RBE4 cells with a width of 178 ± 11 μm under control conditions (Fig. 3). The width of the LY-positive cells was reduced to 101 ± 5 μm when the GNOME LP process was performed in the presence of the gap junction inhibitor CBX (Fig. 3).

The SL/DT technique can only be applied on cells growing in 2D. We tested whether the GNOME LP/DT could be applied to 3D tissues such as blood vessels. Pseudo vessels were generated by cultivation of the GM-7373 cells in glass capillaries. First it is striking that the cells were able to grow and line the inner surface of the glass capillaries imitating a vessel lumen (Fig. 4). This allowed us to introduce the AuNP into the pseudo vessels and to perform GNOME LP/DT (Fig. 4a). Using GNOME LP/DT we found a LY-positive cell band of approximately 160 μm indicating that cells which were not located within the width of the laser beam (Ø 88 μm) were able to acquire the dye from neighboring cells by diffusion through gap junctions (Fig. 4b). Furthermore, the width of the LY-positive cells was clearly reduced in CBX-treated cells (Fig. 4b). These experiments give evidence that GNOME LP/DT could be applied to 3D tissues.

Discussion

Gold nanoparticle-mediated laser perforation (GNOME LP) was previously found as a cell friendly rapid method to deliver substances, for example dextrans or siRNA into cells (Heinemann et al. 2013; Kalies et al. 2013). In the present report we show the method can also be used to introduce gap junction permeable dyes into cells to evaluate the level of gap junction coupling in the cell monolayer (Fig. 2). Our experimental set-up with a laser beam of 88 μm, which, by interacting with large gold nanoparticles (Ø 200 nm) in vicinity of the cell membrane, permeabilizes the plasma membrane (Heinemann et al. 2013; Kalies et al. 2013, 2014) allowed the uptake of the dye, which then diffused laterally in the cell monolayer through gap junctions. After a diffusion time of 10 min, a LY-positive cell band of 179 μm was observed. The lateral diffusion through gap junctions was demonstrated by experiments in which the GNOME LP/DT was applied in presence of the gap junction blocker CBX (Fig. 2). CBX reduced the LY-positive cell band to 95 μm (2–3 cell rows) corresponding to the cells which were directly permeabilized by the laser beam of about 88 μm. The observation that when GNOME LP/DT was applied in presence of both the gap junction permeable LY and the gap junction impermeable 4.4 kDa TRITC-dextran, LY diffused laterally while the dextran stayed constrained in a cell band of about 90 μm also supports our assumption that the laser permeabilized the cells, which then absorbed the dye in the external solution. These

Fig. 3 Analysis of gap junction coupling in RBE4 cells using SL/DT and GNOME LP/DT. **a** Micrographs of RBE4 cells showing undesirable disruptions, such as shredded (upper section) or squeezed (lower section) cells at the edge of the scrape, as result of mechanical scraping. Consequently, the dye diffusion distance could not be estimated. LY

fluorescence is shown in white and the cells were additionally imaged with the differential interference contrast (DIC). **b** The LY uptake and diffusion in RBE4 cells revealed by GNOME LP/DT. The width of the band of LY-positive cells was reduced when GNOME LP/DT was performed in the presence of CBX. Scale bars represent 100 μm

cells transmitted the dye laterally through gap junctions if the dye was gap junction permeable.

Using SL/DT, we recently showed that forskolin and other stimulators of cAMP production were able to enhance the gap junction coupling in GM-7373 cells (Begandt et al. 2010; Fig.1). A forskolin-related enhancement of the gap junction coupling could also be reproduced using the GNOME LP/DT
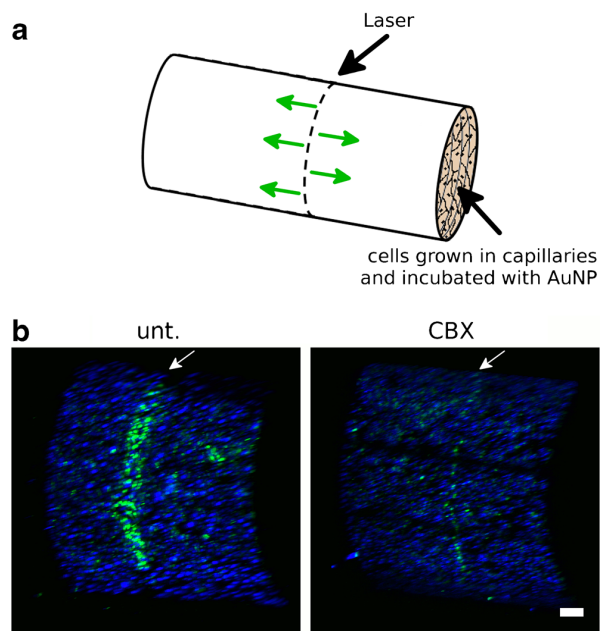
Fig. 4 **a** Schematic representation of GM-7373 cells grown in glass capillaries. Arrows indicate the expected direction of the dye diffusion. **b** Section of a three-dimensional microscopic image of GM-7373 cells in a glass capillary (inner diameter: 1.1 mm) after GNOME LP/DT. The band of LY-positive cells (arrows) can be clearly recognized. CBX reduced the width of the LY-positive cell band. Cell nuclei were stained with Hoechst 33342 (blue) for better visualization of the cells. Scale bar represents 100 μm

(Fig. 2). We show that while DMSO, which was used as vehicle for forskolin, did not influence the gap junction coupling compared to control conditions, the cultivation of the cells in presence of forskolin increased the dye diffusion distance in the monolayers (Fig. 2). Relative to the cells cultivated in the presence of DMSO, cell cultivation with forskolin for 6 h enhanced the gap junction coupling up to 203 % (Fig. 2). It is striking that the effect of forskolin observed using GNOME LP/DT is reinforced compared with the effect observed using the mechanical SL/DT (Begandt et al. 2010; Fig.1). The interpretation for this observation is that GNOME LP/DT may be less invasive for the cells. Performing dye loading or transfection using optoperforation techniques such as GNOME LP, it was shown that the loading of the cells with molecules present in the extracellular milieu was compatible with a cell viability of up to 90 % (Kalies et al. 2014; Baumgart et al. 2012). How the mechanical SL/DT affects the viability of the injured cells is not known, but from the observation of the cells on the edges of the mechanical scrapes, it can be speculated that many injured cells die before they transfer the dye into neighboring cells. It has been shown that mechanically damaging tissues rapidly reduces the gap junction coupling in the affected cells (Carbone et al. 2014). Therefore, we assume that the invasive SL/DT technique underestimates the degree of gap junction coupling in a cell monolayer and most likely leads to underestimation of the regulating effect of physiological and pharmacological agents on the gap junction coupling. Collectively, our results show that GNOME LP/DT can advantageously replace mechanical SL/DT for the analysis of gap junction coupling in cell monolayers.

As mentioned above, the geometric variability of the mechanic scrape produced during SL/DT experiment (Fig. 1) hinders the automation of experiment processing. During GNOME LP/DT experiments, the cell permeabilization is

achieved by a laser beam which interacts with nanoparticles in close vicinity of the cell membrane (Heinemann et al. 2013; Kalies et al. 2013, 2014). By reducing the mechanical intervention of the experimenter, an accurate band of LY-positive cells (Fig. 2) was produced in cell monolayers cultivated in the wells of a 24 multiwell plate, which could then be automatically imaged and evaluated using a java-based ImageJ-plugin. This automation offers the corollary advantage of rapidity and avoidance of experimenter-related biases. The automatic plot profile generation of the three fluorescent images per well of a 24 multiwell plate, the transfer of the images to the MATLAB software and the evaluation of the dye diffusion distances in a complete excel table were accomplished within 30 min. To generate and evaluate the same amount of data using the traditional scrape loading method (Begandt et al. 2010, 2013), required more than 3 h and necessitated the continuous presence of an experimenter. Moreover, the automation can still be improved by integrating the washing and fixation steps, as well as optics for fluorescence imaging and further documentation in the GNOME laser apparatus.

Because of the invasiveness of the SL/DT technique, we found that cells such as HUVEC or RBE4 cells could not be studied. They formed monolayers which were destroyed during the SL/DT process (Fig. 3a). The GNOME LP/DT as an optic-based method did not alter adhesion of the cells on the culture surface, rendering possible the estimation of gap junction coupling in these cells. As shown in Fig. 3, after application of GNOME LP/DT technique a band of LY-loaded RBE4 cells with a width of 178 μm could be found after a diffusion time of 10 min. The width of the LY-positive cells was reduced to 101 μm when the gap junction inhibitor CBX was present during the GNOME LP/DT process, clearly indicating that gap junction coupling was necessary for a lateral diffusion of the dye in the RBE-4 cell monolayer.

The SL/DT technique is used on cells cultivated in 2D on hard and even materials such as glass cover slips. We show in this report that the GNOME LP/DT technology can be applied on cells grown in 3D. As shown in Fig. 4, cells which formed a 3D pseudo vessel when cultured in glass capillaries could be addressed by GNOME LP/DT. It is shown that the width of the band of LY-positive cells could be reduced by the gap junction inhibitor CBX, clearly indicating that the method can be used to access the degree of gap junction coupling in 3D structures. These experiments open a possibility to analyze gap junction coupling in 3D tissue and even in living animal tissues such as blood vessels. The vascular cells exhibit homocellular gap junction coupling between the endothelial cells and between the smooth muscle cells as well as heterocellular gap junctions between the endothelial and the surrounding smooth muscle cells (Figueroa and Duling 2009). The analysis of the gap junction coupling in 3D tissue structures would appreciably increase our understanding of the role played by gap junctions in the physiology of various tissues

such as the heart, the brain and the blood vessels (Nielsen et al. 2012; Goodenough and Paul 2009; Figueroa and Duling 2009). However, physiological assays to access the coupling in 3D structures are still missing. Using our pseudo vessels, we show that the GNOME LP/DT could be applied on 3D tissues for example isolated, dissected vessels for ex vivo investigations or direct in vivo studies. However, some improvements for an optimal in vivo usage are still required. The application set-up for in vivo investigations will need adaptation to tissues and animals. The accessibility of the AuNP, the excitatory laser beam as well as the imaging system to deep layers in the tissue are issues that will need new considerations. While the introduction of the AuNP to cell layers in tissue still is a challenging issue, the excitation of the AuNP and imaging in deep layers of tissue can be solved, at least to a certain extent, by the usage of multiphoton systems (Werkmeister et al. 2007; Osswald and Winkler 2013).

In conclusion, we show that GNOME LP/DT is a fast and reliable method for high-throughput analyses of gap junction coupling in different cell types. Unlike SL/DT, GNOME LP/DT does not require the cultivation of the cells on a hard and even surface. The technique can therefore be used to analyze gap junction coupling of cells cultivated in 3D or on softer materials, e. g. matrigel. Additionally, the scanning parameters (power of the laser beam and the scanning velocity) can be adapted to different cell types and to specific cultivation conditions. Moreover, by adapting the application unit, the technology could be used for analysis of gap junction coupling in tissue even in vivo.

References

Abbaci M, Barberi-Heyob M, Blondel W, Guillemin F, Didelon J (2008) Advantages and limitations of commonly used methods to assay the molecular permeability of gap junctional intercellular communication. Biotechniques 45(33–52):56–62. doi:10.2144/000112810

Baumgart J, Humbert L, Boulais É, Lachaine R, Lebrun J, Meunier M (2012) Off-resonance plasmonic enhanced femtosecond laser optoporation and transfection of cancer cells. Biomaterials 33: 2345–2350. doi:10.1016/j.biomaterials.2011.11.062

Begandt D, Bader A, Dreyer L, Eisert N, Reeck T, Ngezahayo A (2013) Biphasic increase of gap junction coupling induced by dipyridamole in the rat aortic a-10 vascular smooth muscle cell line. J Cell Commun Signal 7:151–160. doi:10.1007/s12079-013-0196-4

Begandt D, Bintig W, Oberheide K, Schlie S, Ngezahayo A (2010) Dipyridamole increases gap junction coupling in bovine GM-7373 aortic endothelial cells by a cAMP-protein kinase a dependent pathway. J Bioenerg Biomembr 42:79–84. doi:10.1007/s10863-009-9262-2

Carbone SE, Wattchow DA, Spencer NJ, Hibberd TJ, Brookes SJ (2014) Damage from dissection is associated with reduced neuro-musclar transmission and gap junction coupling between circular muscle

cells of guinea pig ileum, *in vitro*. Front Physiol 5:319. doi:10.3389/fphys.2014.00319

el-Fouly MH, Trosko JE, Chang CC (1987) Scrape-loading and dye transfer. A rapid and simple technique to study gap junctional intercellular communication. Exp Cell Res 168(2):422–430

Figueroa XF, Duling BR (2009) Gap junctions in the control of vascular function. Antioxid. Redox Signal. 11:251–266. doi:10.1089/ars.2008.2117

Goodenough DA, Paul DL (2009) Gap junctions. Cold Spring Harb Perspect Biol 1:a002576. doi:10.1101/cshperspect.a002576

Harris AL (2007) Connexin channel permeability to cytoplasmic molecules. Prog Biophys Mol Biol 94:120–143. doi:10.1016/j.pbiomolbio.2007.03.011

Heinemann D, Schomaker M, Kalies S, Schieck M, Carlson R, Murua Escobar H, Ripken T, Meyer H, Heisterkamp A (2013) Gold nanoparticle mediated laser transfection for efficient siRNA mediated gene knock down. PLoS One 8:e58604. doi:10.1371/journal.pone.0058604

Kalies S, Birr T, Heinemann D, Schomaker M, Ripken T, Heisterkamp A, Meyer H (2014) Enhancement of extracellular molecule uptake in plasmonic laser perforation. J Biophotonics 7:474–482. doi:10.1002/jbio.201200200

Kalies S, Heinemann D, Schomaker M, Escobar HM, Heisterkamp A, Ripken T, Meyer H (2013) Plasmonic laser treatment for morpholino oligomer delivery in antisense applications. J Biophotonics. doi:10.1002/jbio.201300056

Ke Q, Li L, Cai B, Liu C, Yang Y, Gao Y, Huang W, Yuan X, Wang T, Zhang Q, Harris AL, Tao L, Xiang AP (2013) Connexin 43 is involved in the generation of human-induced pluripotent stem cells. Hum Mol Genet 22:2221–2233. doi:10.1093/hmg/ddt074

Kelsell DP, Dunlop J, Hodgins MB (2001) Human diseases: clues to cracking the connexin code? Trends Cell Biol 11(1):2–6

Lee C, Chen I, Lee C, Chi C, Tsai M, Tsai J, Lin H (2010) Inhibition of gap junctional intercellular communication in WB-F344 rat liver epithelial cells by triphenyltin chloride through MAPK and PI3-kinase pathways. J Occup Med Toxicol 5:17. doi:10.1186/1745-6673-5-17

Nielsen MS, Axelsen LN, Sorgen PL, Verma V, Delmar M, Holstein-Rathlou N (2012) Gap junctions. Compr Physiol 2:1981–2035. doi:10.1002/cphy.c110051

Osswald M, Winkler F (2013) Insights into cell-to-cell and cell-to-blood-vessel communications in the brain: in vivo multiphoton microscopy. Cell Tissue Res 352:149–159. doi:10.1007/s00441-013-1580-3

Schomaker M, Fehlauer H, Bintig W, Ngezahayo A, Nolte, I, Murua-Escobar, H, Lubatschowski H, Heisterkamp A (2010) Fs- laser cell perforation using gold nanoparticles of different shapes. Proceedings of SPIE 7589:75890C-75890C-5

Schomaker M, Killian D, Willenbrock S, Heinemann D, Kalies S, Ngezahayo A, Nolte I, Ripken T, Junghanss C, Meyer H, Escobar HM, Heisterkamp A (2014) Biophysical effects in off-resonant gold nanoparticle mediated (GNOME) laser transfection of cell lines, primary- and stem cells using fs laser pulses. J Biophotonics 9999. doi:10.1002/jbio.201400065

Stevenson D, Gunn-Moore F, Campbell P, Dholakia K (2010) Transfection by optical injection. In: Tuchin V (ed) Handbook of photonics for biomedical science. CRC Press, Taylor and Francis Group, London, pp. 87–118

Werkmeister E, Kerdjoudj H, Marchal L, Stoltz JF, Dumas D (2007) Multiphoton microscopy for blood vessel imaging: new non-invasive tools (Spectral, SHG, FLIM). Clin Hemorheol Microcirc 37(1–2):77–88

Willecke K, Eiberger J, Degen J, Eckardt D, Romualdi A, Guldenagel M, Deutsch U, Sohl G (2002) Structural and functional diversity of connexin genes in the mouse and human genome. Biol Chem 383:725–737. doi:10.1515/BC.2002.076

Xia Y, Gong K, Xu M, Zhang Y, Guo J, Song Y, Zhang P (2009) Regulation of gap-junction protein connexin 43 by beta-adrenergic receptor stimulation in rat cardiomyocytes. Acta Pharmacol Sin 30:928–934. doi:10.1038/aps.2009.92

Zoidl G, Dermietzel R (2010) Gap junctions in inherited human disease. Pflügers Arch. 460:451–466. doi:10.1007/s00424-010-0789-1

4 General discussion and further perspectives

In the second chapter of this work the regulation of gap junction coupling in cerebral endothelial cells by adenosine receptor-dependent signalling mechanims was analysed. It was shown that 2-phenylaminoadenosine (2-PAA), predominantely activating the A_{2B} adenosine receptor subtype, increased the gap junction coupling and the amount of Cx43 gap junction plaques in the cerebral microvascular endothelial cell line hCMEC/D3. This was due to an increase in the intracellular cAMP concentration with cAMP in turn activating cyclic nucleotide-gated (CNG) channels. A subsequent increase in Ca^{2+} was responsible for the increased gap junction coupling. The presented report for the first time identified CNG channels as link between adenosine receptor activation and gap junctions in endothelial cells (Chapter 2, Bader *et al.* 2017).

4.1 Role of the A_{2B} adenosine receptor subtype

The important role of the A_{2B} adenosine receptor subtype in regulation of gap junction coupling in hCMEC/D3 cells was shown with several approaches. Firstly, the A_{2B} adenosine receptor subtype-specific inhibitor MRS1754 alone nearly completely blocked the 2-PAA-induced increase in gap junction coupling (Chapter 2, Bader *et al.* 2017), while the A_{2A} adenosine receptor subtype-specific inhibitor SCH58261 only slightly attenuated the 2-PAA-induced increase in gap junction coupling (Chapter 2, Bader *et al.* 2017). Secondly, in siRNA-treated cells with a reduced A_{2B} adenosine receptor subtype expression 2-PAA failed to induce a significant increase in the dye diffusion distance (Chapter 2, Bader *et al.* 2017). Further new data not included in Chapter 2 confirmed that the A_{2B} adenosine receptor specifically affected the gap junction coupling of the cerebral microvascular endothelial cells hCMEC/D3. We observed that the A_{2B} adenosine receptor-specific agonist BAY60-6583 (Hinz *et al.* 2014, van der Hoeven *et al.* 2011) induced a significantly increased dye diffusion distance in scrape loading/dye transfer

assays, comparable to 2-PAA (Figure 4.1 A), while the specific A_{2A} adenosine receptor subtype agonist CGS21680 (Phillis 1990, Klotz *et al.* 2000) did not induce an increased dye diffusion distance (Chapter 2, Bader *et al.* 2017).
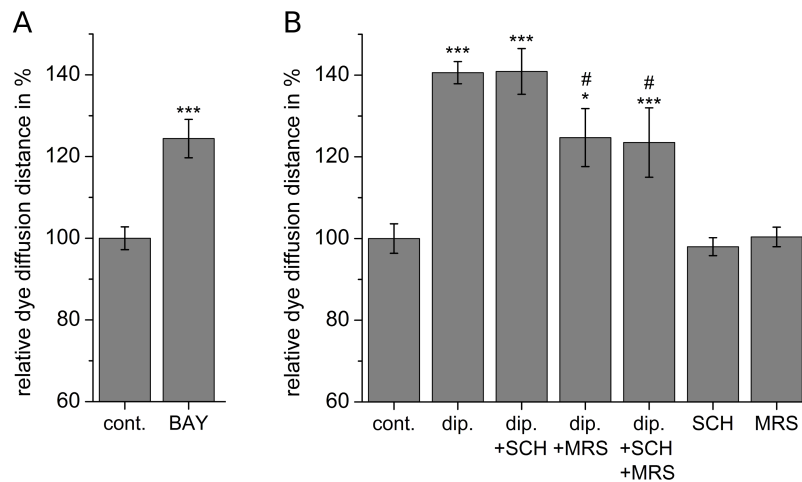

Figure 4.1: Activation of the A_{2B} adenosine receptor subtype increases the gap junction coupling in hCMEC/D3 cells. A) The A_{2B} adenosine receptor subtype-specific agonist BAY60-6583 (BAY, 100 nM) significantly increased the dye diffusion distance compared to the vehicle control (cont.) within 1 h. B) The increased gap junction coupling induced by dipyridamole (dip., 25 µM, 4 h) was significantly attenuated by simultaneous application of the A_{2B} adenosine receptor subtype-specific antagonist MRS1754 (MRS, 100 nM) but not by the A_{2A} adenosine receptor subtype-specific antagonist SCH58261 (SCH, 100 nM). ∗ Significant differences to vehicle control, # significant differences to dipyridamole, Student's *t*-test: ∗, # $P < 0.05$, ∗∗∗ $P < 0.001$.

Activation of adenosine receptors and a subsequent increase in gap junction coupling can also be achieved by pharmaceutical compounds as we demonstrated for the antithrombotic drug dipyridamole that is used to prevent recurrent strokes, often in combination with acetylsalicylic acid (Eisert 2006, Kim & Liao 2008, Isabel *et al.* 2016, Rothlisberger & Ovbiagele 2015). Dipyridamole increases the extracellular adenosine concentration by blocking equilibrative nucleoside transporters (Molina-Arcas *et al.* 2009, Eisert 2006) and increased the gap junction coupling in aortic endothelial (Begandt *et al.* 2010, 2013b) and smooth muscle cells (Begandt *et al.* 2013a). The same effect was oberserved in hCMEC/D3 cells in scrape loading/dye transfer experiments (Figure 4.1 B). The enhanced gap junction coupling was due to activation of adenosine receptors and, as for 2-PAA, mainly depended on activation of the A_{2B} adenosine receptor subtype since the application of dipyridamole together with the A_{2B} adenosine receptor subtype inhibitor MRS1754 (Figure 4.1 B) significantly attenuated the increased dye diffusion

distance as compared to dipyridamole alone. The A_{2A} adenosine receptor subtype inhibitor SCH58261 did not have an effect (Figure 4.1 B). The effect of dipyridamole on gap junction coupling of vascular cells (Figure 4.1 B, Begandt *et al.* 2010, 2013a,b) is not considered in its current therapeutic application that targets platelets (Eisert 2006). However, the gap junction-dependent intercellular communication of vascular cells might be an important therapeutic target (Willebrords *et al.* 2016, Green & Nicholson 2008).

The A_{2B} adenosine receptor subtype is activated by high adenosine concentrations in the micromolar range in contrast to the other three adenosine receptor subtypes (Fredholm *et al.* 2001a, Fredholm 2007, Chen *et al.* 2013). A sustained systemic increase of the external adenosine concentration to micromolar ranges mostly correlates with pathophysiological situations such as inflammation or hypoxia, suggesting that the A_{2B} adenosine receptor is only activated under pathological conditions (Fredholm 2007, Eltzschig 2009, Chen *et al.* 2013). However, local increases of external adenosine levels under non-pathological conditions have been found in tissue such as the brain (Nguyen *et al.* 2014, Nguyen & Venton 2015) and in the vasculature in respose to changed flow or mechanical stretch (Bodin *et al.* 1991, Bodin & Burnstock 2001, Burnstock & Knight 2017). This indicates that an activation of the A_{2B} adenosine receptor subtype under non-pathological conditions is possible. The A_{2B} adenosine receptor subtype is widely expressed in endothelial cells and is involved in many vascular signalling mechanisms (Chen *et al.* 2013, Yang *et al.* 2006). Several studies indicated that activation of the A_{2B} adenosine receptor subtype by temporarily increased adenosine levels can have beneficial tissue-protective effects (Karmouty-Quintana *et al.* 2013). It can protect against vascular injury (Yang *et al.* 2008), inflammation and excessive leukocyte adhesion (Yang *et al.* 2006) and prevent hypoxia-induced vascular leakage (Eltzschig *et al.* 2003, Eckle *et al.* 2008) as well as hyperoxic-induced vascular leakage in the lung (Davies *et al.* 2014). The A_{2B} adenosine receptor subtype is also involved in ischemic preconditioning in the heart (Eckle *et al.* 2007) and lung (Choukèr *et al.* 2012) and stimulates angiogenesis (Feoktistov *et al.* 2002, Du *et al.* 2015).

In our studies the effects of A_{2B} adenosine receptor activation on gap junction coupling were evaluated during a time scale of one to a few hours. Furthermore, we found that application of 2-PAA to hCMEC/D3 cells for 5 or 10 min and performing scrape loading/ dye transfer assays 1 h later resulted in an increased dye diffusion distance (Figure 4.2). This indicates that in contrast to constantly increased adenosine levels during chronic disease states, activation of A_{2B} adenosine receptors and a subsequently enhanced gap junction coupling can occur during transiently increased adenosine concentrations.
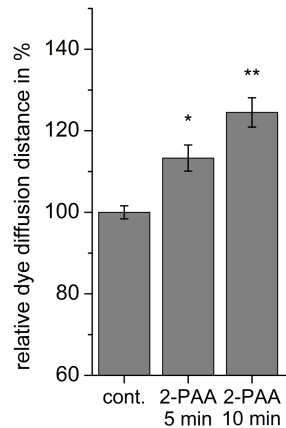
Figure 4.2: A short-time stimulation of adenosine receptors increases the gap junction coupling. Applying 2-PAA ($20\,\mu M$) for 5 min or 10 min was sufficient to observe a significantly increased dye diffusion distance in scrape loading/dye transfer assays 1 h later compared to the vehicle control (cont.). $*$ Significant differences to vehicle control, Student's t-test: $* \, P < 0.05$, $** \, P < 0.01$.

In conclusion, our results show that the A_{2B} adenosine receptor subtype is also linked to regulation of gap junction coupling (Chapter 2, Bader *et al.* 2017). Many reports concentrated on the macroscopic outcome of adenosine receptor activation on physiological level. How gap junctions could be involved in these events is not clear yet. However, both A_{2B} adenosine receptor activation and gap junction coupling are associated with the same physiological processes, for example regulation of inflammatory response or angiogenesis (Fredholm 2007, Blackburn *et al.* 2009, Chen *et al.* 2013, Scheckenbach *et al.* 2011, Willebrords *et al.* 2016). During acute inflammation A_{2B} adenosine receptor activation is mostly beneficial and attenuated vascular barrier leakage and tissue damage (Yang *et al.* 2006, 2008, Karmouty-Quintana *et al.* 2013). Endothelial Cx43 is often upregulated during inflammation (Scheckenbach *et al.* 2011, Willebrords *et al.* 2016, Green & Nicholson 2008, Sarieddine *et al.* 2009, Parthasarathi *et al.* 2006, O'Donnell *et al.* 2014, Kandasamy *et al.* 2015). In several studies upregulation of Cx43 gap junctions correlated with increased vascular permeability (O'Donnell *et al.* 2014, Kandasamy *et al.* 2015, Zhang *et al.* 2015) and it was proposed that spreading pro-inflammatory signals through gap junctions contributed to these effects (Parthasarathi *et al.* 2006). Increased levels of Cx43 were also found to impair wound healing (Green & Nicholson 2008, Chen *et al.* 2015). It was further shown that activating A_{2B} adenosine receptors induced angiogenesis (Du *et al.* 2015, Feoktistov *et al.* 2002). Upregulation of endothelial Cx43 also

increased angiogenesis (Dhein *et al.* 2015) while downregulation of endothelial Cx43 impaired angiogenesis (Gärtner *et al.* 2012). How A_{2B} adenosine receptor activation and subsequently increased gap junction coupling as observed in our study (Chapter 2, Bader *et al.* 2017) are involved in processes such as cellular responses to inflammation or regulation of angiogenesis cannot be concluded at this point, especially since the effects of adenosine receptor signalling and gap junction regulation can differ, depending on the vascular bed and surrounding tissue (Green & Nicholson 2008, Karmouty-Quintana *et al.* 2013). Many studies analysing A_{2B} adenosine receptor subtype- and Cx43-dependent effects during inflammation concentrated on pulmonary cells and not much is known for the specialised endothelial cells of the blood-brain barrier. Taken together, we propose that the role of gap junction coupling should be integrated into the signalling events stimulated by A_{2B} adenosine receptor activation to gain a detailed understanding of the underlying mechanisms regulating the physiological effects of A_{2B} adenosine receptor activation in different tissue.

4.2 Mechanisms regulating the gap junction coupling

In hCMEC/D3 cells the activation of adenosine receptors and subsequently CNG channels led to an increase in the intracellular Ca^{2+} concentration which was responsible for the increase in gap junction coupling (Chapter 2, Bader *et al.* 2017). Ca^{2+} is an important second messenger involved in a plethora of cellular signalling cascades (Pani & Singh 2009). To this point it is not clear how the increased amount of Ca^{2+} affected the gap junction coupling but different interacting molecules and pathways could be involved (Figure 4.3, Bader *et al.* 2017).

In hCMEC/D3 cells a spatially restricted Ca^{2+} increase after CNG channel activation was assumed to explain the low measured increase in intracellular Ca^{2+} and the efficacy of BAPTA to suppress the 2-PAA-induced increase in gap junction coupling in contrast to EGTA (Chapter 2, Bader *et al.* 2017, Rousset *et al.* 2004). Microdomains enable the spatial separation of cellular signalling (Pani & Singh 2009, Cooper & Tabbasum 2014, D'Ambrosi & Volonté 2013) and therefore ubiquitous second messengers like Ca^{2+} or cAMP can exhibit specific effects on different effectors (Pani & Singh 2009, Feinstein *et al.* 2012). Microdomains can be formed in lipid rafts which are cholesterol- and sphingolipid-rich regions within the cell membrane (Lingwood & Simons 2010, Reeves *et al.* 2012, Pani & Singh 2009). Various Ca^{2+} channels and their regulatory interaction partners as well as their effectors have been shown to be located in lipid rafts (Pani & Singh 2009,
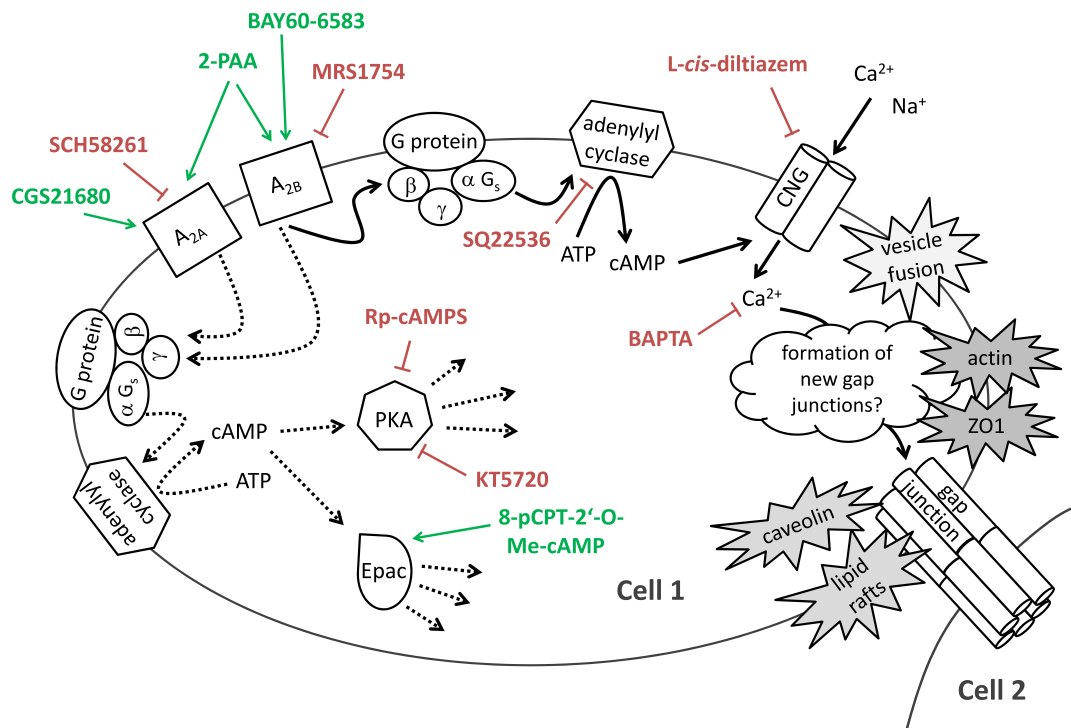
Figure 4.3: Postulated signalling pathway induced by A_{2B} adenosine receptor activation in hCMEC/D3 cells. Solid lines indicate the presented signalling mechanism, dashed lines indicate other possible signalling pathways. A_{2B} adenosine receptor activation induced cAMP synthesis and subsequent activation of CNG channels. This led to a Ca^{2+} influx that increased the gap junction coupling. Grey, jagged text boxes show mechanisms possibly involved in the increased gap junction coupling. This could rely on increased formation of new gap junctions through enhanced vesicle fusion of connexon-containing vesicles with the cell membrane. A caveolin- or lipid raft-mediated regulation of connexons as well as a ZO1- and actin-dependent regulation of gap junctions could also be possible. Modified from Bader *et al.* (2017).

Balijepalli *et al.* 2006, Wang *et al.* 2005). Lipid rafts are often structured and organised by specialised proteins, for example by caveolins that form caveolae (Reeves *et al.* 2012, Pani & Singh 2009). Caveolae are elongated invaginations within the cell membrane that are involved in endocytosis and transcytosis and provide signalling platforms for various signal transduction events (Reeves *et al.* 2012). They can also serve as small intracellular Ca^{2+} stores in endothelial cells (Isshiki *et al.* 2013). Caveolae are especially abundant in endothelial cells (Reeves *et al.* 2012, Minshall *et al.* 2003) and have been shown to regulate the expression of junction-associated proteins in brain microvascular endothelial cells (Song *et al.* 2007).

For our proposed signalling mechanism that links adenosine receptor stimulation, CNG channel activation and gap junctions (Chapter 2, Bader *et al.* 2017), lipid rafts could act as structural elements that cluster the participating proteins A_{2B} adenosine receptors, the adenylyl cyclase and CNG channels in close proximity. It is well known that adenylyl cyclases (Cooper & Tabbasum 2014) and CNG channels (Rich *et al.* 2000, Brady *et al.* 2004, Ding *et al.* 2008) are targeted to and regulated by caveolear and non-caveolar lipid rafts (Brady *et al.* 2004, Ding *et al.* 2008). Adenosine receptors are also known to be located in lipid rafts (D'Ambrosi & Volonté 2013, Lasley 2011), although only a few studies exist showing that the A_{2B} adenosine receptor subtype specifically associates with caveolins (Sitaraman *et al.* 2002). Microdomains could explain the restricted cAMP elevation to only about 130% after 2-PAA application (Chapter 2, Bader *et al.* 2017). Brady *et al.* (2004) observed cAMP-dependent opening of CNG channels in response to prostaglandin E1 application, although whole-cell cAMP increases were not measurable (Brady *et al.* 2004). Similarly, it was shown that stimulation of A_{2B} adenosine receptor subtypes in airway epithelial cells stimulated cAMP production in local compartments containing A-kinase anchoring proteins to immobilise the PKA (Huang *et al.* 2000). Phosphodiesterases can spatially restrict cAMP diffusion in these compartments (Barnes *et al.* 2005). We therefore assume compartmentalisation of the signalling cascade leading from the stimulated A_{2B} adenosine receptor and its coupled adenylyl cyclase to gap junctions via activation of CNG channels.

Connexins and gap junctions are associated with and regulated by caveolins as well (Schubert *et al.* 2002, Langlois *et al.* 2008, Ampey *et al.* 2016, Saliez *et al.* 2008, Hervé *et al.* 2012). In keratinocytes caveolin-1 and caveolin-2 were associated with Cx43 already in the Golgi apparatus and caveolins regulated the Cx43-dependent gap junction coupling (Langlois *et al.* 2008). A co-trafficking of caveolins and connexins to the cell membrane and a targeted introduction of connexins in lipid rafts (Schubert *et al.* 2002, Langlois *et al.* 2008) could be a possible mechanism that regulates the observed rapid increases in gap junction coupling and Cx43 gap junction plaques (Chapter 2, Bader *et al.* 2017). In hCMEC/D3 cells we showed co-localisation of Cx43 and caveolin-1 with double immunofluorescence stainings (Figure 4.4 A) and proximity ligation assays (Söderberg *et al.* 2006, Jarvius *et al.* 2007, Figure 4.4 B). Experiments after activation of adenosine receptors with 2-PAA were not conclusive till now, so it remains unclear if caveolin-1-mediated mechanisms play a role in the 2-PAA-induced increase in gap junction coupling.

An increase in gap junction coupling may result from an increased open probability of gap junction channels, an increase in gap junction channel permeability, or an in-
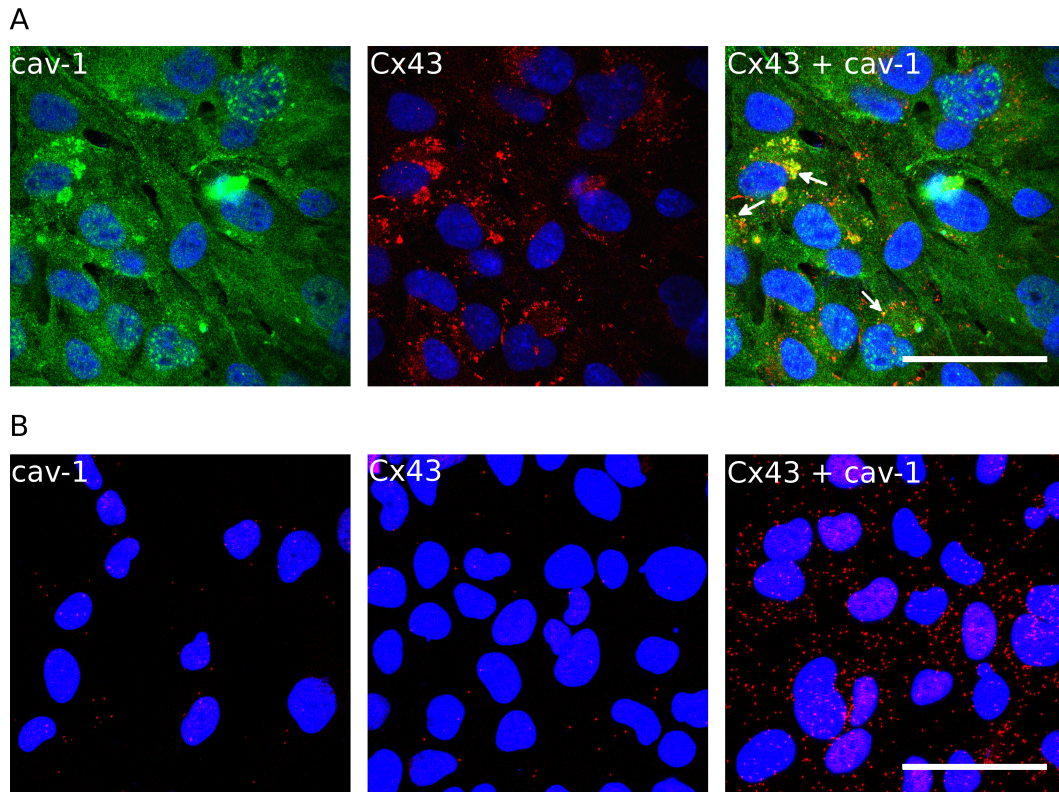
Figure 4.4: Co-localisation of Cx43 and caveolin-1. A) Immunofluorescence images after co-stainig caveolin-1 (cav-1, green) and Cx43 (red). Nuclei were counterstained with 4',6-diamidino-2-phenylindole (DAPI, blue). Arrows point to co-localised particles. B) Proximity ligation assays confirmed co-localisation of Cx43 and caveolin-1. Experiments were performed with only the anti-caveolin-1 antibody (left), only the anti-Cx43 antibody (middle) or both antibodies (right). Co-localised proteins are clearly visualised by red spots. Scale bars represent 50 μm.

creased amount of gap junction channels in the cell membrane. The latter explanation could be favoured in the presented signalling mechanism because we observed a significant increase in cells with Cx43 gap junction plaques and an increased gap junction plaque area in high-resolution microscopic images after 2-PAA treatment (Chapter 2, Bader *et al.* 2017). Since an increase in the overall Cx43 amount was not observed and the increase in gap junction coupling occurred within 1 h we assumed that the increased amount of Cx43 gap junction channels depended on already synthesised connexons (Chapter 2, Bader *et al.* 2017). The transport of connexon-containing vesicles to the cell membrane or the fusion of these vesicles with the cell membrane could be enhanced through a 2-PAA-induced Ca^{2+}-dependent signalling pathway. Ca^{2+} is a well-known regulator of endothelial vesicle fusion and exocytosis (Pulido *et al.* 2011, Zhu

et al. 2015, Lowenstein *et al.* 2005). Analysing the involvement of Ca^{2+} in the vesicle fusion of connexon-containing vesicles with the cell membrane could be an approach for future studies. Ca^{2+}-sensing proteins in the vesicle membrane, for example synaptotagmins or synaprotagmin-like proteins could be involved in this mechanism (Frampton 2013, Bierings *et al.* 2012, van Breevoort *et al.* 2014). Further targets could be the soluble N-ethylmaleimide-sensitive-factor attachment receptors or synaptosomal-associated proteins (SNAPs), for example SNAP-23 (Pulido *et al.* 2011, Zhu *et al.* 2015).

Another explanation for the rapid 2-PAA-induced increase in gap junction coupling could be the formation of new gap junctions from connexons that are already inserted in the cell membrane and rapidly recruited to existing gap junction plaques (Rhett *et al.* 2011, Laing *et al.* 2005, Olk *et al.* 2009). The cytoskeleton, especially actin filaments, are known to be regulated by Ca^{2+}-dependent signalling pathways (Vandenbroucke *et al.* 2008, Tsai *et al.* 2015, Shen *et al.* 2009). The cytoskeleton is an important partner for gap junction proteins, being the transport track for gap junctions to the cell membrane (Smyth *et al.* 2012, Shaw *et al.* 2007, Olk *et al.* 2009), anchoring the gap junctions into the cell membrane (Olk *et al.* 2009, Rhett *et al.* 2011, Hervé *et al.* 2012), and regulating gap junction remodelling and degradation (Rhett *et al.* 2011, Rhett & Gourdie 2012, Olk *et al.* 2009, Hervé *et al.* 2012). The cytoskeleton also participates in the regulation of gap junction coupling, for example via RhoA-dependent modulation of actin filaments (Derangeon *et al.* 2008) or directed microtubule-dependent transport of connexons to gap junction plaques (Shaw *et al.* 2007).

Special interest has been paid to the interaction between ZO1 and connexins. ZO1 binds to Cx43 and tethers it to actin filaments (Chen *et al.* 2015, Rhett *et al.* 2011, Derangeon *et al.* 2008, Hunter *et al.* 2005, Laing *et al.* 2005, Hervé *et al.* 2012, 2014). It has been shown that ZO1 regulates gap junction plaque size by binding to Cx43 at gap junction plaque edges and recruiting actin to these points (Hunter *et al.* 2005, Rhett *et al.* 2011, Rhett & Gourdie 2012, Zhu *et al.* 2005). Rhett *et al.* (2011) proposed that ZO1 mainly binds to unopposed Cx43 connexons at the edge of gap junction plaques and controls the insertion of these connexons into gap junction plaques (Rhett *et al.* 2011, Rhett & Gourdie 2012). Only gap junctional ZO1-Cx43 complexes were bound to actin filaments (Rhett *et al.* 2011, Rhett & Gourdie 2012). Disrupting the binding of Cx43 and ZO1 or knocking down ZO1 expression resulted in significantly enlarged gap junction plaques and increased gap junction coupling (Hunter *et al.* 2005, Rhett *et al.* 2011). Similarly, activation of the small GTPase RhoA decreased Cx43-ZO1 interactions and increased gap junction plaque size and dye transfer in cardiomyocytes via actin

remodelling mechanisms (Derangeon *et al.* 2008). In contrast to these studies, Laing *et al.* (2005) observed that interrupting the binding between ZO1 and Cx43 in osteoblastic cells decreased the gap junction coupling (Laing *et al.* 2005). They proposed that lipid raft-associated, inactive Cx43 connexons could rapidly be recruited into actin-anchored gap junction plaques by ZO1 but also noted that ZO1 could differently regulate the gap junction coupling in different cell types (Laing *et al.* 2005). Recently, Thévenin *et al.* (2017) suggested that upon specific phosphorylation of Cx43, ZO1 recruited closed Cx43 connexons to gap junction edges. When Cx43 and ZO1 could not disengage, the gap junction plaque size and number increased, probably because the gap junctions were kept in an open state and Cx43 half-life was increased (Thévenin *et al.* 2017). Chen *et al.* (2015) showed that in microvascular cerebral endothelial cells disrupting the interaction between Cx43 and ZO1 resulted in remodelling of the actin filaments and regulated cell motility and wound healing independently of gap junction channel function (Chen *et al.* 2015).

ZO1-dependent mechanisms regulating Cx43 gap junction coupling and gap junction plaque size (Rhett *et al.* 2011, Hunter *et al.* 2005, Derangeon *et al.* 2008, Hervé *et al.* 2014) could play a role in the signalling link between A_{2B} adenosine receptor activation and gap junctions since we observed an increase in gap junction coupling and Cx43 gap junction plaques without changes in the overall Cx43 levels (Chapter 2, Bader *et al.* 2017). Therefore, we also postulated that the formation of new gap junctions from already synthesised connexons could be responsible for the increased gap junction coupling (Chapter 2, Bader *et al.* 2017). We applied the peptide αCT1 to interrupt the interaction between Cx43 and ZO1 (Chen *et al.* 2015, Rhett *et al.* 2011) to hCMEC/D3 cells and observed a significantly increased dye diffusion distance in dye transfer assays similar to adenosine receptor activation with 2-PAA (Figure 4.5). These findings are in agreement with previous results (Rhett *et al.* 2011) and could possibly indicate a ZO1- and actin-dependent remodelling of gap junctions (Rhett *et al.* 2011, Derangeon *et al.* 2008) induced in hCMEC/D3 cells after adenosine receptor stimulation. Since it has been shown that ZO1 contains a calmodulin binding site (Paarmann *et al.* 2008) it could be possible that Ca^{2+}-dependent signalling mechanisms influence ZO1. We did not observe a significant restructuring in the actin cytoskeleton after application of αCT1 (data not shown) like Chen *et al.* (2015) in cerebral microvascular endothelial cells.

The results concerning αCT1 application are preliminary and need to be confirmed with additional experiments. The specific role of ZO1 could be evaluated by knocking down its expression and analysing the impact on gap junction coupling. The involvement
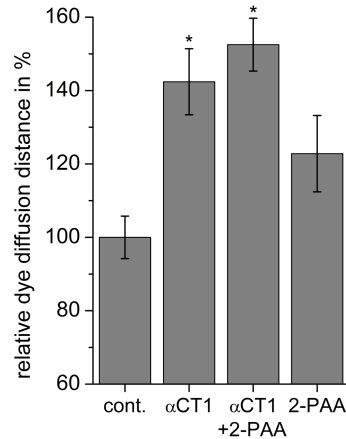
Figure 4.5: Adding the peptide αCT1 (150 µM) for 4 h to hCMEC/D3 cells to disrupt the binding of Cx43 and ZO1 increased the gap junction coupling in gold nanoparticle-mediated laser perforation/dye transfer assays (Chapter 3). Additional application of 2-PAA (20 µM) for 1 h led to an even enhanced increase. ∗ Significant differences to vehicle control (cont.), Student's t-test: ∗ $P < 0.05$.

of actin should also be analysed more detailed, for example by applying actin remodelling agents like cytochalasin and phalloidin (Derangeon *et al.* 2008) and analysing the gap junction coupling after 2-PAA application. Following the fate of Cx43 proteins, for example with pulse-chase labelling and time-lapse microscopy (Boassa *et al.* 2010, Gaietta *et al.* 2002), could shed more light on the mechanisms regulating connexin transport, insertion of connexons into gap junctions and redistribution of connexons or gap junctions in the cell membrane in hCMEC/D3 cells after adenosine receptor stimulation.

4.3 Comparison of endothelial cells of different vascular beds

In bovine aortic endothelial GM-7373 cells it was shown that the equilibrative nuleoside transporter inhibitor dipyridamole increased the gap junction coupling by activation of adenosine receptors (Begandt *et al.* 2010, 2013b). The increase in gap junction coupling was cAMP- and PKA-dependent (Figure 4.6 A, Begandt *et al.* 2010). Similarly, 2-PAA significantly increased the dye diffusion distance in GM-7373 cells in scrape loading/dye transfer assays and this increase could be suppressed by simultaneous application of the PKA inhibitors Rp-cAMPS or KT5720 (Figure 4.6 A, Begandt *et al.* 2010). In contrast, in the human cerebral endothelial cell line hCMEC/D3 neither the dipyridamole- nor

the 2-PAA-induced increase in gap junction coupling could completely be suppressed by PKA inhibition (Figure 4.6 B, Bader *et al.* 2017). In these cells activation of CNG channels was responsible for the 2-PAA-induced increase in gap junction coupling (Chapter 2, Bader *et al.* 2017).

Differences between the different endothelial cells were also noted for the time course of the increased gap junction coupling. The gap junction coupling in bovine aortic endothelial GM-7373 cells increased consistently within 6 h of dipyridamole treatment and continued to increase up to 24 h (Begandt *et al.* 2013b). In the human microvascular cerebral endothelial cell line hCMEC/D3 the gap junction coupling reached a maximum within 1 h (Chapter 2, Bader *et al.* 2017). Apart from the signalling pathways involving the PKA in GM-7373 cells and CNG channels in hCMEC/D3 cells, the varying kinetics of gap junction regulation resemble a difference between the cell lines. Primary cells or endothelial cells *in vivo* could respond differently than cell lines used as *in vitro* model. Furthermore, it cannot be excluded that species variations between the two cell lines from bovine and human origin, respectively, led to the observed differences. However, since both cell lines derive from different vascular beds, i.e. the aorta and the cerebral microvasculature, the differences could also be due to specialised endothelial functions. Cerebral microvascular endothelial cells forming the blood-brain barrier exhibit specific properties, including polarisation and tight junction formation (Section 1.1.3, Abbott *et al.* 2006, Correale & Villa 2009, Weiss *et al.* 2009). Considering that endothelial cells from different vascular beds could exhibit different signalling pathways to regulate gap junctions, the role of gap junctions for maintaining the blood-brain barrier properties in cerebral micovascular endothelial cells should be analysed in more detail.

To evaluate the gap junction coupling and its regulation in a more *in vivo*-like setting, the cell culture of blood-brain barrier-forming endothelial cells would have to be improved. A more appropriate model of the blood-brain barrier would be the co-culture of endothelial cells with pericytes and/or astrocytes as found *in vivo* (Figure 1.2, Gromnicova *et al.* 2013, Sreekanthreddy *et al.* 2015, Thomsen *et al.* 2015, Zhang *et al.* 2011, Czupalla *et al.* 2014, Wilhelm *et al.* 2011). Furthermore, three-dimensional cell culture systems would be advantageous (Cucullo *et al.* 2008, 2011, Bogorad *et al.* 2015). The more complex the cell culture set-up is, the more complicated it is to investigate the cells. The scrape loading/dye transfer technique for example would not be applicable in the above-mentioned set-ups. Alternative methods are needed and have to be adapted to the studied cell culture models. We established a new non-invasive method to ana-
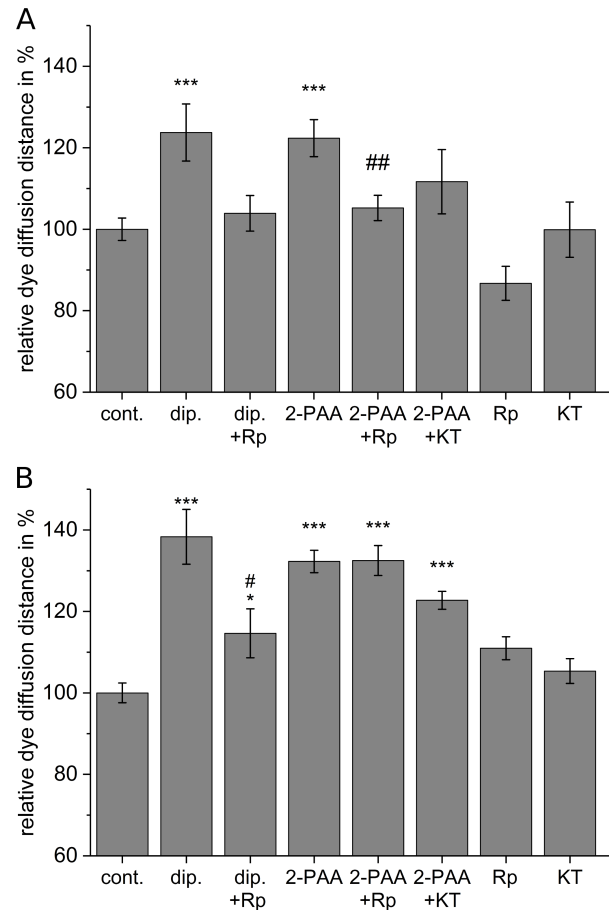
Figure 4.6: The adenosine receptor-dependent increase in gap junction coupling is PKA-dependent in aortic, but not in microvascular cerebral endothelial cells. A) Applying the nucleoside transporter inhibitor dipyridamole (dip., 50 µM, 6 h) to GM-7373 bovine aortic endothelial cells increased the dye diffusion distance in scrape loading/dye transfer assays and this could be suppressed by the PKA inhibitor Rp-cAMPS (Rp, 200 µM). Similar results were observed after 2-PAA incubation (50 µM, 6 h) with or without Rp-cAMPS or another PKA inhibitor, KT5720 (KT, 1 µM). B) The dipyridamole- (dip., 25 µM, 6 h) induced increase in the dye diffusion distance in human cerebral microvascular endothelial hCMEC/D3 cells could not completely be blocked by Rp-cAMPS (200 µM). Neither Rp-cAMPS (200 µM) nor KT5720 (1 µM) had an effect on the 2-PAA- (20 µM) induced increase in dye transfer within 1 h (modified from Bader *et al.* (2017)). ∗ Significant differences to the vehicle control, # significant differences to dipyridamole or 2-PAA, respectively, Student's *t*-test: ∗, # $P < 0.05$, ## $P < 0.01$, ∗∗∗ $P < 0.001$.

lyse the gap junction coupling via dye transfer, using gold nanoparticle-mediated laser perforation to introduce the dye into the cells (Chapter 3, Begandt *et al.* 2015).

4.4 Applicability of GNOME LP/dye transfer in complex endothelial cell culture models

The scrape loading/dye transfer technique is limited to analysing cells that are robust enough for the mechanically challenging scraping and is usually applied in two-dimensional cell culture systems. For the analysis of gap junction coupling in complex tissue-like cell culture systems the development of new techniques is necessary. Gold nanoparticle-mediated laser perforation (GNOME LP) has proved to be a cell-friendly method to deliver various molecules into cells (Heinemann *et al.* 2013, 2014, Kalies *et al.* 2013). In general, high cell viabilities have been found after GNOME LP, ranging above 80-90 % (Kalies *et al.* 2013, Heinemann *et al.* 2013, Schomaker *et al.* 2014, 2015). Many studies have shown that relatively large gold nanoparticles as used for the dye transfer experiments (diameter 200 nm) were well tolerated by cells and did not exhibit profound cytotoxic properties (Pan *et al.* 2007, Connor *et al.* 2005, Schomaker *et al.* 2014, 2015, Krawinkel *et al.* 2016). Additionally, in our experiments the incubation period with the gold nanoparticles could be kept short (3 h, Chapter 3, Begandt *et al.* 2015, Heinemann *et al.* 2013, Kalies *et al.* 2013). The mechanisms by which the gold nanoparticles enable the temporal perforation of the cell membrane through a weakly focused laser beam is still under investigation (Kalies *et al.* 2015, Schomaker *et al.* 2015). It has been shown that thermal as well as plasmon resonance effects are involved in the membrane permeabilisation (Heinemann *et al.* 2013, Schomaker *et al.* 2015). Likewise, it is not known how long the cells should be permeabilised to allow efficient dye uptake without detrimental effects. However, as Lucifer yellow that was used to analyse the gap junction coupling is a small molecule (443 Da) it can efficiently be introduced into cells with GNOME LP using low laser power (Schomaker *et al.* 2014). This reduces the probability of unwanted stress-induced effects on the analysed cells. Therefore, after adapting the experimental parameters laser power and scanning velocity the GNOME LP/dye transfer (GNOME LP/DT) method could be applied to analyse the gap junction coupling.

The GNOME LP/DT method displayed similar results as the scrape loading/dye transfer method (Chapter 3, Begandt *et al.* 2015). Therefore, GNOME LP/DT promised to be a new approach to analyse the gap junction coupling in diverse cell culture systems, for example on soft and flexible growth surfaces or in three-dimensional cell culture systems. Co-culturing cerebral microvascular endothelial cells with astrocytes and/or pericytes better resembles the *in vivo* situation because the other cells of the neurovascular unit are known to influence the barrier properties of the endothelial

cells (Wilhelm *et al.* 2011, Hawkins *et al.* 2015, Thomsen *et al.* 2015, Abbott *et al.* 2006). Three-dimensional cell culture can further improve the cell culture models (Cucullo *et al.* 2008, 2011, Adriani *et al.* 2017). The different cell types could be cultivated in extracellular matrix gels like collagen I or matrigel (Bogorad *et al.* 2015, McCoy *et al.* 2016, Allen *et al.* 2011, Adriani *et al.* 2017), or the endothelial cells could be cultured in blood vessel-like structures under flow conditions (Wong & Searson 2014, Bogorad *et al.* 2015, Cucullo *et al.* 2008, 2011).

With GNOME LP/DT it was possible to analyse the gap junction coupling in cells grown in three-dimensional cell culture systems. GM-7373 cells were cultured in glass capillaries to form pseudo-vessels and GNOME LP/DT experiments were performed (Chapter 3, Begandt *et al.* 2015). The cells successfully incorporated the dye along the laser perforation line and the width of the stained cell band was significantly narrowed when the experiments were performed in presence of the gap junction blocker carbenoxolone (CBX, Chapter 3, Begandt *et al.* 2015). This additionally opens the possibility to apply the GNOME LP/DT method in *ex vivo* settings, for example in isolated blood vessels, or directly *in vivo*. Considering the non-focused laser system (Heinemann *et al.* 2013) the perforation of whole blood vessels should be possible without major changes. An adaption of the image acquisition, for example integration of a microscopic imaging system adapted to tissue imaging, could be necessary (Chapter 3, Begandt *et al.* 2015).

Regarding alternative growth surfaces it was possible to directly apply the GNOME LP/DT technique without modifications to cells grown in transwell inserts on porous polyethylene terephthalate (PET) membranes (Figure 4.7). In this set-up a co-culture of different cell types would be possible. For blood-brain barrier models endothelial cells could be cultured inside the transwell inserts and astrocytes or pericytes in the well bottom or on the abluminal side of the transwell inserts (Figure 4.7 A, Thomsen *et al.* 2015, Nakagawa *et al.* 2009, Hatherell *et al.* 2011, Zhang *et al.* 2011, Wilhelm *et al.* 2011). The gap junction coupling of only the cells cultivated on one side of the insert could be analysed with GNOME LP/DT as shown for hCMEC/D3 cells cultured inside transwell inserts (Figure 4.7 B). The dye diffusion distance after GNOME LP/DT was clearly reduced in cells perforated in the presence of CBX (Figure 4.7 B). This set-up would enable the combination of different physiological assays in one cell culture, for example analysis of transepithelial or transendothelial resistance measurements and gap junction coupling of the same cells grown in transwell inserts. The possibility to perform different physiological analyses within one single cell culture would be advantegeous for cells that are costly to isolate and thus precious, for example primary cells (Nakagawa *et al.* 2009,

Thomsen *et al.* 2015). These cell culture systems would also open the possibility to link gap junction and tight junction function and for example analyse a co-regulation of tight junctions and gap junctions as observed in blood-brain barrier endothelial cells by Nagasawa *et al.* (2006). A co-regulation of gap junctions and tight junctions could also be important in other blood-tissue barriers, for example the blood-testis or blood-retinal barrier (Li *et al.* 2013) or in epithelial barriers, for example in the colon (Choi *et al.* 2017) or the lung (Schlingmann *et al.* 2015).
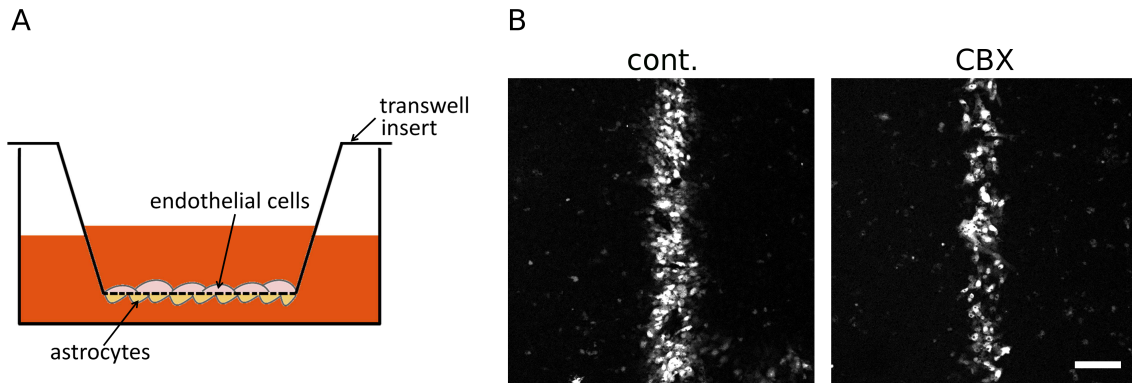

Figure 4.7: GNOME LP/DT in transwell inserts. A) Schematic drawing of a co-culture model of blood-brain barrier-forming microvascular endothelial cells grown inside a transwell insert and astrocytes cultured on the abluminal side of the porous PET membrane (dashed line). B) Dye diffusion after GNOME LP/DT experiments in hCMEC/D3 cerebral endothelial cells grown in transwell inserts, control (cont.) or in presence of CBX. Scale bar represents 100 µm.

Since adenosine receptors have been proposed as targets for blood-brain barrier permeabilisation for drug delivery (Carman *et al.* 2011, Gao *et al.* 2014, Kim & Bynoe 2015, Bynoe *et al.* 2015), a possible influence of adenosine receptor-dependent gap junction regulation in this context could be analysed. Furthermore, the role of especially A_{2B} adenosine receptor activation in preventing vascular leakage and increasing vascular barrier function is well-decribed (Section 4.1, Lennon *et al.* 1998, Eltzschig *et al.* 2003, Eckle *et al.* 2008, Zhou *et al.* 2011, Umapathy *et al.* 2010). The A_{2B} adenosine receptor-dependent regulation of gap junctions found in microvascular cerebral endothelial cells (Chapter 2, Bader *et al.* 2017) could be linked to these events. The role of gap junction coupling in vascular barrier modulation after A_{2B} adenosine receptor activation could be analysed with GNOME LP/DT in transwell inserts and facilitate a deeper understanding of the detailed signalling mechanisms regulating vascular barrier function in different tissue.

Bibliography

Abbaci M., Barberi-Heyob M., Blondel W., Guillemin F. & Didelon J. (2008), Advantages and limitations of commonly used methods to assay the molecular permeability of gap junctional intercellular communication, *Biotechniques* **45**(1), 33–52, 56–62.

Abbott N. J., Rönnbäck L. & Hansson E. (2006), Astrocyte–endothelial interactions at the blood–brain barrier, *Nat Rev Neurosci* **7**(1), 41–53.

Adriani G., Ma D., Pavesi A., Kamm R. D. & Goh E. L. K. (2017), A 3D neurovascular microfluidic model consisting of neurons, astrocytes and cerebral endothelial cells as a blood-brain barrier, *Lab Chip* **17**(3), 448–459.

Allen P., Melero-Martin J. & Bischoff J. (2011), Type I collagen, fibrin and PuraMatrix matrices provide permissive environments for human endothelial and mesenchymal progenitor cells to form neovascular networks, *J Tissue Eng Regen Med* **5**(4), e74–e86.

Ampey B. C., Morschauser T. J., Ramadoss J. & Magness R. R. (2016), Domain-Specific Partitioning of Uterine Artery Endothelial Connexin43 and Caveolin-1, *Hypertension* **68**(4), 982–988.

Antonioli L., Blandizzi C., Pacher P. & Haskó G. (2013), Immunity, inflammation and cancer: A leading role for adenosine, *Nat Rev Cancer* **13**(12), 842–857.

Babica P., Sovadinová I. & Upham B. L. (2016), Scrape Loading/Dye Transfer Assay, *Methods Mol Biol* **1437**, 133–144.

Bader A., Bintig W., Begandt D., Klett A., Siller I. G., Gregor C., Schaarschmidt F., Weksler B., Romero I., Couraud P.-O., Hell S. W. & Ngezahayo A. (2017), Adenosine receptors regulate gap junction coupling of the human cerebral microvascular endothelial cells hCMEC/D3 by Ca^{2+} influx through cyclic nucleotide-gated channels, *J Physiol* **595**(8), 2497–2517.

Balijepalli R. C., Foell J. D., Hall D. D., Hell J. W. & Kamp T. J. (2006), Localization of cardiac L-type Ca^{2+} channels to a caveolar macromolecular signaling complex is required for β2-adrenergic regulation, *Proc Natl Acad Sci* **103**(19), 7500–7505.

Ballarín M., Fredholm B. B., Ambrosio S. & Mahy N. (1991), Extracellular levels of adenosine and its metabolites in the striatum of awake rats: Inhibition of uptake and metabolism, *Acta Physiol Scand* **142**(1), 97–103.

Barnes A. P., Livera G., Huang P., Sun C., O'Neal W. K., Conti M., Stutts M. J. & Milgram S. L. (2005), Phosphodiesterase 4D Forms a cAMP Diffusion Barrier at the Apical Membrane of the Airway Epithelium, *J Biol Chem* **280**(9), 7997–8003.

Begandt D., Bader A., Antonopoulos G. C., Schomaker M., Kalies S., Meyer H., Ripken T. & Ngezahayo A. (2015), Gold nanoparticle-mediated (GNOME) laser perforation: a new method for a high-throughput analysis of gap junction intercellular coupling, *J Bioenerg Biomembr* **47**(5), 441–449.

Begandt D., Bader A., Dreyer L., Eisert N., Reeck T. & Ngezahayo A. (2013a), Biphasic increase of gap junction coupling induced by dipyridamole in the rat aortic A-10 vascular smooth muscle cell line, *J Cell Commun Signal* **7**(2), 151–160.

Begandt D., Bader A., Gerhard L., Lindner J., Dreyer L., Schlingmann B. & Ngezahayo A. (2013b), Dipyridamole-related enhancement of gap junction coupling in the GM-7373 aortic endothelial cells correlates with an increase in the amount of connexin 43 mRNA and protein as well as gap junction plaques, *J Bioenerg Biomembr* **45**(4), 409–419.

Begandt D., Bintig W., Oberheide K., Schlie S. & Ngezahayo A. (2010), Dipyridamole increases gap junction coupling in bovine GM-7373 aortic endothelial cells by a cAMP-protein kinase A dependent pathway, *J Bioenerg Biomembr* **42**(1), 79–84.

Begandt D., Good M. E., Keller A. S., DeLalio L. J., Rowley C., Isakson B. E. & Figueroa X. F. (2017), Pannexin channel and connexin hemichannel expression in vascular function and inflammation, *BMC Cell Biol* **18**(Suppl 1), 2.

Berthoud V. M., Minogue P. J., Laing J. G. & Beyer E. C. (2004), Pathways for degradation of connexins and gap junctions, *Cardiovasc Res* **62**(2), 256–267.

Berthoud V. M. & Ngezahayo A. (2017), Focus on lens connexins, *BMC Cell Biol* **18**(Suppl 1), 6.

Beyer E. C. & Berthoud V. M. (2009), The Family of Connexin Genes, in Harris A. L. & Locke D., ed., *Connexins: A Guide*, Humana Press, New York, 3–26.

Bierings R., Hellen N., Kiskin N., Knipe L., Fonseca A.-V., Patel B., Meli A., Rose M., Hannah M. J. & Carter T. (2012), The interplay between the Rab27A effectors Slp4-a and MyRIP controls hormone-evoked Weibel-Palade body exocytosis, *Blood* **120**(13), 2757–2767.

Blackburn J. P., Peters N. S., Yeh H.-I., Rothery S., Green C. R. & Severs N. J. (1995), Upregulation of Connexin43 Gap Junctions During Early Stages of Human Coronary Atherosclerosis, *Arterioscler Thromb Vasc Biol* **15**(8), 1219–1228.

Blackburn M. R., Vance C. O., Morschl E. & Wilson C. N. (2009), Adenosine receptors and inflammation, in Wilson C. N. & Mustafa S. J., ed., *Handbook of Experimental Pharmacology: Adenosine Receptors in Health and Disease*, Vol. 193, Springer Verlag Berlin Heidelberg, 215–269.

Boassa D., Solan J. L., Papas A., Thornton P., Lampe P. D. & Sosinsky G. E. (2010), Trafficking and Recycling of the Connexin43 Gap Junction Protein during Mitosis, *Traffic* **11**(11), 1471–1486.

Bodin P., Bailey D. & Burnstock G. (1991), Increased flow-induced ATP release from isolated vascular endothelial cells but not smooth muscle cells, *Br J Pharmacol* **103**(1), 1203–1205.

Bodin P. & Burnstock G. (2001), Evidence that release of adenosine triphosphate from endothelial cells during increased shear stress is vesicular, *J Cardiovasc Pharmacol* **38**(6), 900–908.

Bogorad M. I., DeStefano J., Karlsson J., Wong A. D., Gerecht S. & Searson P. C. (2015), Review: *In vitro* microvessel models, *Lab Chip* **15**(22), 4242–4255.

Bouma M. G., van den Wildenberg F. A. & Buurman W. A. (1996), Adenosine inhibits cytokine release and expression of adhesion molecules by activated human endothelial cells, *Am J Physiol* **270**(2 Pt 1), C522–529.

Brady J. D., Rich T. C., Le X., Stafford K., Fowler C. J., Lynch L., Karpen J. W., Brown R. L. & Martens J. R. (2004), Functional Role of Lipid Raft Microdomains in Cyclic Nucleotide-Gated Channel Activation, *Mol Pharmacol* **65**(3), 503–511.

Brink P. R., Valiunas V., Gordon C., Rosen M. R. & Cohen I. S. (2012), Can gap junctions deliver?, *Biochim Biophys Acta* **1818**(8), 2076–2081.

Burnstock G. & Knight G. E. (2017), Cell culture: Complications due to mechanical release of ATP and activation of purinoceptors, *Cell Tissue Res* **370**(1), 1–11.

Bynoe M. S., Viret C., Yan A. & Kim D. G. (2015), Adenosine receptor signaling: a key to opening the blood-brain door, *Fluids Barriers CNS* **12**, 20.

Caporarello N., Olivieri M., Cristaldi M., Scalia M., Toscano M. A., Genovese C., Addamo A., Salmeri M., Lupo G. & Anfuso C. D. (2017), Blood–Brain Barrier in a *Haemophilus influenzae* Type a In Vitro Infection: Role of Adenosine Receptors A_{2A} and A_{2B} , *Mol Neurobiol* 1–16.

Carman A. J., Mills J. H., Krenz A., Kim D. G. & Bynoe M. S. (2011), Adenosine receptor signaling modulates permeability of the blood-brain barrier, *J Neurosci* **31**(37), 13272–13280.

Chadjichristos C. E., Scheckenbach K. E. L., van Veen T. A. B., Richani Sarieddine M. Z., de Wit C., Yang Z., Roth I., Bacchetta M., Viswambharan H., Foglia B., Dudez T., van Kempen M. J. A., Coenjaerts F. E. J., Miquerol L., Deutsch U., Jongsma H. J., Chanson M. & Kwak B. R. (2010), Endothelial-specific deletion of connexin40 promotes atherosclerosis by increasing CD73-dependent leukocyte adhesion, *Circulation* **121**(1), 123–131.

Chen C. H., Mayo J. N., Gourdie R. G., Johnstone, Isakson B. E. & Bearden S. E. (2015), The connexin 43/ZO-1 complex regulates cerebral endothelial F-actin architecture and migration, *Am J Physiol Cell Physiol* **309**(9), C600–607.

Chen J.-F., Eltzschig H. K. & Fredholm B. B. (2013), Adenosine receptors as drug targets–what are the challenges?, *Nat Rev Drug Discov* **12**(4), 265–286.

Cheng C. C., Yang Y. L., Liao K. H. & Lai T. W. (2016), Adenosine receptor agonist NECA increases cerebral extravasation of fluorescein and low molecular weight dextran independent of blood-brain barrier modulation, *Sci Rep* **6**, 23882.

Choi W., Yeruva S. & Turner J. R. (2017), Contributions of intestinal epithelial barriers to health and disease, *Exp Cell Res* **358**(1), 71–77.

Choukèr A., Ohta A., Martignoni A., Lukashev D., Zacharia L. C., Jackson E. K., Schnermann J., Ward J. M., Kaufmann I., Klaunberg B., Sitkovsky M. V. & Thiel M. (2012), *In vivo* hypoxic preconditioning protects from warm liver ischemia-reperfusion injury through the adenosine A_{2B} receptor, *Transplantation* **94**(9), 894–902.

Connor E. E., Mwamuka J., Gole A., Murphy C. J. & Wyatt M. D. (2005), Gold Nanoparticles Are Taken Up by Human Cells but Do Not Cause Acute Cytotoxicity, *Small* **1**(3), 325–327.

Cooper D. M. F. & Tabbasum V. G. (2014), Adenylate cyclase-centred microdomains, *Biochem J* **462**(2), 199–213.

Correale J. & Villa A. (2009), Cellular elements of the blood-brain barrier, *Neurochem Res* **34**(12), 2067–2077.

Cronin M., Anderson P. N., Cook J. E., Green C. R. & Becker D. L. (2008), Blocking connexin43 expression reduces inflammation and improves functional recovery after spinal cord injury, *Mol Cell Neurosci* **39**(2), 152–160.

Cucullo L., Couraud P. O., Weksler B., Romero I. A., Hossain M., Rapp E. & Janigro D. (2008), Immortalized human brain endothelial cells and flow-based vascular modeling: A marriage of convenience for rational neurovascular studies, *J Cereb Blood Flow Metab* **28**(2), 312–328.

Cucullo L., Marchi N., Hossain M. & Janigro D. (2011), A dynamic *in vitro* BBB model for the study of immune cell trafficking into the central nervous system, *J Cereb Blood Flow Metab* **31**(2), 767–777.

Czupalla C. J., Liebner S. & Devraj K. (2014), In vitro models of the blood-brain barrier, in Milner R., ed., *Cerebral Angiogenesis: Methods and Protocols*, Humana Press, New York, 415–437.

Dahl G. (2015), ATP release through pannexon channels, *Philos Trans R Soc Lond B Biol Sci* **370**(1672), 20140191.

D'Ambrosi N. & Volonté C. (2013), Metabotropic Purinergic Receptors in Lipid Membrane Microdomains, *Curr Med Chem* **20**(1), 56–63.

Davies J., Karmouty-Quintana H., Le T. T., Chen N.-Y., Weng T., Luo F., Molina J., Moorthy B. & Blackburn M. R. (2014), Adenosine promotes vascular barrier function in hyperoxic lung injury, *Physiol Rep* **2**(9), e12155.

de Bock M., Culot M., Wang N., da C. A., Decrock E., Bol M., Bultynck G., Cecchelli R. & Leybaert L. (2012), Low extracellular Ca^{2+} conditions induce an increase in brain endothelial permeability that involves intercellular Ca^{2+} waves, *Brain Res* **1487**, 78–87.

de Bock M., Decrock E., Wang N., Bol M., Vinken M., Bultynck G. & Leybaert L. (2014), The dual face of connexin-based astroglial Ca^{2+} communication: A key player in brain physiology and a prime target in pathology, *Biochim Biophys Acta* **1843**(10), 2211–2232.

de Bock M., Leybaert L. & Giaume C. (2017), Connexin Channels at the Glio-Vascular Interface: Gatekeepers of the Brain, *Neurochem Res* **42**(9), 2519–2536.

de Wit C., Roos F., Bolz S.-S., Kirchhoff S., Kruger O., Willecke K. & Pohl U. (2000), Impaired Conduction of Vasodilation Along Arterioles in Connexin40-Deficient Mice, *Circ Res* **86**(6), 649–655.

Derangeon M., Bourmeyster N., Plaisance I., Pinet-Charvet C., Chen Q., Duthe F., Popoff M. R., Sarrouilhe D. & Hervé J.-C. (2008), RhoA GTPase and F-actin dynamically regulate the permeability of Cx43-made channels in rat cardiac myocytes, *J Biol Chem* **283**(45), 30754–30765.

Dhein S. (2004), Pharmacology of gap junctions in the cardiovascular system, *Cardiovasc Res* **62**(2), 287–298.

Dhein S., Gärtner C., Georgieff C., Salameh A., Schlegel F. & Mohr F.-W. (2015), Effects of isoprenaline on endothelial connexins and angiogenesis in a human endothelial cell culture system, *Naunyn Schmiedebergs Arch Pharmacol* **388**(1), 101–108.

Ding X.-Q., Fitzgerald J. B., Matveev A. V., McClellan M. E. & Elliott M. H. (2008), Functional Activity of Photoreceptor Cyclic Nucleotide-Gated Channels Is Dependent on the Integrity of Cholesterol- and Sphingolipid-Enriched Membrane Domains, *Biochem* **47**(12), 3677–3687.

Donaldson P., Kistler J. & Mathias R. T. (2001), Molecular solutions to mammalian lens transparency, *News Physiol Sci* **16**(4-6), 118–123.

Du X., Ou X., Song T., Zhang W., Cong F., Zhang S. & Xiong Y. (2015), Adenosine A_{2B} receptor stimulates angiogenesis by inducing VEGF and eNOS in human microvascular endothelial cells, *Exp Biol Med (Maywood)* **240**(11), 1472–1479.

Eckle T., Faigle M., Grenz A., Laucher S., Thompson L. F. & Eltzschig H. K. (2008), A_{2B} adenosine receptor dampens hypoxia-induced vascular leak, *Blood* **111**(4), 2024–2035.

Eckle T., Krahn T., Grenz A., Köhler D., Mittelbronn M., Ledent C., Jacobson M. A., Osswald H., Thompson L. F., Unertl K. & Eltzschig H. K. (2007), Cardioprotection by ecto-5'-nucleotidase (CD73) and A_{2B} adenosine receptors, *Circulation* **115**(12), 1581–1590.

Eisert W. G. (2006), Dipyridamole, in Michelson A. D., ed., *Platelets*, 2nd edn, Academic Press, Amsterdam, 1165–1179.

Eltzschig H. K. (2009), Adenosine: an old drug newly discovered, *Anesthesiology* **111**(4), 904–915.

Eltzschig H. K., Eckle T., Mager A., Küper N., Karcher C., Weissmüller T., Boengler K., Schulz R., Robson S. C. & Colgan S. P. (2006), ATP Release From Activated Neutrophils Occurs via Connexin 43 and Modulates Adenosine-Dependent Endothelial Cell Function, *Circ Res* **99**(10), 1100–1108.

Eltzschig H. K., Ibla J. C., Furuta G. T., Leonard M. O., Jacobson K. A., Enjyoji K., Robson S. C. & Colgan S. P. (2003), Coordinated adenine nucleotide phosphohydrolysis and nucleoside signaling in posthypoxic endothelium: role of ectonucleotidases and adenosine A_{2B} receptors, *J Exp Med* **198**(5), 783–796.

Eugenin E. A., Basilio D., Sáez J. C., Orellana J. A., Raine C. S., Bukauskas F., Bennett M. V. L. & Berman J. W. (2012), The Role of Gap Junction Channels During Physiologic and Pathologic Conditions of the Human Central Nervous System, *J Neuroimmune Pharmacol* **7**(3), 499–518.

Falk M. M., Bell C. L., Kells Andrews R. M. & Murray S. A. (2016), Molecular mechanisms regulating formation, trafficking and processing of annular gap junctions, *BMC Cell Biol* **17**(Suppl 1), 22.

Feinstein W. P., Zhu B., Leavesley S. J., Sayner S. L. & Rich T. C. (2012), Assessment of cellular mechanisms contributing to cAMP compartmentalization in pulmonary microvascular endothelial cells, *Am J Physiol Cell Physiol* **302**(6), C839–852.

Feoktistov I., Goldstein A. E., Ryzhov S., Zeng D., Belardinelli L., Voyno-Yasenetskaya T. & Biaggioni I. (2002), Differential expression of adenosine receptors in human

endothelial cells: role of A_{2B} receptors in angiogenic factor regulation, *Circ Res* **90**(5), 531–538.

Figueroa X. F. & Duling B. R. (2009), Gap Junctions in the Control of Vascular Function, *Antioxid Redox Signal* **11**(2), 251–266.

Figueroa X. F., Isakson B. E. & Duling B. R. (2006), Vascular gap junctions in hypertension, *Hypertension* **48**(5), 804–811.

Foote C. I., Zhou L., Zhu X. & Nicholson B. J. (1998), The Pattern of Disulfide Linkages in the Extracellular Loop Regions of Connexin 32 Suggests a Model for the Docking Interface of Gap Junctions, *J Cell Biol* **140**(5), 1187–1197.

Frampton J. (2013), *Synaptotagmins and Weibel-Palade Body Exocytosis in Human Endothelial Cells*, Phd Thesis, National Institute for Medical Research, Mill Hill, London.

Fredholm B. B. (2007), Adenosine, an endogenous distress signal, modulates tissue damage and repair, *Cell Death Differ* **14**(7), 1315–1323.

Fredholm B. B., IJzerman A. P., Jacobson K. A., Klotz K.-N. & Linden J. (2001b), International Union of Pharmacology. XXV. Nomenclature and Classification of Adenosine Receptors, *Pharmacol Rev* **53**(4), 527–552.

Fredholm B. B., Irenius E., Kull B. & Schulte G. (2001a), Comparison of the potency of adenosine as an agonist at human adenosine receptors expressed in Chinese hamster ovary cells, *Biochem Pharmacol* **61**(4), 443–448.

Gaietta G., Deerinck T. J., Adams S. R., Bouwer J., Tour O., Laird D. W., Sosinsky G. E., Tsien R. Y. & Ellisman M. H. (2002), Multicolor and Electron Microscopic Imaging of Connexin Trafficking, *Science* **296**(5567), 503–507.

Gao X., Qian J., Zheng S., Changyi Y., Zhang J., Ju S., Zhu J. & Li C. (2014), Overcoming the blood-brain barrier for delivering drugs into the brain by using adenosine receptor nanoagonist, *ACS Nano* **8**(4), 3678–3689.

Gärtner C., Ziegelhöffer B., Kostelka M., Stepan H., Mohr F.-W. & Dhein S. (2012), Knock-down of endothelial connexins impairs angiogenesis, *Pharmacol Res* **65**(3), 347–357.

Giepmans B. N. G. (2004), Gap junctions and connexin-interacting proteins, *Cardiovasc Res* **62**(2), 233–245.

Green C. R. & Nicholson L. F. (2008), Interrupting the inflammatory cycle in chronic diseases–do gap junctions provide the answer?, *Cell Biol Int* **32**(12), 1578–1583.

Gromnicova R., Davies H. A., Sreekanthreddy P., Romero I. A., Lund T., Im Roitt, Phillips J. B. & Male D. K. (2013), Glucose-coated gold nanoparticles transfer across human brain endothelium and enter astrocytes *in vitro*, *PLoS One* **8**(12), e81043.

Haefliger J.-A., Nicod P. & Meda P. (2004), Contribution of connexins to the function of the vascular wall, *Cardiovasc Res* **62**(2), 345–356.

Hamada K., Takuwa N., Yokoyama K. & Takuwa Y. (1998), Stretch Activates Jun N-terminal Kinase/Stress-activated Protein Kinase in Vascular Smooth Muscle Cells through Mechanisms Involving Autocrine ATP Stimulation of Purinoceptors, *J Biol Chem* **273**(11), 6334–6340.

Haskó G. & Cronstein B. N. (2004), Adenosine: An endogenous regulator of innate immunity, *Trends Immunol* **25**(1), 33–39.

Haskó G., Linden J., Cronstein B. & Pacher P. (2008), Adenosine receptors: Therapeutic aspects for inflammatory and immune diseases, *Nat Rev Drug Discov* **7**(9), 759–770.

Hassanian S. M., Dinarvand P. & Rezaie A. R. (2014), Adenosine regulates the proinflammatory signaling function of thrombin in endothelial cells, *J Cell Physiol* **229**(9), 1292–1300.

Hatherell K., Couraud P.-O., Romero I. A., Weksler B. & Pilkington G. J. (2011), Development of a three-dimensional, all-human *in vitro* model of the blood–brain barrier using mono-, co-, and tri-cultivation Transwell models, *J Neurosci Meth* **199**(2), 223–229.

Hawkins B. T., Grego S. & Sellgren K. L. (2015), Three-dimensional culture conditions differentially affect astrocyte modulation of brain endothelial barrier function in response to transforming growth factor β1, *Brain Res* **1608**, 167–176.

Heinemann D., Kalies S., Schomaker M., Ertmer W., Murua Escobar H., Meyer H. & Ripken T. (2014), Delivery of proteins to mammalian cells via gold nanoparticle mediated laser transfection, *Nanotechnology* **25**(24), 245101.

Heinemann D., Schomaker M., Kalies S., Schieck M., Carlson R., Murua Escobar H., Ripken T., Meyer H. & Heisterkamp A. (2013), Gold nanoparticle mediated laser transfection for efficient siRNA mediated gene knock down, *PLoS One* **8**(3), e58604.

Hervé J.-C., Derangeon M., Sarrouilhe D. & Bourmeyster N. (2014), Influence of the scaffolding protein Zonula Occludens (ZOs) on membrane channels, *Biochim Biophys Acta* **1838**(2), 595–604.

Hervé J.-C., Derangeon M., Sarrouilhe D., Giepmans B. N. G. & Bourmeyster N. (2012), Gap junctional channels are parts of multiprotein complexes, *Biochim Biophys Acta* **1818**(8), 1844–1865.

Hinz S., Lacher S. K., Seibt B. F. & Müller C. E. (2014), BAY60-6583 acts as a partial agonist at adenosine A_{2B} receptors, *J Pharmacol Exp Ther* **349**(3), 427–436.

Ho M.-F. & Rose'Meyer R. B. (2013), Vascular Adenosine Receptors; Potential Clinical Applications, *Curr Vasc Pharmacol* **11**(3), 327–337.

Huang P., Trotter K., Boucher R. C., Milgram S. L. & Stutts M. J. (2000), PKA holoenzyme is functionally coupled to CFTR by AKAPs, *Am J Physiol Cell Physiol* **278**(2), C417–422.

Hunter A. W., Barker R. J., Zhu C. & Gourdie R. G. (2005), Zonula occludens-1 alters connexin43 gap junction size and organization by influencing channel accretion, *Mol Biol Cell* **16**(12), 5686–5698.

Isabel C., Calvet D. & Mas J.-L. (2016), Stroke prevention, *Press Med* **45**(12, Part 2), e457 – e471.

Isshiki M., Nishimoto M., Mizuno R. & Fujita T. (2013), FRET-based sensor analysis reveals caveolae are spatially distinct Ca^{2+} stores in endothelial cells, *Cell Calcium* **54**(6), 395–403.

Jacobson K. A. & Gao Z.-G. (2006), Adenosine receptors as therapeutic targets, *Nat Rev Drug Discov* **5**(3), 247–264.

Jarvius M., Paulsson J., Weibrecht I., Leuchowius K.-J., Andersson A.-C., Wählby C., Gullberg M., Botling J., Sjöblom T., Markova B., Ostman A., Landegren U. & Söderberg O. (2007), *In situ* detection of phosphorylated platelet-derived growth factor receptor β using a generalized proximity ligation method, *Mol Cell Proteomics* **6**(9), 1500–1509.

Johnson A. M., Roach J. P., Hu A., Stamatovic S. M., Zochowski M. R., Keep R. F. & Andjelkovic A. V. (2018), Connexin 43 gap junctions contribute to brain endothelial

barrier hyperpermeability in familial cerebral cavernous malformations type III by modulating tight junction structure, *FASEB J* fj.201700699R.

Johnstone S., Isakson B. & Locke D. (2009), Biological and biophysical properties of vascular connexin channels, *Int Rev Cell Mol Biol* **278**, 69–118.

Jordan K., Chodock R., Hand A. R. & Laird D. W. (2001), The origin of annular junctions: a mechanism of gap junction internalization, *J Cell Sci* **114**(Pt. 4), 763–773.

Kalies S., Antonopoulos G. C., Rakoski M. S., Heinemann D., Schomaker M., Ripken T. & Meyer H. (2015), Investigation of biophysical mechanisms in gold nanoparticle mediated laser manipulation of cells using a multimodal holographic and fluorescence imaging setup, *PLoS One* **10**(4), e0124052.

Kalies S., Heinemann D., Schomaker M., Escobar H. M., Heisterkamp A., Ripken T. & Meyer H. (2013), Plasmonic laser treatment for Morpholino oligomer delivery in antisense applications, *J Biophotonics* **7**(10), 825–833.

Kandasamy K., Escue R., Manna J., Adebiyi A. & Parthasarathi K. (2015), Changes in endothelial connexin 43 expression inversely correlate with microvessel permeability and VE-cadherin expression in endotoxin-challenged lungs, *Am J Physiol Lung Cell Mol Physiol* **309**(6), L584–L592.

Karmouty-Quintana H., Xia Y. & Blackburn M. R. (2013), Adenosine signaling during acute and chronic disease states, *J Mol Med (Berl)* **91**(2), 173–181.

Kim D. G. & Bynoe M. S. (2015), A2A Adenosine Receptor Regulates the Human Blood-Brain Barrier Permeability, *Mol Neurobiol* **52**(1), 664–678.

Kim H.-H. & Liao J. K. (2008), Translational therapeutics of dipyridamole, *Arterioscler Thromb Vasc Biol* **28**(3), s39–42.

Kirchhoff S., Kim J.-S., Hagendorff A., Thönnissen E., Krüger O., Lamers W. H. & Willecke K. (2000), Abnormal Cardiac Conduction and Morphogenesis in Connexin40 and Connexin43 Double-Deficient Mice, *Circ Res* **87**(5), 399–405.

Klotz K. N., Hessling J., Hegler J., Owman C., Kull B., Fredholm B. B. & Lohse M. J. (2000), Comparative pharmacology of human adenosine receptor subtypes - characterization of stably transfected receptors in CHO cells, *Naunyn-Schmiedeberg's Arch Pharmacol* **357**(1), 1–9.

Kong F.-Y., Zhang J.-W., Li R.-F., Wang Z.-X., Wang W.-J. & Wang W. (2017), Unique Roles of Gold Nanoparticles in Drug Delivery, Targeting and Imaging Applications, *Molecules* **22**(9), E1445.

Krattinger N., Capponi A., Mazzolai L., Aubert J. F., Caille D., Nicod P., Waeber G., Meda P. & Haefliger J. A. (2007), Connexin40 regulates renin production and blood pressure, *Kidney Int* **72**(7), 814–822.

Krawinkel J., Torres-Mapa M. L., Werelius K., Heisterkamp A., Rüttermann S., Romanos G. E. & Gerhardt-Szép S. (2016), Gold Nanoparticle-Mediated Delivery of Molecules into Primary Human Gingival Fibroblasts Using ns-Laser Pulses: A Pilot Study, *Materials* **9**(5), E397.

Krüger O., Plum A., Kim J. S., Winterhager E., Maxeiner S., Hallas G., Kirchhoff S., Traub O., Lamers W. H. & Willecke K. (2000), Defective vascular development in Cx45-deficient mice, *Development* **127**(19), 4179–4193.

Kumar N. M. & Gilula N. B. (1996), The gap junction communication channel, *Cell* **84**(3), 381–388.

Kwak B. R., Mulhaupt F., Veillard N., Gros D. B. & Mach F. c. (2002), Altered Pattern of Vascular Connexin Expression in Atherosclerotic Plaques, *Arterioscler Thromb Vasc Biol* **22**(2), 225–230.

Kwak B. R., Veillard N., Pelli G., Mulhaupt F., James R. W., Chanson M. & Mach F. c. (2003), Reduced Connexin43 Expression Inhibits Atherosclerotic Lesion Formation in Low-Density Lipoprotein Receptor\textendashDeficient Mice, *Circulation* **107**(7), 1033–1039.

Laing J. G., Chou B. C. & Steinberg T. H. (2005), ZO-1 alters the plasma membrane localization and function of Cx43 in osteoblastic cells, *J Cell Sci* **118**(Pt 10), 2167–2176.

Laird D. W. (2006), Life cycle of connexins in health and disease, *Biochem J* **394**(Pt 3), 527–543.

Lampe P. D. & Lau A. F. (2004), The effects of connexin phosphorylation on gap junctional communication, *Int J Biochem Cell Biol* **36**(7), 1171–1186.

Langlois S., Cowan K. N., Shao Q., Cowan B. J. & Laird D. W. (2008), Caveolin-1 and -2 interact with connexin43 and regulate gap junctional intercellular communication in keratinocytes, *Mol Biol Cell* **19**(3), 912–928.

Lasley R. D. (2011), Adenosine receptors and membrane microdomains, *Biochim Biophys Acta* **1808**(5), 1284–1289.

Lennon P. F., Taylor C. T., Stahl G. L. & Colgan S. P. (1998), Neutrophil-derived 5'-Adenosine Monophosphate Promotes Endothelial Barrier Function via CD73-mediated Conversion to Adenosine and Endothelial A_{2B} Receptor Activation, *J Exp Med* **188**(8), 1433–1443.

Lewis B. M., Pexa A., Francis K., Verma V., McNicol A. M., Scanlon M., Deussen A., Evans W. H., Rees D. A. & Ham J. (2006), Adenosine stimulates connexin 43 expression and gap junctional communication in pituitary folliculostellate cells, *FASEB J* **20**(14), 2585–2587.

Leybaert L., Lampe P. D., Dhein S., Kwak B. R., Ferdinandy P., Beyer E. C., Laird D. W., Naus C. C., Green C. R. & Schulz R. (2017), Connexins in Cardiovascular and Neurovascular Health and Disease: Pharmacological Implications, *Pharmacol Rev* **69**(4), 396–478.

Li M. W. M., Mruk D. D. & Cheng C. Y. (2013), Gap junctions and blood-tissue barriers, in Cheng C. Y., ed., *Biology and Regulation of Blood-Tissue Barriers*, Springer, New York, 260–280.

Liao Y., Day K. H., Damon D. N. & Duling B. R. (2001), Endothelial cell-specific knockout of connexin 43 causes hypotension and bradycardia in mice, *Proc Natl Acad Sci U S A* **98**(17), 9989–9994.

Linden J. (2011), Chapter 4 - Regulation of Leukocyte Function by Adenosine Receptors, in Jacobson K. A. & Linden J., ed., *Pharmacology of Purine and Pyrimidine Receptors*, Vol. 61 of *Advances in Pharmacology*, Academic Press, 95–114.

Lingwood D. & Simons K. (2010), Lipid Rafts As a Membrane-Organizing Principle, *Science* **327**(5961), 46–50.

Löffler M., Morote-Garcia J. C., Eltzschig S. A., Coe I. R. & Eltzschig H. K. (2007), Physiological Roles of Vascular Nucleoside Transporters, *Arterioscler Thromb Vasc Biol* **27**(5), 1004–1013.

Lohman A. W. & Isakson B. E. (2014), Differentiating connexin hemichannels and pannexin channels in cellular ATP release, *FEBS Lett* **588**(8), 1379–1388.

Lowenstein C. J., Morrell C. N. & Yamakuchi M. (2005), Regulation of Weibel–Palade Body Exocytosis, *Trends Cardiovasc Med* **15**(8), 302–308.

MacDonald P. E., Braun M., Galvanovskis J. & Rorsman P. (2006), Release of small transmitters through kiss-and-run fusion pores in rat pancreatic β cells, *Cell Metab* **4**(4), 283–290.

McCoy M. G., Seo B. R., Choi S. & Fischbach C. (2016), Collagen I hydrogel microstructure and composition conjointly regulate vascular network formation, *Acta Biomater* **44**(Supplement C), 200–208.

Melani A., Am Pugliese & Pedata F. (2014), Adenosine receptors in cerebral ischemia, *Int Rev Neurobiol* **119**, 309–348.

Mills J. H., Alabanza L., Weksler B. B., Couraud P.-O., Romero I. A. & Bynoe M. S. (2011), Human brain endothelial cells are responsive to adenosine receptor activation, *Purinergic Signal* **7**(2), 265–273.

Minshall R. D., Sessa W. C., Stan R. V., Anderson R. G. & Malik A. B. (2003), Caveolin regulation of endothelial function, *Am J Physiol Lung Cell Mol Physiol* **285**(6), L1179–1183.

Molina-Arcas M., Casado F. J. & Pastor-Anglada M. (2009), Nucleoside transporter proteins, *Curr Vasc Pharmacol* **7**(4), 426–434.

Moreno A. P. & Lau A. F. (2007), Gap junction channel gating modulated through protein phosphorylation, *Prog Biophys Mol Biol* **94**(1-2), 107–119.

Nagasawa K., Chiba H., Fujita H., Kojima T., Saito T., Endo T. & Sawada N. (2006), Possible involvement of gap junctions in the barrier function of tight junctions of brain and lung endothelial cells, *J Cell Physiol* **208**(1), 123–132.

Nakagawa S., Deli M. A., Kawaguchi H., Shimizudani T., Shimono T., Kittel Á., Tanaka K. & Niwa M. (2009), A new blood–brain barrier model using primary rat brain endothelial cells, pericytes and astrocytes, *Neurochem Int* **54**(3), 253–263.

Neyton J. & Trautmann A. (1985), Single-channel currents of an intercellular junction, *Nature* **317**(6035), 331–335.

Nguyen M. D., Lee S. T., Ross A. E., Ryals M., Choudhry V. I. & Venton B. J. (2014), Characterization of spontaneous, transient adenosine release in the caudate-putamen and prefrontal cortex, *PLoS One* **9**(1), e87165.

Nguyen M. D. & Venton B. J. (2015), Fast-scan Cyclic Voltammetry for the Characterization of Rapid Adenosine Release, *Comput Struct Biotechnol J* **13**, 47–54.

Nicholson B. J. (2003), Gap junctions - from cell to molecule, *J Cell Sci* **116**(22), 4479–4481.

Nicholson S. M. & Bruzzone R. (1997), Gap junctions: getting the message through, *Curr Biol* **7**(6), R340–R344.

Nielsen M. S., Axelsen L. N., Sorgen P. L., Verma V., Delmar M. & Holstein-Rathlou N.-H. (2012), Gap junctions, *Compr Physiol* **2**(3), 1981–2035.

O'Donnell J. J. I., Birukova A. A., Beyer E. C. & Birukov K. G. (2014), Gap junction protein connexin43 exacerbates lung vascular permeability, *PLoS One* **9**(6), e100931.

Oldendorf W. H., Cornford M. E. & Brown W. J. (1977), The large apparent work capability of the blood-brain barrier: a study of the mitochondrial content of capillary endothelial cells in brain and other tissues of the rat, *Ann Neurol* **1**(5), 409–417.

Olk S., Zoidl G. & Dermietzel R. (2009), Connexins, cell motility, and the cytoskeleton, *Cell Motil Cytoskeleton* **66**(11), 1000–1016.

Opsahl H. & Rivedal E. (2000), Quantitative Determination of Gap Junction Intercellular Communication by Scrape Loading and Image Analysis, *Cell Adhes Commun* **7**(5), 367–375.

Paarmann I., Lye M. F., Lavie A. & Konrad M. (2008), Structural requirements for calmodulin binding to membrane-associated guanylate kinase homologs, *Protein Sci* **17**(11), 1946–1954.

Pan Y., Neuss S., Leifert A., Fischler M., Wen F., Simon U., Schmid G., Brandau W. & Jahnen-Dechent W. (2007), Size-Dependent Cytotoxicity of Gold Nanoparticles, *Small* **3**(11), 1941–1949.

Pani B. & Singh B. B. (2009), Lipid rafts/caveolae as microdomains of calcium signaling, *Cell Calcium* **45**(6), 625–633.

Parthasarathi K., Ichimura H., Monma E., Lindert J., Quadri S., Issekutz A. & Bhattacharya J. (2006), Connexin 43 mediates spread of Ca^{2+} -dependent proinflammatory responses in lung capillaries, *J Clin Invest* **116**(8), 2193–2200.

Pedata F., Corsi C., Melani A., Bordoni F. & Latini S. (2001), Adenosine Extracellular Brain Concentrations and Role of A2A Receptors in Ischemia, *Ann N Y Acad Sci* **939**(1), 74–84.

Phelan P. (2005), Innexins: Members of an evolutionarily conserved family of gap-junction proteins, *Biochim Biophys Acta* **1711**(2), 225–245.

Phillis J. W. (1990), The selective adenosine A2 receptor agonist, CGS 21680, is a potent depressant of cerebral cortical neuronal activity, *Brain Res* **509**(2), 328–330.

Plum A., Hallas G., Magin T., Dombrowski F., Hagendorff A., Schumacher B., Wolpert C., Kim J., Lamers W. H., Evert M., Meda P., Traub O. & Willecke K. (2000), Unique and shared functions of different connexins in mice, *Curr Biol* **10**(18), 1083–1091.

Podgorska M., Kocbuch K. & Pawelczyk T. (2005), Recent advances in studies on biochemical and structural properties of equilibrative and concentrative nucleoside transporters, *Acta Biochim Pol* **52**(4), 749–758.

Pulido I. R., Jahn R. & Gerke V. (2011), VAMP3 is associated with endothelial weibel-palade bodies and participates in their Ca(2+)-dependent exocytosis, *Biochim Biophys Acta* **1813**(5), 1038–1044.

Reaume A. G., de Sousa P. A., Kulkarni S., Langille B. L., Zhu D., Davies T. C., Juneja S. C., Kidder G. M. & Rossant J. (1995), Cardiac malformation in neonatal mice lacking connexin43, *Science* **267**(5205), 1831–1834.

Reeves V. L., Thomas C. M. & Smart E. J. (2012), Lipid Rafts, Caveolae and GPI-Linked Proteins, in Jasmin J. F., Frank P. G. & Lisanti M. P., ed., *Caveolins and Caveolae*, Springer, New York, 3–13.

Rhett J. M. & Gourdie R. G. (2012), The perinexus: A new feature of Cx43 gap junction organization, *Heart Rhythm* **9**(4), 619–623.

Rhett J. M., Jourdan J. & Gourdie R. G. (2011), Connexin 43 connexon to gap junction transition is regulated by zonula occludens-1, *Mol Biol Cell* **22**(9), 1516–1528.

Rich T. C., Fagan K. A., Nakata H., Schaack J., Cooper D. M. & Karpen J. W. (2000), Cyclic nucleotide-gated channels colocalize with adenylyl cyclase in regions of restricted cAMP diffusion, *J Gen Physiol* **116**(2), 147–161.

Rignault S., Haefliger J.-A., Waeber B., Liaudet L. & Feihl F. (2007), Acute inflammation decreases the expression of connexin 40 in mouse lung, *Shock* **28**(1), 78–85.

Robertson J., Lang S., Lambert P. A. & Martin P. E. (2010), Peptidoglycan derived from Staphylococcus epidermidis induces Connexin43 hemichannel activity with consequences on the innate immune response in endothelial cells, *Biochem J* **432**(1), 133–143.

Rothlisberger J. M. & Ovbiagele B. (2015), Antiplatelet therapies for secondary stroke prevention: An update on clinical and cost-effectiveness, *J Comp Eff Res* **4**(4), 377–384.

Rousset M., Cens T., Vanmau N. & Charnet P. (2004), Ca^{2+}-dependent interaction of BAPTA with phospholipids, *FEBS Lett* **576**(1-2), 41–45.

Sai K., Kanno J., Hasegawa R., Trosko J. E. & Inoue T. (2000), Prevention of the down-regulation of gap junctional intercellular communication by green tea in the liver of mice fed pentachlorophenol, *Carcinogenesis* **21**(9), 1671–1676.

Saliez J., Bouzin C., Rath G., Ghisdal P., Desjardins F., Rezzani R., Rodella L. F., Vriens J., Nilius B., Feron O., Balligand J.-L. & Dessy C. (2008), Role of Caveolar Compartmentation in Endothelium-Derived Hyperpolarizing Factor\textendashMediated Relaxation, *Circulation* **117**(8), 1065–1074.

Sarieddine M. Z., Scheckenbach K. E. L., Foglia B., Maass K., Garcia I., Kwak B. R. & Chanson M. (2009), Connexin43 modulates neutrophil recruitment to the lung, *J Cell Mol Med* **13**(11-12), 4560–4570.

Scheckenbach K. E. L., Crespin S., Kwak B. R. & Chanson M. (2011), Connexin channel-dependent signaling pathways in inflammation, *J Vasc Res* **48**(2), 91–103.

Schlingmann B., Molina S. A. & Koval M. (2015), Claudins: Gatekeepers of lung epithelial function, *Semin Cell Dev Biol* **42**, 47–57.

Schomaker M., Heinemann D., Kalies S., Willenbrock S., Wagner S., Nolte I., Ripken T., Murua Escobar H., Meyer H. & Heisterkamp A. (2015), Characterization of nanoparticle mediated laser transfection by femtosecond laser pulses for applications in molecular medicine, *J Nanobiotechnology* **13**, 10.

Schomaker M., Killian D., Willenbrock S., Heinemann D., Kalies S., Ngezahayo A., Nolte I., Ripken T., Junghanss C., Meyer H., Escobar H. M. & Heisterkamp A. (2014), Biophysical effects in off-resonant gold nanoparticle mediated (GNOME) laser transfection of cell lines, primary- and stem cells using fs laser pulses, *J Biophotonics* **8**(8), 646–658.

Schubert A.-L., Schubert W., Spray D. C. & Lisanti M. P. (2002), Connexin Family Members Target to Lipid Raft Domains and Interact with Caveolin-1, *Biochem* **41**(18), 5754–5764.

Sedlakova R., Shivers R. R. & Del Maestro R. F. (1999), Ultrastructure of the blood-brain barrier in the rabbit, *J Submicrosc Cytol Pathol* **31**(1), 149–161.

Segretain D. & Falk M. M. (2004), Regulation of connexin biosynthesis, assembly, gap junction formation, and removal, *Biochim Biophys Acta* **1662**(1-2), 3–21.

Sellgren K. L., Hawkins B. T. & Grego S. (2015), An optically transparent membrane supports shear stress studies in a three-dimensional microfluidic neurovascular unit model, *Biomicrofluidics* **9**(6), 061102.

Shaw R. M., Fay A. J., Puthenveedu M. A., von Zastrow M., Jan Y.-N. & Jan L. Y. (2007), Microtubule plus-end-tracking proteins target gap junctions directly from the cell interior to adherens junctions, *Cell* **128**(3), 547–560.

Shen Q., Wu M. H. & Yuan S. Y. (2009), Endothelial contractile cytoskeleton and microvascular permeability, *Cell Health Cytoskelet* **2009**(1), 43–50.

Shryock J. C. & Belardinelli L. (1997), Adenosine and Adenosine Receptors in the Cardiovascular System: Biochemistry, Physiology, and Pharmacology, *Am J Cardiol* **79**(12, Supplement 1), 2–10.

Simon A. M., Goodenough D. A., Li E. & Paul D. L. (1997), Female infertility in mice lacking connexin 37, *Nature* **385**(6616), 525–529.

Simon A. M., Goodenough D. A. & Paul D. L. (1998), Mice lacking connexin40 have cardiac conduction abnormalities characteristic of atrioventricular block and bundle branch block, *Curr Biol* **8**(5), 295–298.

Simon A. M. & McWhorter A. R. (2003), Role of connexin37 and connexin40 in vascular development, *Cell Commun Adhes* **10**(4-6), 379–385.

Sitaraman S. V., Wang L., Wong M., Bruewer M., Hobert M., Yun C.-H., Merlin D. & Madara J. L. (2002), The Adenosine 2b Receptor Is Recruited to the Plasma Membrane and Associates with E3KARP and Ezrin upon Agonist Stimulation, *J Biol Chem* **277**(36), 33188–33195.

Smyth J. W., Vogan J. M., Buch P. J., Zhang S.-S., Fong T. S., Hong T.-T. & Shaw R. M. (2012), Actin Cytoskeleton Rest Stops Regulate Anterograde Traffic of Connexin 43 Vesicles to the Plasma Membrane, *Circ Res* **110**(7), 978–989.

Söderberg O., Gullberg M., Jarvius M., Ridderstråle K., Leuchowius K. J., Jarvius J., Wester K., Hydbring P., Bahram F., Larsson L. G. & Landegren U. (2006), Direct observation of individual endogenous protein complexes in situ by proximity ligation, *Nat Methods* **3**(12), 995–1000.

Söhl G. & Willecke K. (2004), Gap junctions and the connexin protein family, *Cardiovasc Res* **62**(2), 228–232.

Solan J. L. & Lampe P. D. (2005), Connexin phosphorylation as a regulatory event linked to gap junction channel assembly, *Biochim Biophys Acta* **1711**(2), 154–163.

Song L., Ge S. & Pachter J. S. (2007), Caveolin-1 regulates expression of junction-associated proteins in brain microvascular endothelial cells, *Blood* **109**(4), 1515–1523.

Sreekanthreddy P., Gromnicova R., Davies H., Phillips J., Romero I. A. & Male D. (2015), A three-dimensional model of the human blood-brain barrier to analyse the transport of nanoparticles and astrocyte/endothelial interactions, *F1000Res* **4**, 1279.

Stevenson D., Gunn-Moore F., Campbell P. & Dholakia K. (2010), Transfection by Optical Injection, in Tuchin V., ed., *Handbook of Photonics for Biomedical science*, CRC Press, London, 87–118.

Su V. & Lau A. F. (2014), Connexins: Mechanisms regulating protein levels and intercellular communication, *FEBS Lett* **588**(8), 1212–1220.

Sun C.-X., Zhong H., Mohsenin A., Morschl E., Chunn J. L., Molina J. G., Belardinelli L., Zeng D. & Blackburn M. R. (2006), Role of A_{2b} adenosine receptor signaling in adenosine-dependent pulmonary inflammation and injury, *J Clin Invest* **116**(8), 2173–2182.

Szentmiklósi A. J., Ujfalusi A., Cseppento Á., Nosztray K., Kovacs P. & Szabó J. Z. (1995), Adenosine receptors mediate both contractile and relaxant effects of adenosine in main pulmonary artery of guinea pigs, *Naunyn-Schmiedeberg's Arch Pharmacol* **351**(4), 417–425.

Thévenin A. F., Kowal T. J., Fong J. T., Kells R. M., Fisher C. G. & Falk M. M. (2013), Proteins and mechanisms regulating gap-junction assembly, internalization, and degradation, *Physiology* **28**(2), 93–116.

Thévenin A. F., Margraf R. A., Fisher C. G., Kells-Andrews R. M. & Falk M. M. (2017), Phosphorylation regulates connexin43/ZO-1 binding and release, an important step in gap junction turnover, *Mol Biol Cell* **28**(25), 3595–3608.

Thomsen L. B., Burkhart A. & Moos T. (2015), A Triple Culture Model of the Blood-Brain Barrier Using Porcine Brain Endothelial cells, Astrocytes and Pericytes, *PLoS One* **10**(8), e0134765.

Trosko J. E., Chang C. C., Wilson M. R., Upham B., Hayashi T. & Wade M. (2000), Gap junctions and the regulation of cellular functions of stem cells during development and differentiation, *Methods* **20**(2), 245–264.

Tsai F.-C., Kuo G.-H., Chang S.-W. & Tsai P.-J. (2015), Ca^{2+} signaling in cytoskeletal reorganization, cell migration, and cancer metastasis, *Biomed Res Int* **2015**, 409245.

Umapathy N. S., Fan Z., Zemskov E. A., Alieva I. B., Black S. M. & Verin A. D. (2010), Molecular mechanisms involved in adenosine-induced endothelial cell barrier enhancement, *Vascul Pharmacol* **52**(5), 199–206.

Upham B. L., Park J. S., Babica P., Sovadinova I., Am Rummel, Trosko J. E., Hirose A., Hasegawa R., Kanno J. & Sai K. (2009), Structure-activity-dependent regulation of cell communication by perfluorinated fatty acids using *in vivo* and *in vitro* model systems, *Environ Health Perspect* **117**(4), 545–551.

van Breevoort D., Snijders A. P., Hellen N., Weckhuysen S., van Hooren K. W. E. M., Eikenboom J., Valentijn K., Fernandez-Borja M., Ceulemans B., de Jonghe P.,

Voorberg J., Hannah M., Carter T. & Bierings R. (2014), STXBP1 promotes Weibel-Palade body exocytosis through its interaction with the Rab27A effector Slp4-a, *Blood* **123**(20), 3185–3194.

van der Hoeven D., Wan T. C., Gizewski E. T., Kreckler L. M., Maas J. E., van Orman J., Ravid K. & Auchampach J. A. (2011), A Role for the Low-Affinity A_{2B} Adenosine Receptor in Regulating Superoxide Generation by Murine Neutrophils, *J Pharmacol Exp Ther* **338**(3), 1004–1012.

Vandenbroucke E., Mehta D., Minshall R. & Malik A. B. (2008), Regulation of Endothelial Junctional Permeability, *Ann N Y Acad Sci* **1123**(1), 134–145.

Walker D. L., Vacha S. J., Kirby M. L. & Lo C. W. (2005), Connexin43 deficiency causes dysregulation of coronary vasculogenesis, *Dev Biol* **284**(2), 479–498.

Wang X.-L., Ye D., Peterson T. E., Cao S., Shah V. H., Katusic Z. S., Sieck G. C. & Lee H.-C. (2005), Caveolae targeting and regulation of large conductance Ca(2+)-activated K+ channels in vascular endothelial cells, *J Biol Chem* **280**(12), 11656–11664.

Weiss N., Miller F., Cazaubon S. & Couraud P.-O. (2009), The blood-brain barrier in brain homeostasis and neurological diseases, *Biochim Biophys Acta* **1788**(4), 842–857.

Wilhelm I., Fazakas C. & Krizbai I. A. (2011), *In vitro* models of the blood-brain barrier, *Acta Neurobiol Exp (Wars)* **71**(1), 113–128.

Willebrords J., Crespo Yanguas S., Maes M., Decrock E., Wang N., Leybaert L., Kwak B. R., Green C. R., Cogliati B. & Vinken M. (2016), Connexins and their channels in inflammation, *Crit Rev Biochem Mol Biol* **51**(6), 413–439.

Willecke K., Eiberger J., Degen J., Eckardt D., Romualdi A., Guldenagel M., Deutsch U. & Sohl G. (2002), Structural and functional diversity of connexin genes in the mouse and human genome, *Biol Chem* **383**(5), 725–737.

Winterhager E., Pielensticker N., Freyer J., Ghanem A., Schrickel J. W., Kim J.-S., Behr R., Grümmer R., Maass K., Urschel S., Lewalter T., Tiemann K., Simoni M. & Willecke K. (2007), Replacement of connexin43 by connexin26 in transgenic mice leads to dysfunctional reproductive organs and slowed ventricular conduction in the heart, *BMC Dev Biol* **7**, 26.

Wong A. D. & Searson P. C. (2014), Live-cell imaging of invasion and intravasation in an artificial microvessel platform, *Cancer Res* **74**(17), 4937–4945.

Wong C. W., Burger F., Pelli G., Mach F. & Kwak B. R. (2003), Dual benefit of reduced Cx43 on atherosclerosis in LDL receptor-deficient mice, *Cell Commun Adhes* **10**(4-6), 395–400.

Yang D., Koupenova M., McCrann D. J., Kopeikina K. J., Kagan H. M., Schreiber B. M. & Ravid K. (2008), The A_{2B} adenosine receptor protects against vascular injury, *Proc Natl Acad Sci* **105**(2), 792–796.

Yang D., Zhang Y., Nguyen H. G., Koupenova M., Chauhan A. K., Makitalo M., Jones, St H. C., Seldin D. C., Toselli P., Lamperti E., Schreiber B. M., Gavras H., Wagner D. D. & Ravid K. (2006), The A_{2B} adenosine receptor protects against inflammation and excessive vascular adhesion, *J Clin Invest* **116**(7), 1913–1923.

Yang Y., Qiu Y., Wang W., Xiao W., Liang H., Zhang C., Yang H., Teitelbaum D. H., Sun L.-H. & Yang H. (2014), Adenosine A_{2B} receptor modulates intestinal barrier function under hypoxic and ischemia/reperfusion conditions, *Int J Clin Exp Pathol* **7**(5), 2006–2018.

Yen M. & Saier JR. M. (2007), Gap junctional proteins of animals: The innexin/pannexin superfamily, *Prog Biophys Mol Biol* **94**(1-2), 5–14.

Yuan D., Sun G., Zhang R., Luo C., Ge M., Luo G. & Hei Z. (2015), Connexin 43 expressed in endothelial cells modulates monocyte-endothelial adhesion by regulating cell adhesion proteins, *Mol Med Rep* **12**(5), 7146–7152.

Zhang J., Yang G.-m., Zhu Y., Peng X.-y., Li T. & Liu L.-m. (2015), Role of connexin 43 in vascular hyperpermeability and relationship to rock1-mlc20 pathway in septic rats, *Am J Physiol Lung Cell Mol Physiol* **309**(11), L1323–L1332.

Zhang Z., Chen G., Zhou W., Song A., Xu T., Luo Q., Wang W., Gu X.-s. & Duan S. (2007), Regulated ATP release from astrocytes through lysosome exocytosis, *Nat Cell Biol* **9**(8), 945–953.

Zhang Z., McGoron A. J., Crumpler E. T. & Li C.-Z. (2011), Co-culture based blood-brain barrier *in vitro* model, a tissue engineering approach using immortalized cell lines for drug transport study, *Appl Biochem Biotechnol* **163**(2), 278–295.

Zheng-Fischhöfer Q., Ghanem A., Kim J.-S., Kibschull M., Schwarz G., Schwab J. O., Nagy J., Winterhager E., Tiemann K. & Willecke K. (2006), Connexin31 cannot functionally replace connexin43 during cardiac morphogenesis in mice, *J Cell Sci* **119**(4), 693–701.

Zhou Y., Schneider D. J., Morschl E., Song L., Pedroza M., Karmouty-Quintana H., Le T., Sun C.-X. & Blackburn M. R. (2011), Distinct roles for the A_{2b} adenosine receptor in acute and chronic stages of bleomycin-induced lung injury, *J Immunol* **186**(2), 1097–1106.

Zhu C., Barker R. J., Hunter A. W., Zhang Y., Jourdan J. & Gourdie R. G. (2005), Quantitative Analysis of ZO-1 Colocalization with Cx43 Gap Junction Plaques in Cultures of Rat Neonatal Cardiomyocytes, *Microsc Microanal* **11**(3), 244–248.

Zhu Q. M., Yamakuchi M. & Lowenstein C. J. (2015), SNAP23 Regulates Endothelial Exocytosis of von Willebrand Factor, *PLoS One* **10**(8), e0118737.

Curriculum Vitae

Name	Almke Bader
Date of Birth	24.11.1988
Place of Birth	Pretoria

Education

2013–2018	PhD student, Institute of Biophysics, Leibniz Universität Hannover
2010–2012	Master studies in Life Science, Leibniz Universität Hannover Major subjects: molecular biology, bioprocess technology, Thesis topic: Analysis of the gap junction-dependent communication of blood-brain barrier microvascular endothelial cells and their regulation by dipyridamole
2011	Internship at the Hebrew University of Jerusalem, The Alexander Silberman Institute of Life Sciences, Israel Topic: Bacterial biosensors
2007–2010	Bachelor studies in Life Science, Leibniz Universität Hannover Thesis topic: Investigation of the molecular biological mode of action of dipyridamole on the gap junctional intercellular communication of smooth muscle cells
2007	Gymnasium Großburgwedel, graduation with university-entrance diploma (Abitur)

Publications

Bader A., Bintig W., Begandt D., Klett A., Siller I. G., Gregor C., Schaarschmidt F., Weksler B., Romero I., Couraud P. O., Hell S. W., Ngezahayo A. (2017) Adenosine receptors regulate gap junction coupling of the human cerebral microvascular endothelial cells hCMEC/D3 by Ca^{2+} influx through CNG channels. *J Physiol*, **595**(8): 2497-2517.
doi: 10.1113/JP273150.

Repanas A.*, **Bader A.***, Klett A., Ngezahayo A., Glasmacher B. (2016) The effect of dipyridamole embedded in a drug delivery system made by electrospun nanofibers on aortic endothelial cells. *J Drug Deliv Sci Technol*, **35**: 343-352.
doi: 10.1016/j.jddst.2016.08.011.

Blödow A., Begandt D., **Bader A.**, Becker A., Burghard A., Kühne D., Kral A., Ngezahayo A. (2016) ATP-sensitive K^+ channels (Kir6.1/SUR1) regulate gap junctional coupling in cochlear-supporting cells. *Pflugers Arch*, **468**(7): 1215-1222.
doi: 10.1007/s00424-016-1815-8.

Begandt D.*, **Bader A.***, Antonopoulos G. C., Schomaker M., Kalies S., Meyer H., Ripken T., Ngezahyo A. (2015) Gold nanoparticle-mediated (GNOME) laser perforation: a new method for a high-throughput analysis of gap junction intercellular coupling. *J Bioenerg Biomembr*, **47**(5): 441-449.
doi: 10.1007/s10863-015-9623-y.

Begandt D., **Bader A.**, Gerhard L., Lindner J., Dreyer L., Ngezahayo A. (2013) Dipyridamole-related enhancement of gap junction coupling in the GM-7373 aortic endothelial cells correlates with an increase in the amount of connexin 43 mRNA and protein as well as gap junction plaques. *J Bioenerg Biomembr*, **45**(4): 409-419.
doi: 10.1007/s10863-013-9518-8.

Begandt D., **Bader A.**, Dreyer L., Eisert N., Reeck T., Ngezahayo A. (2013) Biphasic increase of gap junction coupling induced by dipyridamole in the rat aortic A-10 vascular smooth muscle cell line. *J Cell Commun Signal*, **7**(2): 151-160.
doi: 10.1007/s12079-013-0196-4.

* These authors contributed equally.

Oral presentations

Bader A., Bintig W., Klett A., Ngezahayo A. (2017) CNG Channel-Dependent Regulation of Gap Junction Coupling Activated by Adenosine Receptors in Cerebral Microvascular Endothelial Cells. International Gap Junction Conference 2017, Glasgow, United Kingdom.

Bader A., Begandt D., Klett A., Bintig W., Ngezahayo A. (2016) Adenosine Receptors Regulate Gap Junction Coupling in Endothelial Cells by Different Pathways. 95th Annual Meeting of the Deutsche Physiologische Gesellschaft, Lübeck, Germany.

Poster presentations

Ngezahayo A., **Bader A.** (2017) Cyclic nucleotide-gated channels integrate adenosine receptors and gap junction coupling in cerebral microvascular endothelial cells. 96th Annual Meeting of the Deutsche Physiologische Gesellschaft, Greifswald, Germany.

Bader A., Klett A., Schmitt K., Ngezahayo A. (2016) Activation of Adenosine Receptors in Endothelial Cells Increases Connexin 43 Gap Junction Plaques: Analysis of Dynamic Changes in Connexin 43 Synthesis and Localisation. 2016 Annual Meeting of the American Society of Cell Biology, San Francisco, USA.

Klett A., **Bader A.**, Schmitt K., Ngezahayo A. (2016) Evaluation of Dynamic Changes of Connexin43 in Endothelial Cells Using Non-Canonical Amino Acid Tagging. 95th Annual Meeting of the Deutsche Physiologische Gesellschaft, Lübeck, Germany.

Bader A., Begandt D., Klett A., Bintig W., Ngezahayo A. (2015) Regulation of Gap Junction Coupling by Adenosine Receptors in Endothelial Cells. 2015 Annual Meeting of the American Society of Cell Biology, San Diego, USA.

Bader A., Begandt D., Bintig W., Ngezahayo, A. (2015) Gap Junctions in Human Blood-Brain Barrier Endothelial Cells hCMEC/D3 are Functionally Linked to Adenosine Receptors via Cyclic Nucleotide Gated Channels. International Gap Junction Conference 2015, Valparaíso, Chile.

Bader A., Begandt D., Bintig W., Ngezahayo A. (2014) Complex Mechanisms Regulate the Gap Junction Coupling of Blood-Brain Barrier Endothelial Cells by Adenosine Receptor Stimulation. 2014 Annual Meeting of the American Society of Cell Biology, Philadelphia, USA.

Begandt D., **Bader A.**, Lorbeer R., Schomaker M., Kalies S., Meyer H., Ngezahayo A. (2014) Gold Nanoparticle-Mediated Laser Perforation as a New Method to Analyze Dye Transfer and Gap Junctional Coupling. 2014 Annual Meeting of the American Society of Cell Biology, Philadelphia, USA.

Bader A., Begandt D., Ngezahayo A. (2013) Adenosine receptors regulate the gap junction coupling of the blood-brain barrier. 2013 Annual Meeting of the American Society of Cell Biology, New Orleans, USA.

Begandt D., **Bader A.**, Dreyer L., Ngezahayo A. (2013) Regulation of Gap Junction Coupling in Aortic Vascular Cells by Dipyridamole. 2013 Annual Meeting der American Society of Cell Biology, New Orleans, USA.

Bader A., Begandt D., Ngezahayo A. (2013) The antithrombic drug dipyridamole enhances the gap junction coupling of the human cerebral microvascular endothelial cell line hCMEC/D3. 92nd Annual Meeting of the Deutsche Physiologische Gesellschaft, Heidelberg, Germany.

Begandt D., **Bader A.**, Dreyer L., Gerhard L., Ngezahayo A. (2012) Gap junction coupling of vascular cells is a target for dipyridamole: the role of the cAMP/PKA dependent pathway. 2012 Annual Meeting of the American Society of Cell Biology, San Fransisco, USA.

Begandt D., **Bader A.**, Dreyer L., Ngezahayo A. (2011) Increase of Gap Junction Coupling in Aortic Vascular Smooth Muscle and Endothelial Cells by Dipyridamole. 2011 Annual Meeting of the American Society of Cell Biology, Denver, USA.

Begandt D., **Bader A.**, Dreyer L., Ngezahayo A. (2011) Is gap junction coupling of vascular cells a target for dipyridamole? International Gap Junction Conference 2011, Gent, Belgium.

Begandt D., **Bader A.**, Dreyer L., Ngezahayo A. (2011) Gap Junction Coupling of Vascular Cells is a Target for Dipyridamole. 90th Annual Meeting of the Deutsche Physiologische Gesellschaft, Regensburg, Germany.

Begandt D., **Bader A.**, Dreyer L., Ngezahayo A. (2010) Dipyridamole Potentiates Gap Junctional Communication of the Vascular System. 2010 Annual Meeting of the American Society of Cell Biology, Philadelphia, USA.

Acknowledgements